

**2DOF External Fixator and
Computer-Assisted Surgical System for
6DOF Orthopedic Correction
Using Axis-Angle Representation**

Submitted in partial fulfillment of the requirements for

the degree of

DOCTOR OF PHILOSOPHY

in

BIOMEDICAL ENGINEERING

Ying Ying Wu

B.Eng., Biomedical Engineering, Imperial College London, UK

Carnegie Mellon University
Pittsburgh, PA

August, 2016

Abstract

Orthopedic deformities are often complex three-dimensional (3D) deformities, and the reconstruction of the original or normal geometry is difficult. In this thesis, the use of external fixators were investigate for long bone deformity correction and clubfoot correction. An external fixator works by attaching to bones or bone fragments and moving them to the target geometry. Its key advantages are that it encourages tissue growth and preserves healthy tissues. However, current six degrees of freedom (6DOF) external fixators are difficult to set up, resulting in long surgeries and steep learning curves for surgeons. They are also bulky and obstruct patient mobility.

The integration of computational methods and surgical assistive device to the surgery to improve the accuracy of external fixation was proposed. A new method of defining orthopedic deformity correction was developed, and the 6DOF correction problem was reduced to just 2DOF using axis-angle representation. Therefore, only two physical trajectory joints are needed so the fixator can be more compact. The planner minimizes the bulk of the external fixator, and optimizes the distraction schedule to avoid overstretching the soft tissues. The surgical assistive device is a passive positioning linkage that assists the surgeon in building an accurate external fixator that can achieve complete correction. It is not actuated but has brakes to hold its end effector pose. The planner and linkage is expected to reduce the learning curve for surgeons and shorten surgery time.

To validate the system, a patient-specific clubfoot model was developed. This model has a 3D printed rigid skeletal structure with an outer layer of gel that mimics human muscles. Thus, it can support bone pin insertions while still maintaining the flexibility to demonstrate the correction.

Four experiments were performed on the foot model. The accuracy of midfoot correction was 11 mm and 3.5 deg without loading, and 41 mm and 11.7 deg with loading. While the external fixator has to be more rigid to overcome resistance against correction, the surgical system itself was able to achieve accurate correction in less than two hours. This is an improvement from the current method which takes 2.5 to 4.5 hours.

Acknowledgement

I would like to thank my advisor, Professor Kenji Shimada, for his guidance. Special thanks to Dr. Anton Plakseychuk for sharing his clinical expertise over the last five years. I would also like to thank Professor Lee Weiss and Professor Phil Campbell for being part of my committee and for their advice.

I would also like to thank my sponsor, the Agency for Science, Technology and Research (A*STAR) for their generous support of my PhD studies, the Disruptive Healthcare Technology Institute for funding part of the thesis (April 2014 Request for Proposal, project title: Office-centered Three-dimensional Ultrasonic Imaging of Rotator Cuff Tears), and the Biomedical Engineering Department for their continued support and reassurances.

I thank the machine shop guys, John, Ed, Jim and Larry for their patience when I leave a trail of broken things. You are out of this world!

I thank my first and only art instructor, Elizabeth Castonguay, for encouraging and helping me to grow as an artist. Thank you to all the other students who made classes so fun and enjoyable.

Special thanks to all friends and family, back home and in town. To friends who reach across the globe to check on me, thank you for keeping me rooted and grounded. To the artsy peeps, the “cool” and “awesome” aisle members, the birding fanatics, the early birds, the coffee addicts, the groceries gang, the shape-conscious, the audiophiles, the climbers, the foodies, and the big-hearted ones, thank you for making this small town gigantic and for keeping my sanity in check.

Thank you for awesome company!

Table of Contents

Abstract	i
Acknowledgement	ii
List of Figures	v
List of Tables	viii
Chapter 1. Introduction	1
1.1 Orthopedic Deformity Correction as Rigid Body Transformation	2
1.2 External Fixation as an Effective Method of Deformity Correction	2
1.3 Recent Advances in Computer Aided Orthopedic Surgery	3
1.4 Problem Statement	3
1.5 Proposed Approach	4
1.5.1 Axis-Angle Representation of Rigid Body Transformation	5
1.5.2 Surgery Workflow	6
1.5.3 Surgical Planner	6
1.5.4 Passive Positioning Linkage	7
1.6 Scope	8
1.7 Contributions	8
1.8 List of Publications	9
1.9 Thesis Outline	10
Chapter 2. 2DOF External Fixator for Long Bone Deformity Correction	11
2.1 Physiology of Distraction Osteogenesis	12
2.2 Current External Fixators for Distraction Osteogenesis	14
2.3 Rotational Osteotomy	15
2.4 Problem Statement	16
2.5 Future Clinical Utilization	16
2.6 Rigid Body Transformation in Long Bone Deformity Correction	17
2.7 2DOF External Fixator for Long Bone Deformity Correction	19
2.8 Optimization of External Fixator Configuration	22
2.9 Conclusion	25
Chapter 3. 2DOF External Fixator for Correction of Relapsed Clubfoot	26
3.1 Clubfoot and Relapsed Clubfoot	28
3.2 Physiology of Relapsed Clubfoot Correction using External Fixators	29
3.3 Current External Fixators for Clubfoot Correction	30
3.4 Problem Statement	30
3.5 Future Clinical Utilization	31
3.6 Rigid Body Transformation in Clubfoot Correction	32
3.7 Patient Data	37
3.8 2DOF External Fixator for Clubfoot Correction	37
3.9 Optimization of External Fixator Configuration	41
3.10 Optimization of Distraction Schedule	43
3.11 Conclusion	51
Chapter 4. Passive Positioning Linkage	52
4.1 Positioning Device	52
4.2 Digitizer	53
4.3 Specifications	53

4.4 Prototypes	55
4.5 End Effector.....	56
4.6 Controller.....	57
4.6.1 Static Braking Profile	58
4.6.2 Dynamic Braking Profile.....	62
4.7 Current Status and Further Work.....	65
Chapter 5. Flexible Clubfoot Model	68
5.1 Current Models.....	68
5.2 Phantom Model	69
5.3 Further Work and Other Applications	72
Chapter 6. Accuracy of Surgical System: Experimental Surgery for Clubfoot Correction	74
6.1 Camera System for Registration and Data Collection.....	75
6.2 Accuracy of Camera Triangulation	77
6.2.1 Results	77
6.2.2 Sources of Error.....	79
6.3 Robot and Universal Positioning Arm for Trajectory Joint Placement.....	79
6.4 Surgery Procedure on Foot Model.....	82
6.5 Accuracy of Correction using 2DOF External Fixator.....	90
6.5.1 Results	91
6.5.1 Sources of Error.....	92
6.6 Qualitative Evaluation of 2DOF External Fixator.....	93
Chapter 7. Conclusion and Further Work	95
7.1 Summary of Contributions	97
7.2 Extensions.....	98
References.....	99
Appendix A. Iterations of 2DOF External Fixator for Clubfoot Correction.....	105
A1. First Prototype	105
A2. Second Prototype.....	109
A3. Third Prototype.....	112
Appendix B. Iterations of Passive Positioning Linkage.....	115
B1. First Prototype.....	115
B2. Second Prototype	116
B3. Third Prototype.....	117
B4. Fourth Prototype	119

List of Figures

Figure 1-1	Illustration of conversion from Euler angles to axis-angle representation.	5
Figure 1-2	Conceptual drawing of passive positioning linkage (purple) in terms of size and dexterity relative to the external fixator. This drawing is specifically for the case of clubfoot correction.	7
Figure 2-1	An integrated surgical system for proposed 2DOF external fixator. ⁸⁰	17
Figure 2-2	Illustration of rigid body transformation of distal bone fragment to correct long bone deformity correction. ⁸⁰ Plane of osteotomy is located at apex of bend.....	18
Figure 2-3	Illustration of rigid body transformation showing frame assignment and target path. ⁸¹	18
Figure 2-4	The proposed 2DOF external fixator for long bone deformity correction. ^{79,80} It is able to correct a full 3D bone deformity in simulation.	19
Figure 2-5	Setup for simulation of four-point bending of 2DOF external fixator attached to cuboid bone models in CAD environment. ⁸⁰ All dimensions are given in mm. “F” indicate stress loading force and arrows indicate stress loading direction.....	20
Figure 2-6	Configurations of 2DOF external fixator configuration for correcting pure bending, pure twisting, and combinations of bending and twisting.	21
Figure 2-7	Results of nested optimization of 2DOF external fixator configuration and trajectory fitting. ^{79,80}	24
Figure 3-1	Illustration of clubfoot showing angulations in three planes. ^{76,77}	26
Figure 3-2	Angulations of clubfoot.....	26
Figure 3-3	Surgery workflow for the proposed fixator system for clubfoot correction.....	32
Figure 3-4	Simplification of clubfoot correction to midfoot deformity and heel deformity.....	33
Figure 3-5	Illustration of how shortening the equinus joint results in a rotation of the foot upwards, reducing equinus.	34
Figure 3-6	Illustration of stretch at heel as equinus is reduced.....	35
Figure 3-7	Illustration of B-spline defined on affected foot and the target spline from the target poses of the calcaneus and the first metatarsus.	36
Figure 3-8	Illustration of control points to estimate medial foot length. CP: control point.....	36
Figure 3-9	Anonymized patient data and measurement made by radiologist.....	37
Figure 3-10	Trajectory joints for second 2DOF external fixator prototype.....	39
Figure 3-11	Photo of third prototype showing new D-shaped plate and longer equinus joint.....	40
Figure 3-12	Front view of third prototype of 2DOF external fixator for clubfoot correction.....	40
Figure 3-13	Illustration of bounding volume relative to foot.....	42
Figure 3-14	Plot of cost function across bounding volume for one particular ankle joint axis and position. Other ankle joint axes and positions yield similar plots.....	42
Figure 3-15	Computer generated 2DOF external fixator configuration after optimization. Blue line indicates the ankle joint axis. Yellow box indicates the bounding volume for the placement of the revolute trajectory joint.	44
Figure 3-16	Control points for B-spline connecting calcaneus and first metatarsus are plotted for every day of the distraction schedule to visualize the amount of stretch in soft tissues. The first step and last step of the correction are plotted in green and blue respectively.	45
Figure 3-17	Results of distraction schedule optimization in experiment 1.....	47
Figure 3-18	Results of distraction schedule optimization in experiment 2.....	48
Figure 3-19	Results of distraction schedule optimization in experiment 3.....	49
Figure 3-20	Results of distraction schedule optimization in experiment 4.....	50
Figure 4-1	Basic elements of passive positioning linkage.	55
Figure 4-2	CAD model of full passive positioning linkage with revolute trajectory joint attached to its end effector.	56
Figure 4-3	Photo of 3-unit linkage and control circuits on Arduino Micro.	57
Figure 4-4	Block diagram of main steps in getting output signal from controller to electromagnet.	57

Figure 4-5 Profile of torque output vs input voltage of the electromagnet.	58
Figure 4-6 Braking profile types to control activation of brake of each joint. Target angle is set at 50 deg.	59
Figure 4-7 LED lights to indicate where the current joint value is relative to the target value. Red: joint value is very far out. Yellow: joint value is closing in on target value. Green: joint value is within accuracy limits of target.	60
Figure 4-8 Setup of single unit of linkage and indicator lights during user study.	60
Figure 4-9 Photo of a user during the user study.	61
Figure 4-10 Results of user study on static braking profiles. None of the profiles gave a significantly improved results.	62
Figure 4-11 Schematic of Kalman filter with additional predict step to estimate the stopping angle. k indicates the current time step and D indicates the activation delay of 12 ms.	64
Figure 4-12 Schematic of modified Kalman filter, which predict and update of current angle and stopping angle. k indicates the current time step and D indicates the activation delay of 12 ms. A history of prediction of stopping angle is maintained to calculate the error term for $dt = 12$ ms.	64
Figure 4-13 Joint trajectory for each user.	65
Figure 4-14 Results of Kalman filters applied to three user data. Each plot in a row shows the results a user data.	67
Figure 5-1 Photo of foot phantom model ⁷⁸ with rigid 3D printed skeletal structure surrounded by elastic ballistic gel.	70
Figure 5-2 Photo of clubfoot model ⁷⁸ manipulated to normal foot shape. Model did not show signs of tear.	71
Figure 6-1 Camera views of common checkerboard pose that establishes a common workspace coordinate. Colored lines on checkerboard indicates the grid intersections identified by the calibration program.	76
Figure 6-2 Ball bearing setup as viewed by one camera. The ball bearings (green circles) were placed approximately in the middle of the camera view for triangulation.	77
Figure 6-3 Triangulated 3D positions of ball bearings (marked 'x') based on selected points on each camera view in Figure 6-2.	78
Figure 6-4 Error plots of measured distance between ball bearings. Error bars: one standard deviation. .	78
Figure 6-5 Error plots of distance between ball bearings triangulated by the camera array as a percentage of the actual distance. Error bars: one standard deviation.	78
Figure 6-6 Photos of base fixture for universal positioning arm in surgery and robot workspaces.	80
Figure 6-7 Photo of universal positioning arm with the adapter and the robot with the custom end effector. Adapter attached to the robot end effector to configure the universal positioning arm to the calculated pose.	81
Figure 6-8 Photo showing revolute trajectory joint attached to the adapter-arm construct, which was configured by the robot. The adapter-arm construct places the trajectory joint in the calculated pose relative to the foot.	81
Figure 6-9 Setup of experimental surgery for clubfoot correction.	82
Figure 6-10 CAD model of clubfoot skeleton with ball bearings at predefined positions.	83
Figure 6-11 Actual foot models with ball bearings for registration to CAD model.	83
Figure 6-12 Tibial and calcaneal frames were attached to the skeleton via bone pins and sometimes k-wires. The first metatarsus had just the bone pins but no plate as a frame.	84
Figure 6-13 Full view of foot model with base frames.	84
Figure 6-14 The ankle axis was located (green circles) using two ball bearings attached to the hinge joints.	85
Figure 6-15 Final configuration from the optimization of fixator configuration. The calcaneus is depicted in green and the first metatarsus in blue. The yellow rectangle indicates the bounding box for the rotation point.	85

Figure 6-16 Robot positioned the base fixture using a special end effector and the base fixture was secured with clamps.	86
Figure 6-17 Robot positioned the end effector in the calculated pose and the universal positioning arm was attached to the end effector via the adapter.	86
Figure 6-18 Universal positioning arm effectively transferred the calculated pose from the robot in the robot workspace to the revolute trajectory joint in the surgery workspace.	87
Figure 6-19 Photos showing one possible way of using rods and clamps to secure the revolute trajectory joint to the calcaneal base frame.	87
Figure 6-20 Prismatic trajectory joint was positioned by the universal positioning arm and secured to the revolute trajectory joint.	88
Figure 6-21 Photo of connection from calcaneal base frame to first metatarsus via the two trajectory joints.	89
Figure 6-22 Completed 2DOF fixator.	89
Figure 6-23 Fiducial marker for checking the accuracy of midfoot correction. The fiducial marker is a planar construct with three ball bearings attached to track the pose of the forefoot.	90
Figure 6-24 Plots of target transformation (black) and measured transformation with loading (red) and without loading (blue), for experiments 1-4. Transformations shown here are relative to the target transformation.	91
Figure 6-25 Photos of the external fixator for two different experiments. Both configurations were compact and simple. They only occupy the volume in front of the shin and above the foot.	94
Figure 6-26 A different view of external fixator showing simplicity of the setup.	94
Figure A-1 First complete design of 2DOF external fixator. Trajectory joints and equinus joint are highlighted in yellow.	106
Figure A-2 CAD illustration of heel and midfoot deformities.	106
Figure A-3 CAD illustration of foot before and after simulated correction. ⁷⁷	107
Figure A-4 Photos of bone pin attachment sites of first 2DOF external fixator prototype.	107
Figure A-5 Side view of first 2DOF external fixator prototype, before and after correction.	108
Figure A-6 Front view of first 2DOF external fixator prototype, before and after correction. ^{76, 77}	108
Figure A-7 Photo of second prototype showing plate and new trajectory joints.	110
Figure A-8 Photos of foot model before and after midfoot correction.	111
Figure A-9 Photo of third prototype showing new D-shaped plate and longer equinus joint.	114
Figure A-10 Front view of third prototype of 2DOF external fixator for clubfoot correction.	114
Figure B-1 First design of a linkage unit. Exploded view shows the electromagnet in copper color and the encoder in black.	115
Figure B-2 Photos of first prototype of linkage unit.	115
Figure B-3 Second iteration of linkage unit. Exploded view shows the electromagnet in copper color and the encoder in black.	116
Figure B-4 Photos of second prototype of linkage unit.	117
Figure B-5 Third design iteration of linkage unit. Exploded view shows the electromagnet in copper color and the encoder in black.	118
Figure B-6 Photos of third prototype of linkage unit.	119
Figure B-7 Fourth design of a linkage unit. Exploded view shows the electromagnet in copper color and the encoder in black. The planetary gear system and the gear train are also shown in the exploded view.	120
Figure B-8 Photo of fourth prototype of linkage unit. Encoder is not attached to prototype.	120

List of Tables

Table 3-1 Must-have specifications, in order of importance.....	38
Table 3-2 Good-to-have specifications, in order of importance.....	38
Table 3-4 Deformity parameters. Negative angle values indicate rotation in the clockwise direction and the rotation axes are positive in the positive z direction.	45
Table 4-1 Must-have specifications, in order of importance.....	53
Table 4-2 Good-to-have specifications, in order of importance.....	54
Table 5-1 Must-have specifications, in order of importance.....	69
Table 5-2 Good-to-have specifications, in order of importance.....	69
Table 6-1 Table of error in position and orientation of midfoot correction.	92
Table A-1 Component count for first prototype.....	109
Table A-2 Component count for second prototype.	112
Table A-3 Component count for third prototype.....	113

Chapter 1. Introduction

This thesis is focused on the use of computation methods to simplify and improve the accuracy of orthopedic surgeries. In particular, the use of external fixators in the correction of orthopedic deformities was explored. As the deformity often involves six degrees of freedom (DOF), the external fixator is a complex device involving multiple mechanical joints and connections. In particular, this thesis focuses on the application of a proposed 2DOF external fixator on long bone deformity correction and clubfoot correction.

The main concept presented in this thesis is the use of axis-angle representation to reduce any 6DOF correction problem to just 2DOF. A 2DOF correction problem requires only two physical joints to perform the correction. With only two joints, the fixator configuration can be simplified and made more compact. A surgical system is also proposed to assist the surgery and to improve the accuracy of the treatment.

In this chapter, an overview of the thesis project is given. Firstly, long bone deformity correction and clubfoot deformity correction are introduced as rigid body transformations. The external fixator is described with respect to its function as a facilitator of orthopedic deformity correction. This is followed by a brief overview of recent advances in computer assisted orthopedic surgeries.

A statement of the problems with current external fixation method is then given. The approach of using axis-angle representation to solve these problems is proposed and the surgical system to implement this approach is described. The scope of this thesis is defined to limit the deformities to idiopathic deformities with no underlying neuromuscular disorders. Finally, three lists summarizing the contributions of this thesis are given: (1) a list of contributions from this thesis to the scientific community; (2) a list of publications generated from this thesis; and (3) a list of patent applications of the designs and concepts developed in this thesis.

1.1 Orthopedic Deformity Correction as Rigid Body Transformation

Both long bone deformity correction and clubfoot correction are concerned mainly with the macro level mechanical deformities involving the geometry of the bone shape. Long bone deformity includes trauma injury, fracture and unequal limb length. The correction procedure essentially aims to restore the original or predicted bone shape. Paley^{55,57} described the importance and role of the mechanical axes of the limbs, especially in weight-bearing lower limbs. The alignment of bone fragments to restore the mechanical axes is a rigid body transformation. Clubfoot correction is the complex procedure of reducing angulation of bones in multiple planes, which is also a rigid body transformation.

These correction procedures are conventionally approached from the medical perspective of reducing angulation of the deformity in the sagittal, coronal and frontal planes. The proposed approach defines the deformity as the transformation of key bone or bone fragments to restore the mechanical axes. This definition simplifies the deformity into a single 6DOF transformation matrix that is then reduced to 2DOF.

1.2 External Fixation as an Effective Method of Deformity Correction

An external fixator is a construct external to the patient's limbs that is connected to the skeleton via bone pins. There are multiple uses for an external fixator. For example, it is used as (1) a stabilizing device to stabilize a fracture; (2) a distraction device to facilitate distraction osteogenesis; and/or (3) a soft tissue distraction device to stimulate soft tissue growth.

For this thesis, the focus is on the use of external fixator as a distraction device, either to facilitate distraction osteogenesis or to stimulate soft tissue growth. In these two applications, the external fixator facilitates the movement of bones or bone fragments relative to each other to reduce the overall deformity. The external fixator is connected to the patient's bones via bone pins or k-wires and has one or more joints that are adjusted over the treatment period. Since the external fixator is attached to the bones, adjusting these joints changes the alignment of the bones or bone fragments. In general, an external fixator is applied

in a single minimally invasive surgery and the patient is discharged shortly after, with instructions to adjust the joints by a few millimeters per day.

An important advantage of external fixation is that it preserves healthy tissues as the device is external to the patient and the only destructive procedure is the insertion of bone pins. When external fixation fails, the solution is to simply modify or remove it, with minimal damage to the patient. The patient can then go on to receive an alternative or a more aggressive treatment. This is in stark contrast to a failed surgery, which would leave scar tissues that makes it difficult to perform any further corrective procedures.

The main disadvantage of external fixation is that the current external fixators are very bulky and may cause discomfort during the treatment period. In addition, since the distraction is done gradually, treatment via external fixation may take several weeks or months, depending on the severity of the deformity. External fixators are also difficult to setup, thus requiring a more experienced surgeon for more complicated deformities.

1.3 Recent Advances in Computer Aided Orthopedic Surgery

Beyond external fixation, many orthopedic surgeries are moving into patient-specific tools and computer-aided procedures. For example, 3D-printed patient-specific tools abound in joint replacement surgeries and have resulted in improve outcome, cost savings and shorter surgeries.^{14, 58}

In external fixation, there are no surgical systems that help the surgeon build the external fixator. The closest surgical system is the planning software that comes with the Taylor Spatial Frame. However, it is not very intuitive and involves a steep learning curve.³⁵

1.4 Problem Statement

Conventional orthopedic deformity correction relies on a 6DOF solution executed with an external fixator with multiple joints. The external fixator is also built manually with limited help beyond experience. This approach results in bulky constructs, long surgeries and difficulty in achieving complete correction.

In addition, there are currently no methods to control the path of the distraction using a fixator that is not already shaped to the target path.

1.5 Proposed Approach

This thesis proposes an approach to reduce the 6DOF correction problem to just 2DOF. With this approach, the external fixator has fewer joints and is thus smaller and less obtrusive. With fewer joints to adjust, the chances of human error during the treatment are also decreased.

To reduce the problem from 6DOF to 2DOF, the pose of the joints performing the 2DOF correction are calculated and constrained. Therefore, a surgical system consisting of a surgical planner and a surgical assistive device is proposed. The planner does: (1) the conversion from 6DOF to 2DOF; (2) the optimization of the external fixator configuration; and (3) the optimization of the distraction schedule. The surgical assistive device is a passive positioning linkage that performs registration of the system to the patient, and assists in the accurate building of the fixator by holding the components in their calculated poses.

The two joints that perform the 2DOF correction are termed the trajectory joints as they control the distraction path. The optimization of the distraction schedule enables the achievement of the target distraction path and distraction rate. This minimizes the risk of soft tissue damage due to overstretching. For distraction osteogenesis, this also regenerates bone tissues in the original bone shape to produce better loading pattern.

A compact fixator with a planner that computes the optimal fixator configuration has a profound impact on a broad range of orthopedic procedures that involve external fixators. The use of external fixators in the regeneration of bone tissues via distraction osteogenesis was established by Dr. Gavril Ilizarov in 1988.⁴⁰ It was so effective at stimulating the growth of bone tissue that it was soon applied to fracture healing, bone lengthening and reconstruction of damaged bone tissues in long bones, and the reconstruction of maxillofacial bones (bones around the face and jaw).⁶⁵ Therefore, this proposed approach is applicable to all bone deformity corrections involving the use of an external fixator. In this thesis, the application of

2DOF external fixators to long bone deformity correction is described in Chapter 2 and the application of 2DOF external fixators to clubfoot deformity correction is described in Chapter 3.

1.5.1 Axis-Angle Representation of Rigid Body Transformation

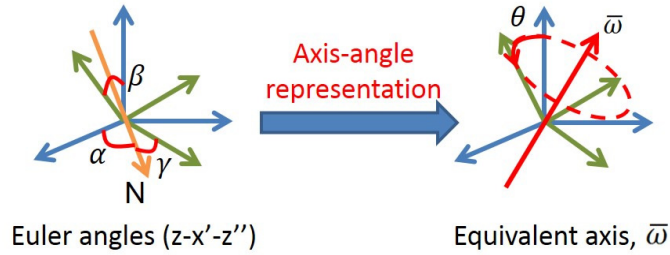


Figure 1-1 Illustration of conversion from Euler angles to axis-angle representation.

Axis-angle representation is a mathematical representation of any 3D rotation as a single rotation about an equivalent axis. As opposed to the conventional approach of rotating about the xyz orthogonal axes by Euler angles to achieve a 3D rotation, axis-angle representation achieves the same 3D rotation using a single rotation about an equivalent axis. Thus, only one physical joint is required as opposed to three.

Figure 1-1 illustrates the conversion from Euler angles to axis-angle representation. The mathematical conversion from a 3x3 rotation matrix is as follows:

$$\theta = \arccos\left(\frac{\text{trace}(R)-1}{2}\right) \quad (1)$$

$$\bar{\omega} = \frac{1}{2 \sin(\theta)} \begin{bmatrix} r_{3,2} - r_{2,3} \\ r_{1,3} - r_{3,1} \\ r_{2,1} - r_{1,2} \end{bmatrix} \quad (2)$$

where R is the desired 3x3 rotation matrix, $r_{i,j}$ is the element in the i -th row and j -th column of R , and θ is the rotation angle about the equivalent rotation axis, $\bar{\omega}$.

While the transformation is calculated at the center of the bone, it is usually not possible to place the center of a physical joint at this position. Taking this into consideration, for a rotation about any off-origin position, the final translation is calculated as:

$$\begin{bmatrix} 0 & \bar{T} \\ 0 & 1 \end{bmatrix} = H \cdot \begin{bmatrix} 0 & \bar{P} \\ 0 & 1 \end{bmatrix} \cdot \begin{bmatrix} R & 0 \\ 0 & 1 \end{bmatrix}^{-1} \cdot \begin{bmatrix} 0 & -\bar{P} \\ 0 & 1 \end{bmatrix} \quad (3)$$

where \bar{T} is the 3x1 translation vector, H is the 4x4 transformation matrix, \bar{P} is the 3x1 rotation point, and R is the 3x3 rotation matrix.

By aligning the physical revolute joint along the rotation axis and the physical prismatic joint along the translation vector, the physical DOFs of the external fixator necessary for correcting a full 3D deformity is reduced from six to two. This reduction is possible as the poses of the trajectory joints are constrained to the calculated axes.

1.5.2 Surgery Workflow

A surgery workflow that integrates computational methods to assist surgeons in achieving greater accuracy with less effort and time is proposed.

Prior to surgery, 2D planar images are obtained and analyzed to generate a 3D patient model. Deformity data is measured or extracted from this model and passed on to a surgical planner that optimizes the surgical plan. The surgical planner is developed for specific procedures as each procedure has its own constraints and conditions for optimality. The planned surgery is then visualized and simulated in the computer so that the surgeon can review it and either approve it or make changes as necessary.

During surgery, a semi-automated method of registering the surgical system to the patient is performed. This enables the planner to update the surgical plan in case there are any changes to the patient's condition. The planner passes along instructions to the surgical assistive device to assist the surgeon in building the device.

1.5.3 Surgical Planner

A surgical planner for the proposed 2DOF external fixator system to assist surgeons in the planning of the treatment was developed. The surgical planner extracts deformity data via medical images and generates a 3D model of the patient's anatomy. It then generates a plan of the external fixator configuration

and the distraction schedule to achieve the target correction without damaging soft tissues. The surgeon reviews the plan and either approves it or make changes to the correction parameters to generate an alternative plan.

During surgery, the model is registered to the patient by either analyzing 3D point cloud data from a digital probe or 2D images from a camera array. The registration enables the planner to verify the deformity data and to generate the necessary instructions for the surgical assistive device.

1.5.4 Passive Positioning Linkage

A passive positioning linkage as a surgical assistive device is conceptualized. This linkage doubles as a positioning device and registration tool. At the start of the surgery, this linkage acts as an encoder chain to obtain a point cloud of bony features to register it relative to the patient and pass that information on to the planner. This enables the planner to locate the patient relative to the linkage and generate the necessary instructions for the linkage. The passive positioning linkage then follow the instructions to place the trajectory joints in the calculated pose relative to the patient as illustrated in **Figure 1-2**.

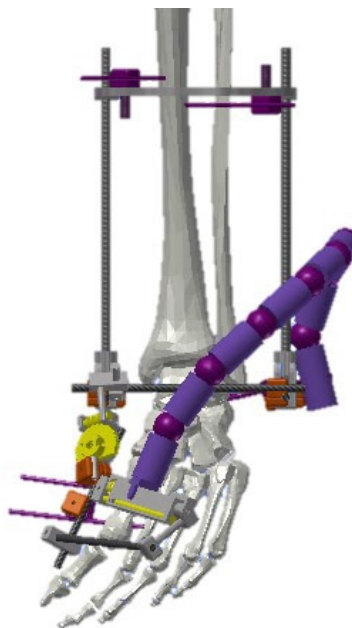


Figure 1-2 Conceptual drawing of passive positioning linkage (purple) in terms of size and dexterity relative to the external fixator. This drawing is specifically for the case of clubfoot correction.

This linkage is still in development and several iterations of the prototypes are completed. Thus, for the experiments described in Chapter 6, an alternative method was used. This alternative method is described in detail in Chapter 6. The iterations and prototypes made thus far are documented in Chapter 4 and Appendix B.

1.6 Scope

The deformities explored in this thesis are limited to long bone deformity from traumatic injury with single apex and idiopathic clubfoot. Other underlying neuromuscular or skeletal diseases complicate the deformity such that it is no longer a geometric problem and requires other forms of treatment.³ Deformities with complications typically have inconsistent prognoses with external fixation.

1.7 Contributions

The original contributions by this thesis are:

1. A mathematical expression of bone deformity correction as a rigid body transformation that enables quantification of correction target and accuracy.
2. A method of optimizing the 2DOF external fixator configuration for long bone deformity correction and clubfoot correction to minimize the overall size of the device.
3. A method of optimizing the device distraction schedule to limit distraction rate in long bone deformity correction and clubfoot correction, and to regenerate the original or contralateral bone shape in distraction osteogenesis.
4. A novel foot phantom model consisting of a rigid skeletal structure embedded in flexible transparent ballistic gel that mimics the consistency of human muscle. This model has generated much interest as a teaching tool for residency programs.

1.8 List of Publications

Journals

1. Wu, Y. Y., A. Plakseychuk, and K. Shimada. 2DOF External Fixator and Surgical System for Clubfoot Deformity Correction. (In preparation)
2. Wu, Y. Y., M. Rajaraman, B. Lee, A. Plakseychuk, and K. Shimada. A Patient-Specific Flexible 3D Printed Orthopedic Model for Training and Teaching of Clubfoot Correction Surgery. *3D Printing and Additive Manufacturing* 3:98-105, 2016.
3. Wu, Y. Y., A. Plakseychuk, and K. Shimada. Computer-aided surgical planner for a new bone deformity correction device using axis-angle representation. *Med. Eng. Phys.* 36:1536-1542, 2014.
4. Wu, Y. Y., R. Lucking, R. Oberreuter, and K. Shimada. New Distraction Osteogenesis Device With Only Two Patient-Controlled Joints by Applying the Axis-Angle Representation on Three-Dimensional Bone Deformation. *Journal of Medical Devices* 7:041010-041010, 2013.

Conferences

1. Wu, Y. Y., A. Plakseychuk, and K. Shimada. 2DOF External Fixator and Surgical System for Clubfoot Correction (Poster). *American Society of Biomechanics* , 2015.
2. Wu, Y. Y., A. Plakseychuk, and K. Shimada. 2DOF Fixator System for Correcting 3D Clubfoot Deformity (Poster). *7th World Congress of Biomechanics 2014* , 2014.
3. Wu, Y. Y. and K. Shimada. Computer-Aided Surgical Planner for a New Bone Deformity Correction Device Using Axis-Angle Representation (Poster). *Innovation in Healthcare Technology Conference 2014* , 2014.

Provisional patents

1. Shimada, K., Y. Y. Wu, and A. Plakseychuk. 2DOF Clubfoot Fixator and Computer-aided Surgical System, 2013 (Provisional patent).
2. Shimada, K., Y. Y. Wu, and M. Rajaraman. Medical Phantom with Tactile Feedback for Medical Training and Evaluation, Pre-operative Planning, Teaching, and Patient Education, 2016 (Provisional patent).

1.9 Thesis Outline

Chapter 2 and 3 elaborate how a 2DOF external fixator system is applied to long bone deformity correction and clubfoot correction respectively. Details of the 2DOF external fixator prototypes and the optimization methods are explained in these chapters for the respective correction. Moving on to the surgical system, Chapter 4 describes the proposed surgical assistive device while Chapter 5 describes the clubfoot model used to validate the external fixator. Chapter 6 details the experiments to validate the accuracy of the proposed surgical system. Chapter 7 concludes the thesis and briefly explores possible further work.

Chapter 2. 2DOF External Fixator for Long Bone Deformity

Correction

Long bone deformities are often 3D deformities, involving a bend, a twist, and/or a mismatch in contralateral bone lengths. These angulations and length discrepancy in the lower limbs can cause difficulty walking and may lead to other compensatory symptoms such as an abnormal walking gait and functional scoliosis. According to the United States Bone and Joint Initiative, in 2006 alone, there are 61.2 million musculoskeletal injury treatment episodes, of which 16.2 million are bone fractures.⁷³

This thesis is focused on lower limb deformities resulting from external trauma without other underlying pathologies. Examples include limb lengthening, mal-union of fractures, and non-union of fractures. The scope is limited to trauma injuries because external fixators are temporary and work best if the bone and musculature are able to regenerate without complications and maintain the correction upon removal of the external fixator.

This chapter describes the application of the proposed 2DOF approach to the correction of long bone deformity. The principles of distraction osteogenesis are described and the method of external fixation to facilitate distraction osteogenesis is explained. While external fixation is a constructive process that results in tissue growth, current external fixators are bulky and difficult to set up.

The proposed approach reduces the 6DOF correction problem to 2DOF, and enables a more compact fixator configuration. A compact 2DOF external fixator was designed specifically for long bone deformity correction. In addition, this approach enables the regeneration of the original or contralateral bone shape by minimizing the maximum deviation of the bone path from the target trajectory. This approach was tested on a Sawbones model (Sawbones, Vashon Island, WA, U.S.A.) and the maximum deviation of the bone path from the target trajectory was 1.8 mm, which was below the threshold of 2 mm.

2.1 Physiology of Distraction Osteogenesis

Distraction osteogenesis (DO) is a method of stimulating bone growth by osteotomizing the bone and gradually distracting bone fragments under a controlled environment with the help of an external fixator. The external fixator is connected across the bone fragments via bone pins and adjusted to pull the bone fragments apart over time. After its conceptualization in 1905 by Codivilla¹¹ as a method for limb lengthening, there were several periods when DO lost support from the medical community because the underlying physiology was poorly understood and the method used indiscriminately, which resulted in inconsistent success rates.⁷⁵ In 1988, Ilizarov conducted a series of studies to understand the underlying physiology and he discovered the optimal distraction rate of 1 mm/day.⁴⁰ If the distraction is greater than 1 mm/day, fibrous tissues may form instead. On the other hand, if distraction is slower than 1 mm/day, the bone fragments may fuse and prevent further distraction. Since the discovery of this optimal rate, doctors began to achieve consistently good results,^{51, 56} and DO is now applied to many other conditions, such as fracture mal-union and non-union, and maxillofacial reconstruction.⁶⁸ Along with the bone, the surrounding soft tissues also grow under tension.³⁰ The exact cellular biological mechanism of how the stretching stimulates growth in both bone and soft tissues is still being studied.³⁴

Treatment using DO with an external fixator can span over months, depending on the severity of the deformity. According to the original Ilizarov method of DO using external fixator,⁴⁰ the external fixator is attached to the bone before the deformed bone is corticotomized. Corticotomy, as opposed to osteotomy, is performed to preserve the soft tissues in the bone marrow and the periosteum. The gap is then stabilized for a week before distraction begins at 1 mm/day. This stabilization period is termed the latency period. Once the target length is achieved, the external fixator is left in place until the new bone in the gap fully ossifies and is able to support the body weight of the patient. In general, unless the external fixator is physically obstructing movement, weight bearing is possible and encouraged.⁵⁶ Many slight variations to this techniques has been developed, but the main principles of maximum soft tissue preservation, slow gradual distraction and maximum tolerable weight-bearing remain unchanged.

Although DO is a slow and uncomfortable procedure, it is preferred by many surgeons as it maximizes soft tissue preservation and is a constructive procedure that results in new bone growth.²⁹ This is in contrast to the loss of healthy tissues with procedures such as limb shortening or wedge closing. The gradual correction when using an external fixator enables greater overall correction than an acute correction performed in a single surgery. Soft tissues are able to stretch by only a limited distance when the stretching is done all at once. However, if the stretching is done gradually over time, the total amount of stretch is much bigger as the soft tissues grow under tension. For instance, neurons under tension are able to grow both *in vitro*⁸⁴ and *in vivo*². In contrast to other implanted solutions, such as a plate or an internal fixator that goes into the marrow of the bone, external fixation enables fast and non-destructive access to the device in cases of failure or changes in the correction plan.

Given the current understanding of DO, it is uncommon for an experienced surgeon to encounter severe complications such as nerve and vasculature damage and joint contractures.^{29, 45, 70} These complications usually arise when soft tissue growth cannot keep up with the distraction rate, and they can be fully treated by simply reversing the direction of distraction and allowing more time for the soft tissues to grow.^{29, 34} Joint contractures can also be alleviated with physical therapy.⁴⁵ Non-union of the fragments may also occur if the distraction site is unstable.⁷ Minor complications such as pin tract infections and pain are very common, but they are usually easy to treat and deep infections are rare.^{23, 29, 34}

Successful external fixation requires spatial skills and an understanding of the mechanism of the human skeleton. Mechanical axes refers to the loading line on the bone and joint in its natural loading condition⁵⁵ and the realignment of the mechanical axes are crucial to the success of the correction procedure. If the mechanical axes are not aligned, as in the case with mal-union of fracture, the unnatural loading pattern on the joint may lead to degradation of the joint.^{55, 64} For young children below eight years old, even severe mal-unions, such as angulations of 20 deg and complete displacement of bone ends, are found to spontaneously correct themselves.²⁵ However, little correction can be expected in older children and adults.²⁵ Thus, it is important to achieve accurate correction and to realign the mechanical axes.

2.2 Current External Fixators for Distraction Osteogenesis

External fixators come in different shapes and sizes, and are classified primarily as either ring or axial. Ring and axial fixators differ mainly in the shape of the main frame of the fixator.

Ring fixators have two or more ring structures that surround the limb and are generally more rigid than unilateral fixators and thus reduce the risk of non-unions. An example is the Taylor Spatial Frame (TSF), which is designed based on the Stewart platform and has 6DOF to correct 3D bone deformities. More generic ring fixators are built using an array of rings and rods assembled together to form a 6DOF external fixator. A disadvantage of a ring fixator is that it is bulky, especially on the femur and on petite patients. Adjusting multiple joints at each step of the correction also increases the risk of human error.

Axial fixators have a rod-like frames that go along one side (usually the lateral side) of the limb, which make these fixators very compact and suitable for the femur and petite patients. The reduced bulk results in reduced rigidity, which increases the risk of non-unions and may limit their application to non-weight-bearing corrections.⁵⁴ Their use is also limited to corrections of up to 3DOF, typically length discrepancy and one or two other angulation(s). Nevertheless, for short distraction lengths⁶ and when mobility during correction is crucial,¹³ axial external fixators have a clear advantage.

Hybrid external fixators such as the Hoffmann II Lower Extremity Ring System (Stryker, Mahwah, NJ, U.S.A.) have components of both the ring and axial fixators and thus inherit the advantages and disadvantages of both fixators, depending on the application. The Multiaxial Correction System (Biomet Orthopedics, Warsaw, IN, U.S.A.) utilizes the Center of Rotation of Angulation (CORA) method described by Paley⁵⁵ to perform the correction. The MAC system has adjustable rotation joints in the form of thick rods to increase rigidity. The CORA method is based on rotation and translation about three orthogonal axes and is planned on 2D planar radiographs.

A key point about the effectiveness of external fixation is that it is dependent on the surgeon's experience.⁴³ Building the external fixator requires sharp spatial sense to place the joints at the right position.⁴³ Despite these challenges, the pre-operative planning is limited to 2D planar x-ray images^{43, 55}

and the surgery is performed without assistive devices. Some external fixators such as the TSF come with a software to assist with the planning, but even then, there is a steep learning curve to use the software.^{20, 66}

There have been some attempts to simplify the process of building external fixators for long bone deformity correction. Koo et. al.⁴³ developed a computer program for the Dynafix unilateral external fixator (EBI Medical, Inc, Parsippany, NJ, U.S.A) that performs the same function as the software for the TSF does. Both obtain the current fixator configuration and the actual deformity either via fiducial markers or manual input, and then calculate the correction plan to achieve complete correction and the necessary adjustments in fixator components or placement.

For other applications where the fixator can be highly specialized, the fixator themselves are custom made so that it corrects the deformity using only 1DOF. In maxillofacial reconstruction, several groups have suggested curvilinear fixator designs that achieve complete correction with one adjustment joint.^{36, 37, 53} For cases such as maxillofacial reconstruction where there are huge spatial limits and less resistance to expensive custom made jigs, such 1DOF curvilinear fixator designs are highly advantageous as they are small enough to fit into the mouth cavity. In generic trauma injury, more generic fixator that can be used in multiple situations would be preferred.

2.3 Rotational Osteotomy

Aside from DO, rotational osteotomy is another technique for correction and it achieves full angular correction using a single rotation axis. This method is described in literature as early as in 1989⁶⁷ and, in 2011, Dobbe¹⁶ discussed the technique further and described a new surgical jig to assist with the orientation of the osteotomy. Briefly, the surgeon performs an osteotomy perpendicular to the rotation axis, and the distal fragment is rotated about the osteotomized surface for the calculated angle to align the bone fragments. The main difference from DO is that, in rotational osteotomy, both bone fragments are always in contact. This method is advantageous as it is easy to perform if the osteotomy direction can be determined, and it does not create a bone gap and therefore does not require any grafting. However, it is limited to angular deformities, and any limb length modifications have to be done using other methods.¹⁶

2.4 Problem Statement

There is a need in the clinic for a compact external fixator that can gradually correct a 3D long bone deformity in all 6DOF and that comes with an intuitive planner to assist the surgeon in building the external fixator.

In this thesis, a new approach to represent 3D long bone deformity as a rotation about a single axis using axis-angle representation, and a translation in 3D space is proposed. In doing so, a 6DOF correction problem is reduced to a 2DOF correction problem, while the gradual correction of a full 3D deformity is still achieved. The original or contralateral bone shape is regenerated by controlling the trajectory of the distal bone fragment during distraction.

As none of the external fixators currently available are able to efficiently implement the axis-angle approach to deformity correction, a new 2DOF external fixator is developed. It has two trajectory joints, namely a revolute joint for rotation and a prismatic joint for translation.

2.5 Future Clinical Utilization

An integrated surgical system for the proposed 2DOF external fixator that is intuitive and simple to use is envisioned. A flowchart of this system is shown in **Figure 2-1**. Firstly, using the hierarchical free-form deformation developed by Gunay et. al.,³² 3D bone models is generated from two or more 2D planar radiographs such as x-ray images. The axes of the 3D bone model and that of a template normal bone model are compared to define the 3D bone deformity. Based on this deformity data, a surgical planner generates the best external fixator configuration and distraction schedule to minimize tissue damage. The process is then simulated and presented to the surgeon for approval. The surgeon may also use this as material for patient education.

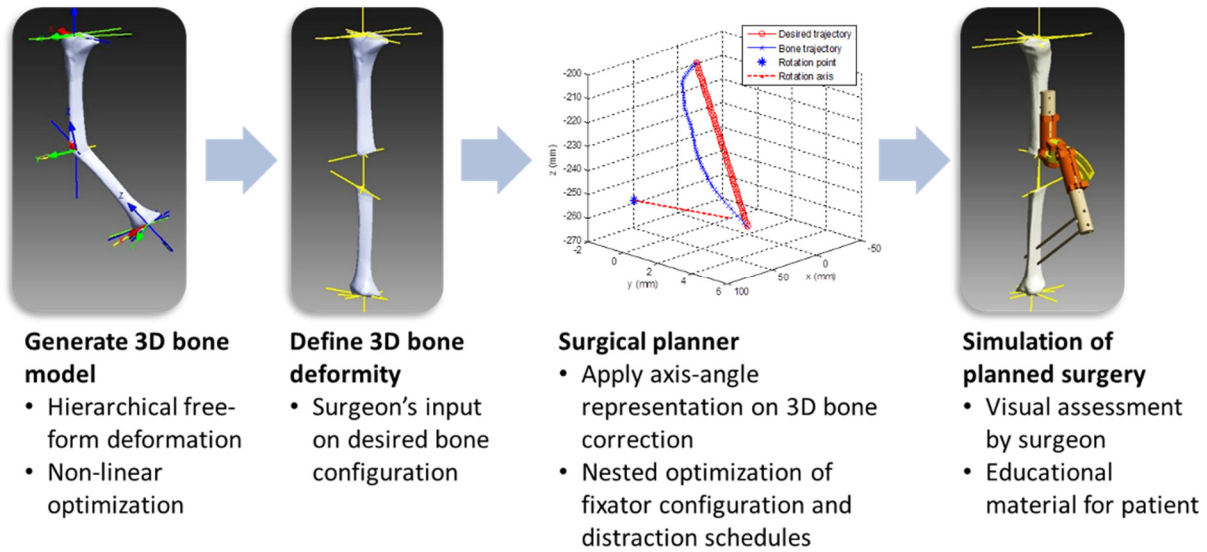
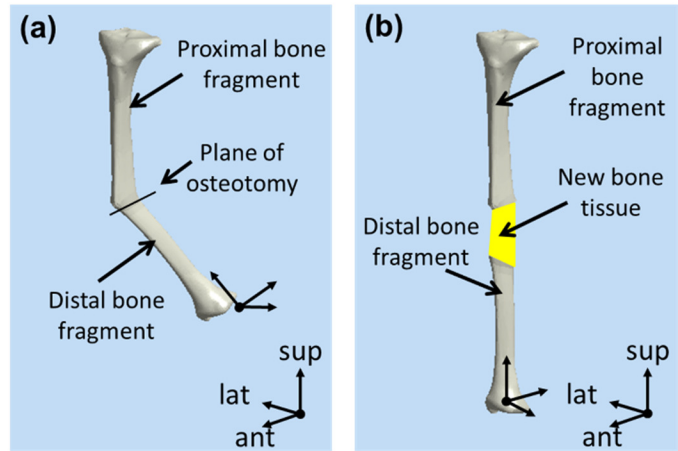


Figure 2-1 An integrated surgical system for proposed 2DOF external fixator.⁸⁰

2.6 Rigid Body Transformation in Long Bone Deformity Correction

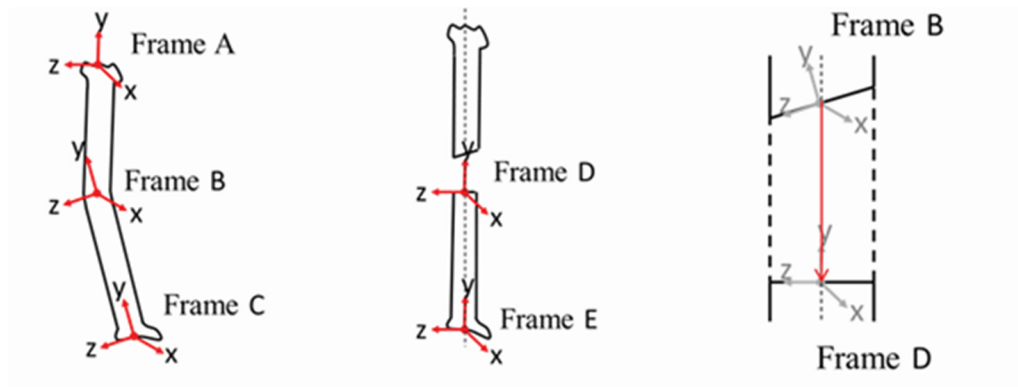
Long bone deformity correction is defined in this thesis as a rigid body transformation of the distal bone fragment from its deformed pose to its target pose as shown in **Figure 2-2**. For a simple single-cut deformity correction, coordinate frames are defined on the two bone fragments as shown in **Figure 2-3**. Deformity correction is simply the transformation of Frame B to Frame D, where Frame B is the deformed pose of the distal fragment and Frame D is the target pose to reduce all angulations and length discrepancies. This 6DOF transformation is then converted using axis-angle representation to 2DOF.



(a) Deformed bone.

(b) Target bone shape.

Figure 2-2 Illustration of rigid body transformation of distal bone fragment to correct long bone deformity correction.⁸⁰ Plane of osteotomy is located at apex of bend.



(a) Deformed bone with assigned frames.

(b) Desired position of bone and associated frames.

(c) Magnified osteotomy site showing transformation (red arrow) from Frame B to Frame D during DO.

Figure 2-3 Illustration of rigid body transformation showing frame assignment and target path.⁸¹

The final shape of the new bone is assumed to follow the trajectory of the distal bone fragment during DO. While the mechanical axis of the bone is crucial to the transfer of the loading stresses to connecting bones and joints, the anatomical bone axis is important for the bone to sustain the loading stresses internally. The natural remodeling by osteoclasts and osteoblasts would most likely remove minor deformation in the bone shape, but the capability to remodel gross deformation in bone shape drastically

decreases after the age of eight years old.²⁵ Thus, in the proposed system, the path planning for the distal bone is included to reduce the workload on the body in shaping the new bone segment.

For long bone, a linear target trajectory across the bone gap is defined as shown in **Figure 2-1**. A linear trajectory is defined because long bones have very slight curvatures and a linear trajectory is a good starting point. In other applications such as maxillofacial reconstruction, the jawline is highly curved and a quadratic distraction path is necessary. In addition to the shape of the trajectory, target poses for each day of correction is defined such that the distraction achieved is not more than 1 mm/day as indicated by Ilizarov's study.⁴⁰

2.7 2DOF External Fixator for Long Bone Deformity Correction

A 2DOF external fixator was designed and a prototype was 3D printed using the Fused Deposition Modelling technique on a Dimension printer (Dimension Elite, Stratasys Ltd, Eden Prairie, MN, U.S.A.). **Figure 2-4** shows an annotated photo of the 3D printed 2DOF external fixator with two trajectory joints. It has a circular revolute joint and a prismatic joint connected in series, and measures 12 in tall by 6 in wide.

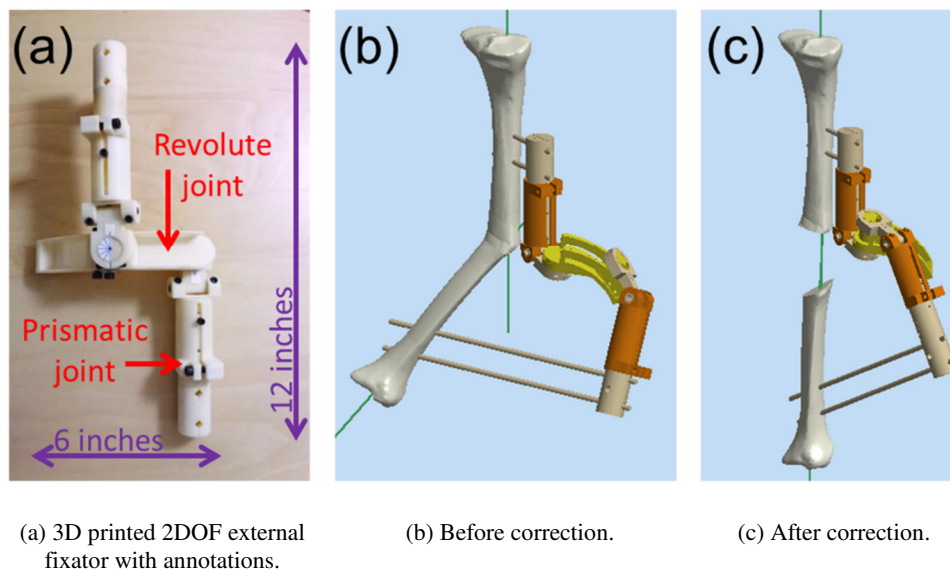


Figure 2-4 The proposed 2DOF external fixator for long bone deformity correction.^{79, 80} It is able to correct a full 3D bone deformity in simulation.

Stress analysis on the CAD model of this 2DOF external fixator is performed because weight-bearing is an important part of external fixation for DO.²⁹ A 100N four-point bending on the model was simulated in the Stress Analysis module in Autodesk Inventor (Autodesk® Inventor™ Professional 2013, Educational Version, Autodesk, Inc.) as shown in **Figure 2-5**. This setup follows the description by Chao et. al.⁸ and more details can be found in this paper⁸⁰.

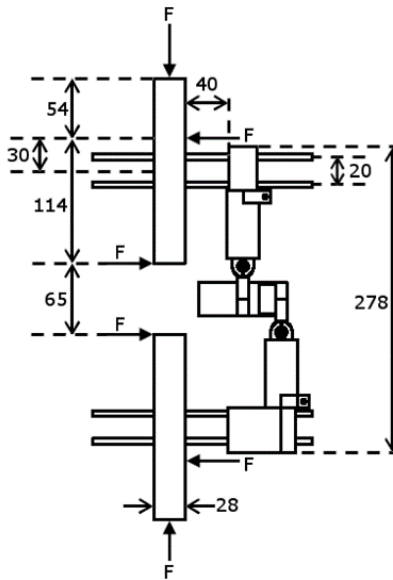


Figure 2-5 Setup for simulation of four-point bending of 2DOF external fixator attached to cuboid bone models in CAD environment.⁸⁰ All dimensions are given in mm. “F” indicate stress loading force and arrows indicate stress loading direction.

The results indicate that, compared to the Orthofix® unilateral external fixator (Orthofix SRL®, Verona, Italy) investigated by Chao et. al.⁸, the 2DOF external fixator is comparably stiff in axial compression, stiffer in the coronal plane and less stiff in the sagittal plane⁸⁰. This result is expected as the 2DOF external fixator design had bone pins that are located closer to each other, which made it less stiff in axial loading. Similarly, since the proposed fixator is thicker perpendicular to the coronal plane, it is expected to be stiffer. All in all, the fixator is comparable in stiffness to current fixators on the market.⁸⁰

Figure 2-6 shows the proposed 2DOF external fixator in different configurations for correcting different deformities. For pure bending, the revolute trajectory joint is angled at 90 deg while for a pure twisting, it is in the neutral position aligned along the bone axis. Realistically, deformities that involve both bending and twisting, such as the ones shown in **Figure 2-6(c,d)**, are more likely.

This design would benefit from a few more design iterations. Due to resource constraints, further iterations of the 2DOF external fixator design for long bone deformity was not pursued. A potential failure mode is instability at the distal bone pins. The gap between the distal part of the fixator and the bone may become too big in some of the fixator configuration. With only the bone pins bridging the gap, this may result in instability and possibly non-union. A solution is to include more joints after the prismatic trajectory joint to bring the fixator closer to the bone and shorten the exposed bone pin segment. As this is not a fundamental design flaw, this design concept is viable even though it requires a few more design iterations.

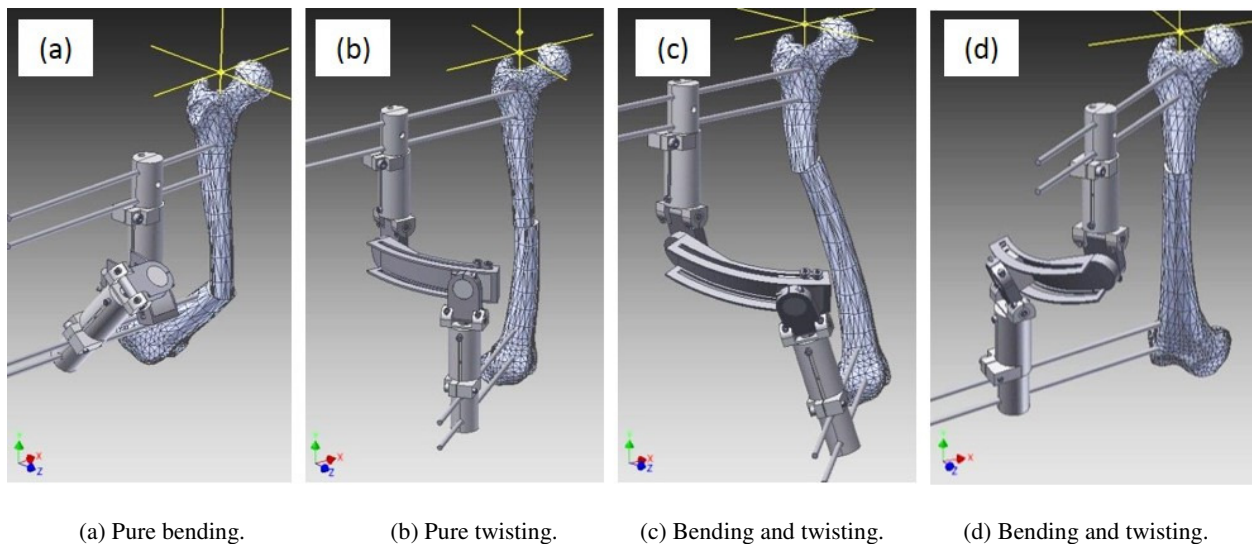


Figure 2-6 Configurations of 2DOF external fixator configuration for correcting pure bending, pure twisting, and combinations of bending and twisting.

2.8 Optimization of External Fixator Configuration

Given the target geometry and distraction trajectory, the external fixator configuration and the distraction schedule were optimized. Both the target correction and trajectory are affected by the position of the revolute trajectory joint and the rate at which the two trajectory joints are adjusted during the correction period. A different position of the revolute trajectory joint results in a different translation component of the correction. The distraction schedule affects the distraction trajectory and thus the final bone shape. For example, performing rotation before translation or translation before rotation will yield a drastically different path.

The target path was set as a linear path with target poses spaced 1 mm apart. The target pose is the pose that the bone should be moved to every day. The target poses were spaced 1 mm apart to maximize the speed of correction without causing soft tissues damage or non-union. Since the path is linear, it is expected that the distraction schedule would include simultaneous rotations and translations in small increments. Deviation from the target path is expected as the path is only controlled by the two trajectory joints. 6DOF is needed for the bone to follow any arbitrary path. Given there are only 2DOF in this case, in general, the deviation will not be zero, but it can be minimized.

To achieve the best distraction schedule, two optimizations were nested: (1) for a particular rotation point, the distraction schedule was optimized to minimize the deviation from the bone trajectory, and (2) the rotation point was optimized to minimize the deviation defined in (1)^{79, 80}. In addition, the rotation point was constrained to an area anterior and lateral to the bone. This ensures that the external fixator will not obstruct walking and that it was placed at a distance from the skin to allow swelling. The distraction schedule were also constrained to be monotonically increasing and the rotation per day was bounded to avoid collision between bone fragments.

The objective function was to minimize deviation from the target path, across all rotation points. Defining deviation as the largest geometric distance between the planned position and target position across all steps, the objective function was expressed as^{79, 80}:

$$\min_{\bar{P}} \left(\max_i (\|\bar{x}_i - \bar{d}_i\|) \right) \quad (4)$$

where \bar{P} is the position of the revolute joint, \bar{x}_i is the bone position at step i (day) of the distraction, and \bar{d}_i is the desired bone position at step i .

The error threshold was set at 2 mm, taking reference from the recommended limit for distal radius fractures.⁵² This constrained optimization was performed using the sequential quadratic programming (SQP) algorithm in MATLAB (Student Version, The MathWorks, Inc.). The final distraction schedule was smoothed to remove any jerky movement.

The external fixation of a Sawbones tibia model with 39 deg of bending and 10 deg of rotation was optimized, and the results are plotted in **Figure 2-7**.^{79,80} As shown in **Figure 2-7(a)**, a bone trajectory within 1.8 mm deviation from the target, which is below the threshold of 2 mm, and with all constraints observed, was achieved. The optimized distraction schedule spans over 63 days and the distraction distance for each day is close to 1 mm, with a maximum distraction of 1.2 mm as shown in **Figure 2-7(b)**. **Figure 2-7(c)** shows that the rotation angle is indeed bounded to prevent bone-bone collision while **Figure 2-7(d)** shows the schedule for each trajectory joint. The final trajectory is plotted against the target trajectory in **Figure 2-7(e)** (note that axes spacing is not equal). The correction as planned was simulated and the resulting fixator configuration before and after correction are shown in **Figure 2-4(b,c)**.

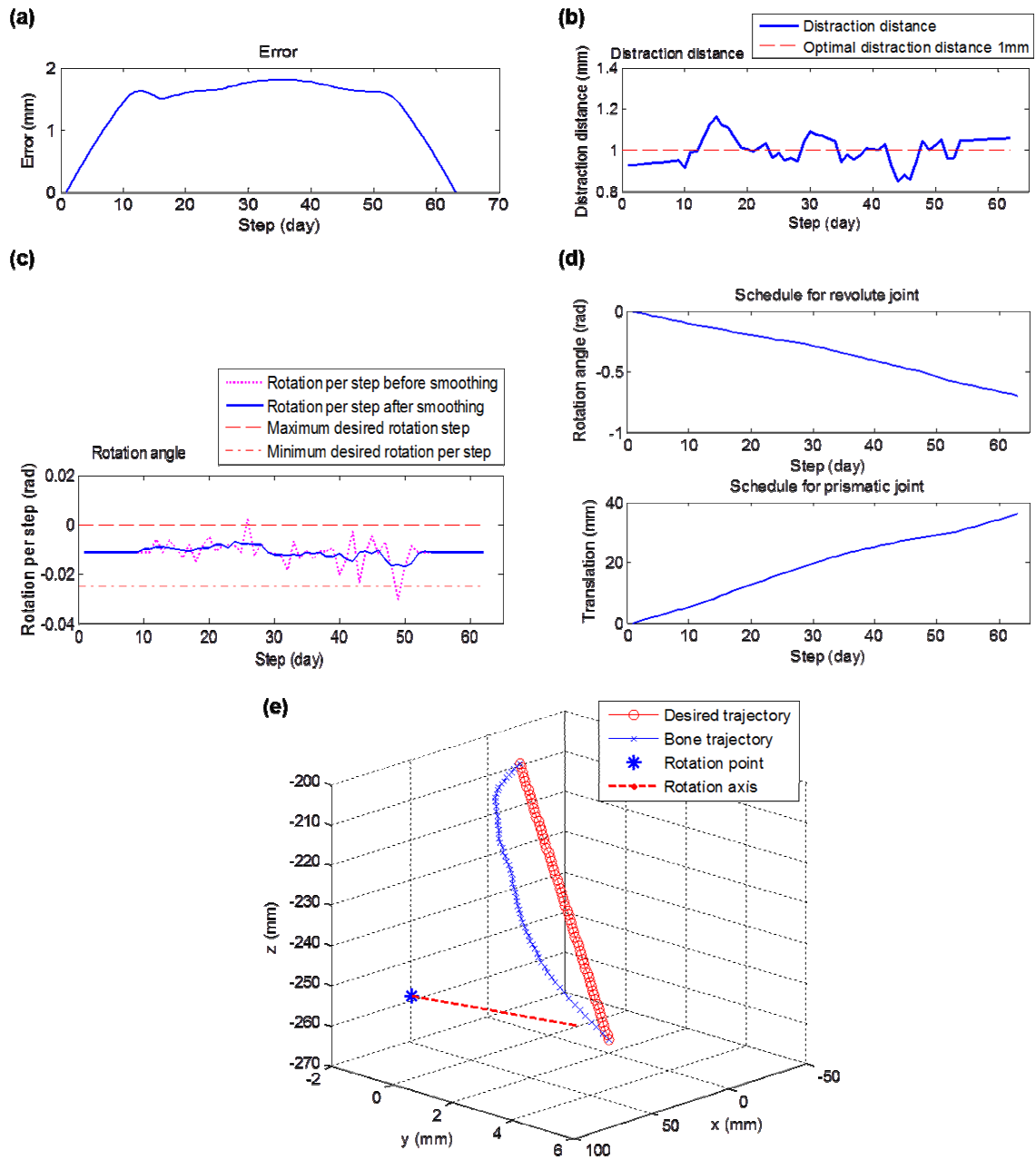


Figure 2-7 Results of nested optimization of 2DOF external fixator configuration and trajectory fitting.^{79, 80}

2.9 Conclusion

In this chapter, the correction of a 6DOF long bone deformity using a 2DOF external fixator was presented and validated. Firstly, long bone deformity correction was introduced as a rigid body transformation. The physiology of distraction osteogenesis was described to explain the external fixation method of correcting long bone deformities.

The approach of using axis-angle representation to reduce the 6DOF long bone deformity correction to 2DOF was described. In addition, to implement this approach, a compact 2DOF external fixator was designed and discussed in terms of its mechanical stiffness.

Furthermore, the concept of regenerating the original or contralateral bone shape by following a target bone trajectory was introduced, and an optimization method was developed to minimize the maximum deviation of the actual bone trajectory from the target bone trajectory. This method was applied to a Sawbones model and a maximum deviation from the target trajectory of 1.8 mm was achieved. This error was below the threshold error of 2 mm.

The main limitation to this approach is the hardware implementation and, at the current stage, further hardware iterations are necessary to achieve sufficient stiffness to support weight-bearing exercises. Nevertheless, the optimization of the external fixator configuration and the distraction schedule was achieved with an error that was within threshold.

Chapter 3. 2DOF External Fixator for Correction of Relapsed Clubfoot

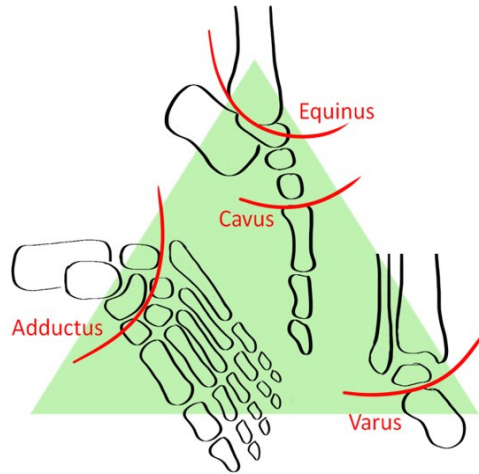


Figure 3-1 Illustration of clubfoot showing angulations in three planes.^{76, 77}

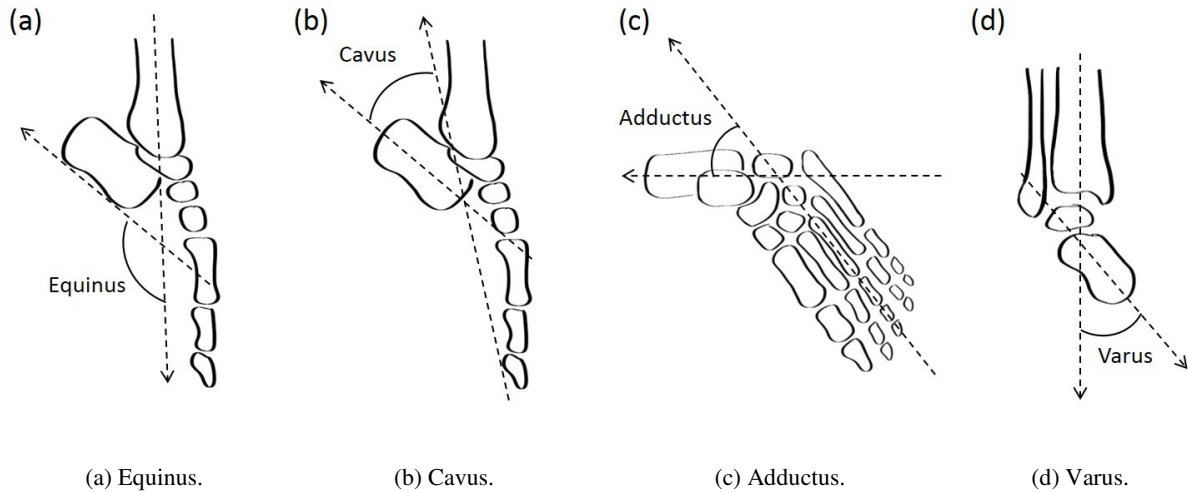


Figure 3-2 Angulations of clubfoot.

Clubfoot, or congenital talipes equinovarus, is a complex three-dimensional (3D) deformity of the foot presented at birth. It presents cavus, adductus, varus and equinus of the foot as illustrated in **Figure 3-1**. **Figure 3-2** illustrates how the angles are measured on radiographs. In a normal foot, there should be no varus, 30 deg adductus, 45 deg cavus and 70 deg equinus.^{28, 74} In the US, clubfoot affects one in 1000 live births and may affect only one or both feet.¹ The affected foot is held rigidly in deformity by shortened ligaments and tendon and stiff muscles. A child with clubfoot walks on the lateral side of the deformed foot in an awkward gait that causes sores and wears out normal shoes. This necessitates the wearing of modified shoes, which stigmatizes the child.

The cause of clubfoot is unclear even though there are multiple conditions that are correlated with clubfoot. It is thought that abnormal amniotic pressure may cause a variety of foot deformities, including clubfoot.⁴⁹ Many other theories, such as interruption in fetal growth, intrauterine positioning, and soft tissues anomalies, are raised but none of the studies are conclusive.^{3, 12, 38}

This chapter first introduces clubfoot deformity and the treatment options. This thesis is focused on specifically relapsed or neglected clubfoot, which is indicated for external fixation. The advantages of external fixation as opposed to surgery are then discussed. The main disadvantage of external fixation for clubfoot correction is that current external fixators are too bulky and not designed for the ankle joint.

By reducing the clubfoot deformity to equinus and midfoot deformity, the 6DOF to 2DOF reduction can be applied to the midfoot deformity. This approach enables minimization of the fixator bulk and optimization of the distraction schedule to avoid soft tissue damage. This method was applied to anonymized patient data and a 2DOF fixator configuration was designed specifically for clubfoot deformity correction. The fixator optimization resulted in a compact fixator with its main bulk concentrated above and in front of the foot. An average soft tissue stretching of 1.6 mm/day, which was below the threshold of 2 mm/day, was achieved.

3.1 Clubfoot and Relapsed Clubfoot

Clubfoot is easily identified at birth and treatment usually begins within the first few months of life. The current consensus for initial clubfoot treatment is soft tissue manipulation with the Ponseti method⁶⁰ to avoid extensive surgery and to restore foot function.^{62, 85} This method involves a series of massages and castings. Approximately once every week, the affected foot is massaged to reduce the deformity and a cast is applied to maintain the incremental correction. This is repeated over several weeks, and different aspects of the deformity are corrected in a specific order.⁶⁰ The infants then undergo a strict bracing regimen for the next several years to maintain the correction. Rigorous adherence to this bracing protocol is essential to achieving permanent correction.^{3, 82} The Ponseti method is highly successful and has close to 100% success rate after initial treatment.^{62, 82, 85}

Despite the initial success, fully treated clubfoot may relapse several years later in early childhood at an incidence of between 11% to over 30%.^{17, 21, 50, 63, 85} The cause of relapse after an apparently successful treatment is not known even though non-compliance has been a major indication.^{46, 83, 85} Clubfoot in older children may be very stiff and involve gross deformity of foot bones and joints. Thus, the goal for treating relapsed clubfoot is to achieve plantigrade foot, or the ability to walk with the sole flat on the ground. A successfully treated relapsed clubfoot may still have a stiff ankle joint and modified gait, but the patient will be able to wear normal shoes and walk on both soles.

Surgical treatment is available for both the initial option or for relapsed clubfoot. However, it is usually not the preferred method as bony procedures results in shortening of the already short deformed foot^{18, 48}, while soft tissue release results in stiffness of the foot¹⁸ and scarring²¹. In addition, the results of surgical methods is unpredictable and they do not obviate the chances of a relapse.^{35, 85}

External fixation is an option limited to only relapsed clubfoot or clubfoot that is neglected and that persisted into early childhood. Sufficient calcification of the bone structure to support the external fixator is necessary for external fixation. Only children with sufficiently calcified skeleton are indicated for external fixation. In general, children older than four years of age are indicated.¹⁹ Nevertheless, since every child develops at a different rate, the actual age depends on the individual.

3.2 Physiology of Relapsed Clubfoot Correction using External Fixators

Since 1990, external fixators have been applied to persistent or relapsed clubfoot with positive results^{24, 31} and it is gaining favor as it is a less destructive method^{21, 27, 35, 47}. The external fixator surrounds the leg and is rigidly attached to the patient via bone pins that are inserted into the tibia, first metatarsus and calcaneus. Joints on this construct are adjusted to push the bones until the foot is plantigrade, and this is done gradually over several weeks to allow the soft tissues to grow and adapt to the new foot position. In general, a distraction rate of 1-2 mm/day^{35, 47} is recommended. In external fixation, the deformity of each foot bone is not as crucial as the shape of the entire foot. Thus, bone pins are inserted into only the tibia, calcaneus and first metatarsus, and it is assumed that the soft tissues will pull all other bones into their natural poses.

Generally, unlike the Ponseti method, there is no order to the correction procedure. Some groups implement the principles of Ponseti method in external fixation, but the advantage of doing so is unclear.⁷² Once correction is achieved, the fixator is left in place for another 4-6 weeks.^{19, 47} Following the removal of the fixator, an ankle cast or foot orthosis may be applied.^{47, 71}

External fixation has been recommended as a highly effective technique for clubfoot deformity correction of relapsed or neglected clubfoot.^{19, 27, 35, 41, 47} Although external fixation may have associated complications such as pin infections, several studies^{35, 41, 47} find the complications mild and without lasting effects. Way back in the 1990s, surgeons reported positive outcomes, including the stimulation of tissue growth and regeneration^{24, 26, 31, 48} and improved mobility¹⁸. It is beneficial even for clubfeet with multiple surgical scars²⁷ and is more effective than casting as it exerts greater corrective forces⁵. External fixation is also effective for the 12.9%³³ of clubfeet associated with neurological dysfunction^{9, 39}, which would otherwise have poor prognosis³. Although further relapse is possible, unlike surgery, external fixation is less destructive as it preserves bone anatomy and thus supports subsequent corrective treatment.⁴⁸

3.3 Current External Fixators for Clubfoot Correction

Despite the difference in anatomy, fixators used for clubfoot correction are the same generic ones, such as the Ilizarov external fixators and TSF, which are designed for correcting long bone deformity. They are bulky and difficult to tolerate^{26,71} when applied to the foot, especially since relapsed clubfeet are treated in young children. This may prevent or limit mobility for the entire treatment period of 12 to 18 weeks.²¹ In the field of orthopedics, patient mobility is highly valued as weight-bearing stimulates regeneration and healing in both bone and soft tissues to achieve better patient outcome.

While external fixation is an effective technique for clubfoot deformity correction, current external fixators are hard to set up.^{5,21,27,47} Setting up a generic fixator such as the Ilizarov external fixator requires good spatial sense to know where to place the joints. Furthermore, current fixators usually do not come with planners or assistive devices, so surgeons have to assess the deformity and build the fixator based on 2D radiographs. Although the TSF comes with a planner⁶⁹, using the device still involves a steep learning curve³⁵. As a result, surgeries tend to be long, averaging 2.5 hours and up to 4.5 hours or even 8 hours with less experience.³⁹ Moreover, as the deformity is complex and 3D in nature, building a fixator that can achieve complete correction is often difficult. Residual deformity that are more severe may require repeat surgery,^{27,39} which in turn increases treatment time and healthcare costs.

3.4 Problem Statement

There is a clinical need for an external fixator specifically for the foot that can gradually correct a 3D foot deformity and that is compact so that it does not obstruct walking. It should also come with an intuitive planner and tools to assist the surgeon in building an accurate external construct.

A fixator system consisting of a compact 2DOF external fixator for clubfoot deformity correction and a computer-assisted surgical system is proposed.^{76,77} Each DOF is defined as a joint that has to be adjusted during treatment. Unlike generic fixators with multiple joints, the proposed 2DOF fixator has only two trajectory joints and is able to correct a full 3D clubfoot deformity.

The surgical system consists of a surgical planner and a surgical assistive device.⁷⁶ The surgical planner finds the most compact fixator configuration and the fastest rate of adjustment of each of the trajectory joints to shorten the total treatment time while preventing soft tissue damage. The surgical assistive device is a passive positioning linkage that accurately places the trajectory joints relative to the patient's foot, thus achieving complete correction with just one fixator setup. This eliminates the need for subsequent adjustment surgery, reduces the total treatment time, and reduces the learning curve for surgeons.

3.5 Future Clinical Utilization

A surgical system for the proposed 2DOF external fixator for clubfeet is envisioned. This system assists the surgeon in planning and building an accurate external fixator to achieve complete correction. The workflow for this fixator system is illustrated in **Figure 3-3**.

An osteotomy is first performed on the calcaneus to reduce slight angulations of the heel, leaving only the equinus. The 3D model of the foot is then created using either 2D radiographs and template models or 3D imaging data such as CT scans. A surgical plan for the 2DOF fixator configuration and the distraction schedule is generated prior to surgery and a simulation of the distraction schedule is presented to the surgeon for approval.

During surgery, the patient's foot is registered using a passive positioning linkage and the ankle joint is located. With the updated registration data, the surgical plan is regenerated and presented to the surgeon for approval. The surgeon sets up the base frames of the 2DOF external fixator and attaches it via bone pins to the tibia, calcaneus and first metatarsus. To achieve accurate placement of the trajectory joints of the external fixator, the same linkage holds them in the poses calculated by the surgical planner while the surgeon builds the rest of the fixator to secure the trajectory joints to the base frames.

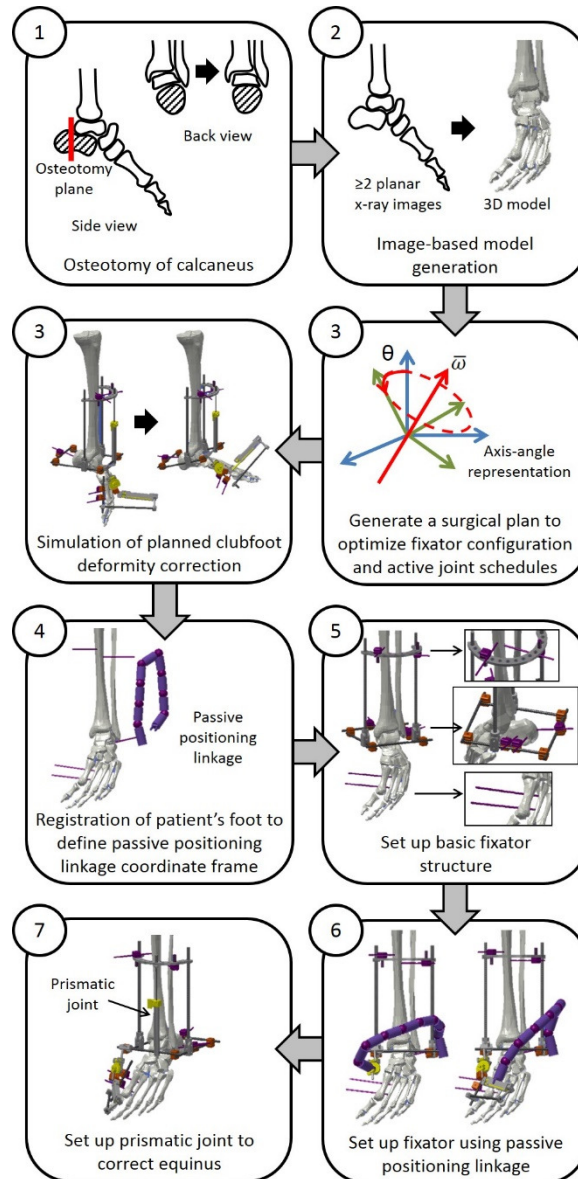


Figure 3-3 Surgery workflow for the proposed fixator system for clubfoot correction.

3.6 Rigid Body Transformation in Clubfoot Correction

Clubfoot deformity is simplified by defining it as the transformation of the first metatarsus from its deformed pose to its target pose. This transformation is further defined as the combined effect of two independent deformities about the midfoot and the heel as illustrated in **Figure 3-4**. The first metatarsus is chosen because the fixator is attached to this bone and thus its pose can be directly controlled via the

external fixator throughout the correction process. The pose of the foot bones are defined using principal coordinate axis (PCA) on the vertices of their respective CAD model. The axis with the largest variance is approximately the long axis of the bone and this is taken as the z-axis.

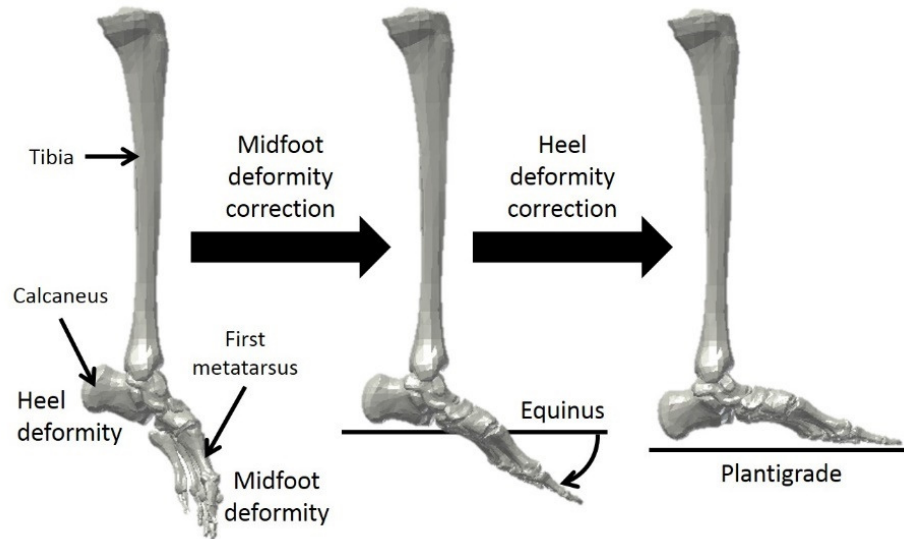


Figure 3-4 Simplification of clubfoot correction to midfoot deformity and heel deformity.

The heel deformity is defined to be a 1DOF upwards rotation about the ankle joint and the midfoot deformity is a 3D deformity requiring 6DOF for correction. It is assumed that osteotomy of the calcaneus can reduce angulation about two axes, leaving only equinus. Since the foot anatomy allows only limited distraction at the ankle, the calcaneus is only rotated and not distracted.

The ankle joint is located by the surgeon. Many studies show that the ankle joint moves as the ankle rotates, and there has been much effort trying to locate the path of the ankle joint.^{15, 59} Many fixators also have tools to find an equivalent or a good approximation of the ankle joint.^{22, 44} The ankle joint is very complex, and the problem of how to best define and locate the ankle joint is beyond the scope of this thesis. The method used by the clinical consultant, Dr. Anton Plakseychuk, MD, is adopted in this project, and this method models the ankle joint as a cylindrical joint. During surgery, the surgeon locates the ankle joint by fitting a circle to the sagittal view of the talus and takes the ankle joint as a line perpendicular to the plane

at the center of this circle. The surgeon manipulates the C-arm, a portable x-ray imaging machine, to locate the correct plane.

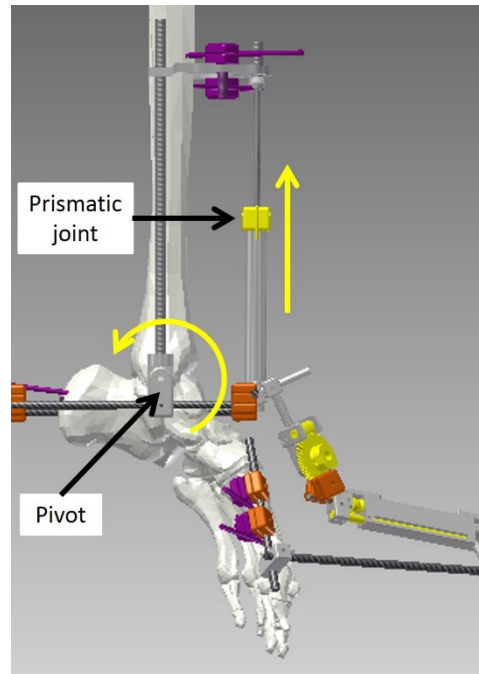


Figure 3-5 Illustration of how shortening the equinus joint results in a rotation of the foot upwards, reducing equinus.

The reduction of equinus is achieved by adjusting the equinus joint. The equinus joint is a prismatic joint located in front of the foot. To reduce equinus, the equinus joint is shortened to rotate the foot. Hinges at both sides of the foot labeled as “pivot” in **Figure 3-5**, are aligned to the ankle joint and ensure that the equinus joint will not crush the ankle joint. The equinus angle is calculated as the rotation to bring the calcaneus from its deformed pose to its target pose. Since the selected ankle joint position is manually selected and is unlikely to exactly rotate the calcaneus from its deformed pose to its target pose, two angles are considered: (1) the angle of rotation that brings the calcaneus to the right position but with the wrong orientation; and (2) the angle of rotation that brings the calcaneus to the right orientation but at the wrong position. Using either extremes could result in a very unnatural foot shape. Since the actual pose of each deformed foot is not as crucial as restoring a normal-looking foot shape, the average of both angles is taken.

The remainder of the deformity is then defined as the 3D midfoot deformity and is reduced using two trajectory joints, namely a revolute joint and a prismatic joint. Midfoot deformity is a 6DOF deformity that is simplified to 2DOF using axis-angle representation as explained in Section 1.5.1. A surgical plan can be made prior to actual surgery, but since the placement of the hinges are not guided, the foot may not rotate about the same ankle joint as identified in the plan. Thus, the surgical plan is updated during the surgery itself and the midfoot deformity has to be re-calculated during surgery.

The amount of soft tissue distraction is defined using the estimated foot length on the medial side of the affected foot. As the distraction happens across the ankle joint, the foot length is segmented into two sections: (1) the distraction at the base of the heel as equinus is reduced; and (2) the distraction at the medial side of the foot as midfoot deformity is corrected. The distraction at the heel is estimated by calculating the increase in circumference as illustrated in **Figure 3-6** when the equinus is rotated at the ankle joint. The radius of rotation is estimated to be 49.8 mm from CAD model of this example.

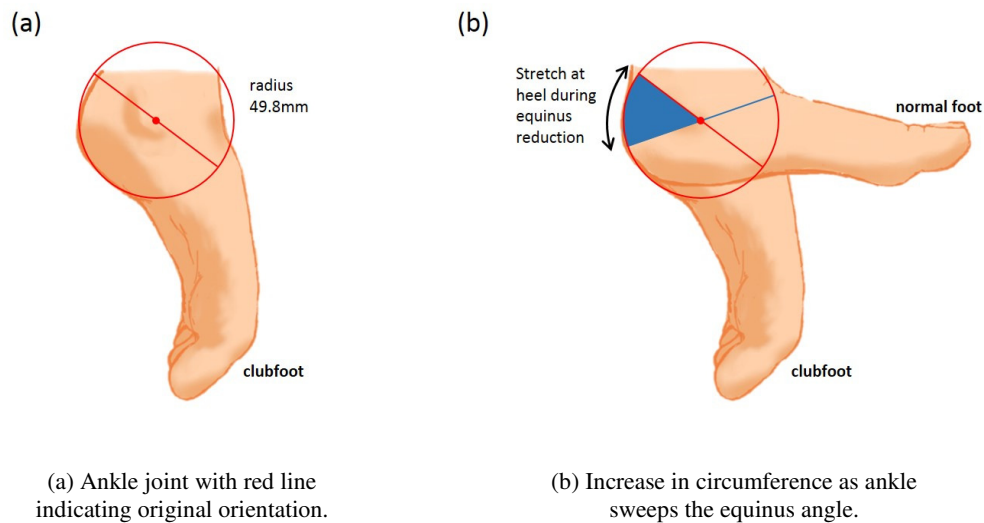


Figure 3-6 Illustration of stretch at heel as equinus is reduced.

The distraction at the medial side of the foot is estimated using a B-spline fitted to the foot bones on the medial side. The first and last control points of the B-spline are the centers of the first metatarsus

and the calcaneus. The second control point is taken along the long axis of the first metatarsus and extended towards the calcaneus for half the length of the first metatarsus. The third control point is taken along the long axis of the calcaneus and extended towards the first metatarsus for half the length of the calcaneus. The splines are shown on the CAD model to illustrate its relationship to the bones in **Figure 3-7**, while the control points are illustrated in **Figure 3-8**. These values are determined empirically and verified visually to give a smooth curve representative of the medial foot length.

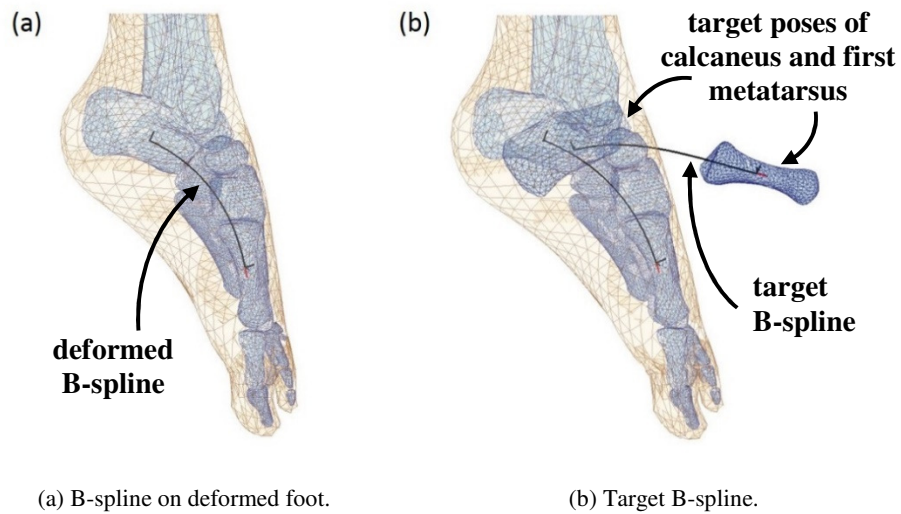


Figure 3-7 Illustration of B-spline defined on affected foot and the target spline from the target poses of the calcaneus and the first metatarsus.

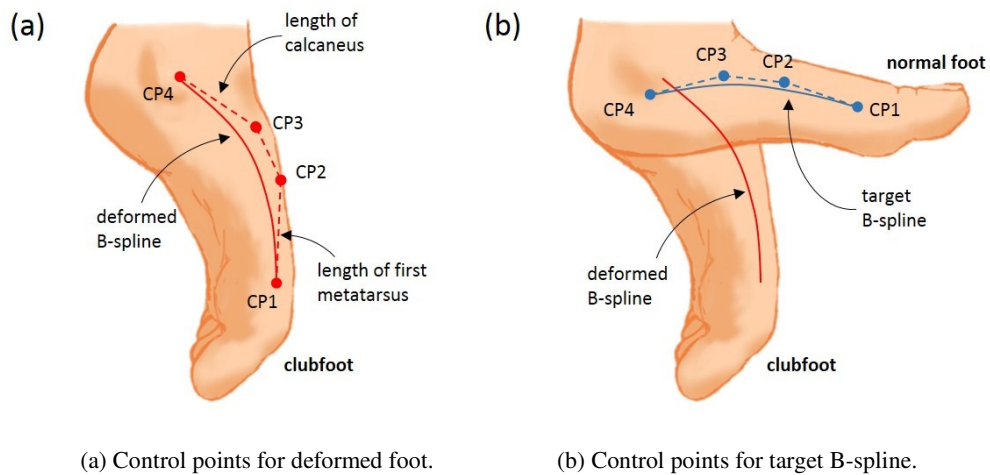


Figure 3-8 Illustration of control points to estimate medial foot length. CP: control point.

Having defined how soft tissue distraction is measured, the distraction rate is controlled by calculating the rate at which the trajectory joints and the equinus joint are adjusted. In clubfoot correction, the actual path of the first metatarsus is less important than the absolute amount of stretching experienced by the soft tissues, as there is no growth of bone tissues.

3.7 Patient Data

An anonymized CT data of a clubfoot was obtained from the clinical consultant. This clubfoot presents 119 deg of equinus, 46 deg of adductus, 34 deg of cavus and 10 deg of varus, as defined in **Figure 3-2**. **Figure 3-9** shows the reconstructed patient model and radiographs at where these measurements were taken by the radiologist. A 2DOF external fixator was designed and tested on a patient-specific clubfoot model segmented from this CT data.

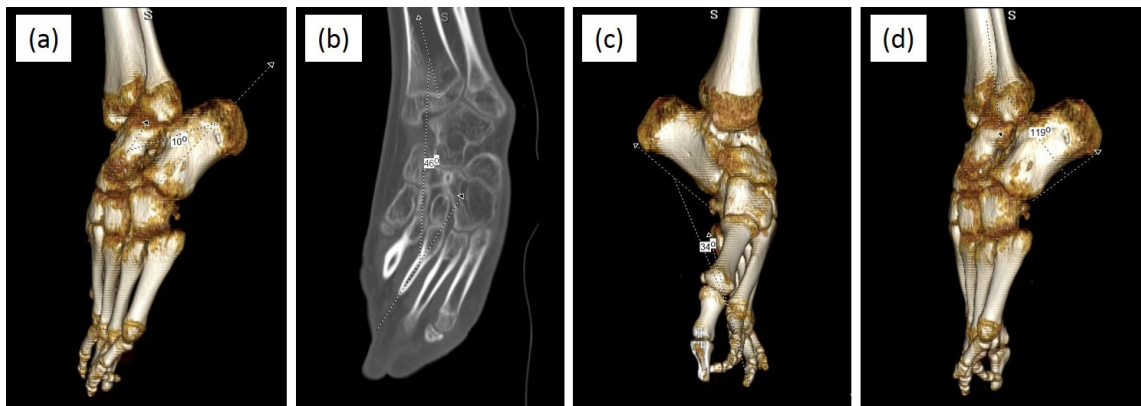


Figure 3-9 Anonymized patient data and measurement made by radiologist.

3.8 2DOF External Fixator for Clubfoot Correction

The design specifications for the external fixator for clubfoot correction is tabulated in **Table 3-1** and **Table 3-2**.

Table 3-1 Must-have specifications, in order of importance.

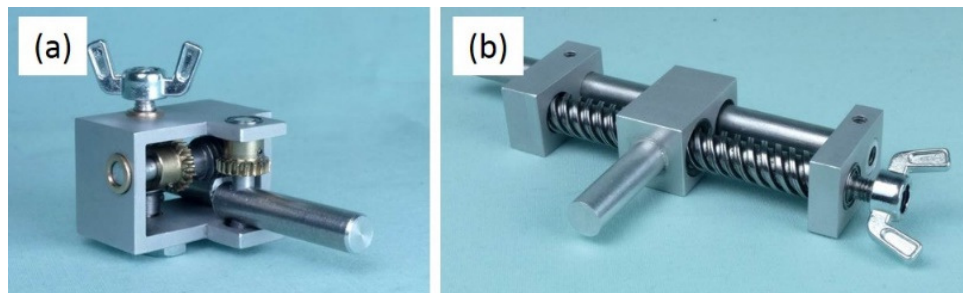
No.	Specifications	Description/ explanation
1	Corrects 60 deg of angulation and 50 mm lengthening	External fixator should cover most cases of clubfoot deformity. These values are estimated as this is a new method of defining clubfoot and there are no prior values to refer to.
2	Device should mostly occupy the area on top of the foot	This minimizes obstruction to walking. Bone pins have to be inserted to the first metatarsus from the medial side. Otherwise, there should be no obstruction on either side of the foot. Device should be entirely above the foot to allow the patient to walk.
3	Rigid	Clubfoot is rigid and will resist correction forces.
4	Large gearing ratio of trajectory joints	A large turn of the joint should only move the leg by a small amount. It is difficult to accurately move a joint by a small amount, so a large gearing ratio would improve accuracy and minimize the risk of overstretching the soft tissues.
5	User friendly interface	Big knobs for joint adjustments to reduce patient's frustration with what is already a long and tedious treatment process. Intuitive interface for surgical system.

Table 3-2 Good-to-have specifications, in order of importance.

No.	Specifications	Description/ explanation
1	Padding for walking	Custom platform/cushion that spreads weight evenly across sole when patient walks during correction period. Sandals are currently available, but fixators are not designed to have these sandals attached.

To increase compatibility with existing external fixators, all components except the trajectory joints were borrowed from existing external fixators. New trajectory joints are designed as there are no components in current external fixators that perform the same function. The revolute trajectory joint has a worm gear mechanism, and the prismatic trajectory joint has 50 mm of extension. The prismatic trajectory joint is constrained so that it does not rotate about its own axis. Current external fixators have prismatic joint components, but those joints are hinged and free to rotate about their own axes, so they cannot be used as a structural component on their own. The final trajectory joints are shown in **Figure 3-10**.

Three iterations of the 2DOF external fixator for clubfoot corrections were made. The final prototype is shown in **Figure 3-11** and a front view of this prototype on the foot model is shown in **Figure 3-12**. The iterations reduce the component count, increase the compatibility with existing components, and increase the rigidity of the external fixator. The D-shaped plate in the final prototype reduces the number of components needed and helps to simplify the fixator. The frame in the final iteration is pre-built before attaching it to the foot to avoid having residual tension in the frame.



(a) Revolute trajectory joint.

(b) Prismatic trajectory joint.

Figure 3-10 Trajectory joints for second 2DOF external fixator prototype.

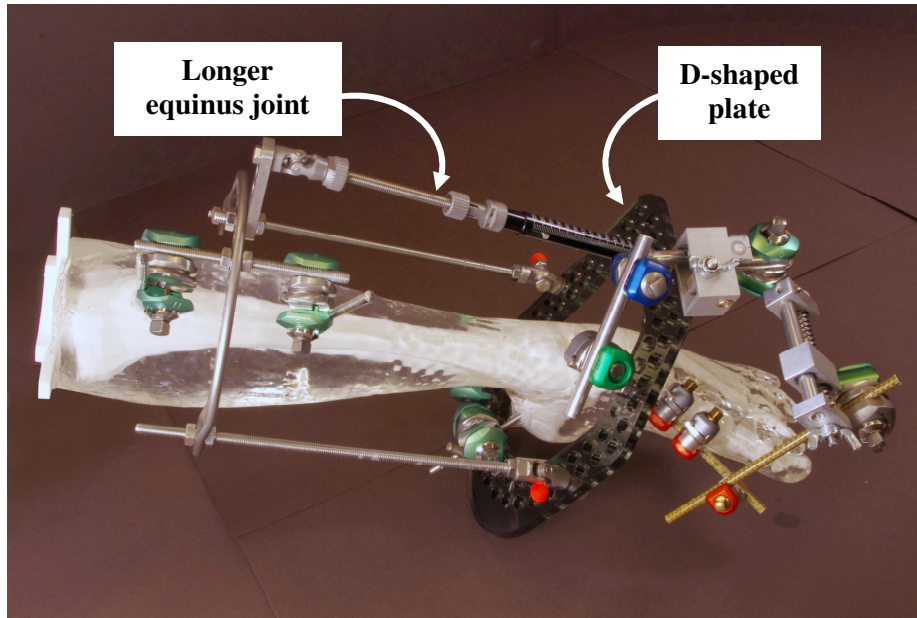


Figure 3-11 Photo of third prototype showing new D-shaped plate and longer equinus joint.

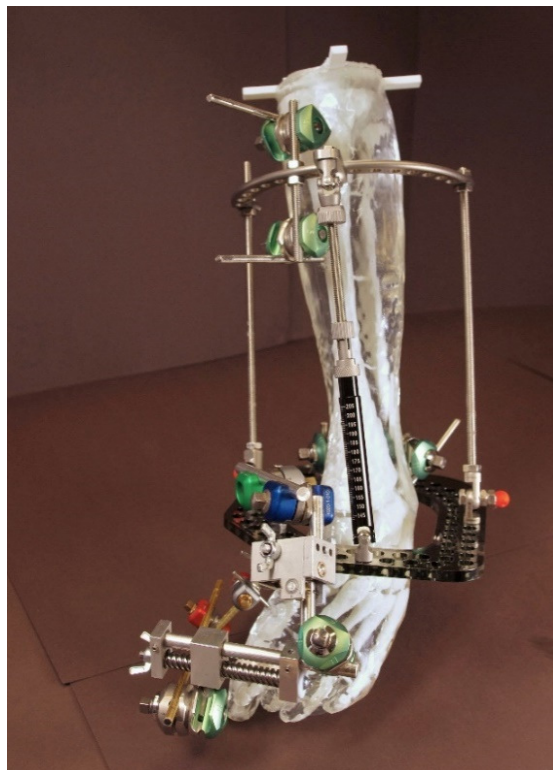


Figure 3-12 Front view of third prototype of 2DOF external fixator for clubfoot correction.

3.9 Optimization of External Fixator Configuration

Unlike the case for long bone deformity correction, the optimization of external fixator configuration for clubfoot correction is independent of the optimization for the distraction schedule. The goal here is only to limit the stretch of the foot to 2 mm/day, as opposed to following a particular trajectory.

For the external fixator configuration, only the midfoot deformity is relevant. The heel deformity or equinus is reduced by lifting the foot with the equinus joint, which results in the rotation of the foot about the ankle hinges. This part of the fixator configuration is straightforward since it is a single prismatic joint that can be placed anywhere in front of the ankle. In contrast, the placement of the revolute trajectory joints affects the magnitude of the translation performed by the prismatic trajectory joint. The bigger this magnitude, the longer and thus larger the joint has to be.

The objective for minimizing the external fixator size was then to minimize the magnitude of translation across all possible rotation points. The cost function heavily penalizes translation that is more than 50 mm and also considers the protrusion of the joint above the plane of the foot. If the joint protrudes out of the foot plane, it not only adds bulk to the fixator, but also may collide with the shin as equinus is corrected. Thus, the objective function was as follows:

$$\min_{\bar{P}} (\|\bar{T}\| + (\bar{n} \cdot \bar{T})^2 + (\|\bar{T}\| > 50) * 1000) \quad (5)$$

where \bar{T} is the 3x1 translation vector from axis-angle representation, $\|\bar{T}\|$ is the 2-norm of \bar{T} , \bar{n} is the 3x1 unit normal to the plane of the foot metatarsus, and \bar{P} is the 3x1 center of rotation.

The revolute trajectory joint was oriented along this rotation axis, while its position was constrained to a bounding volume above the foot, as shown in **Figure 3-13**, to ensure that it will not obstruct walking. Since the translation vector and magnitude was calculated as the remaining transformation after equinus was reduced, the planned correction was always completed with respect to the first metatarsus.

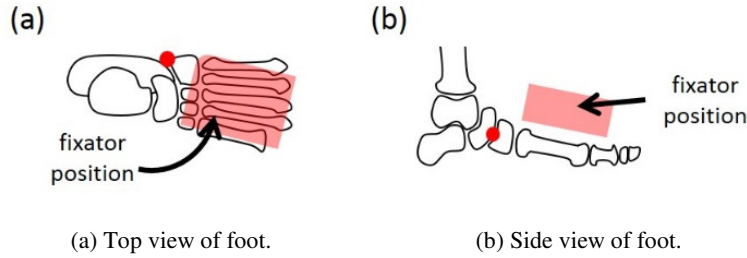


Figure 3-13 Illustration of bounding volume relative to foot.

This optimization was performed using the sequential quadratic programming (SQP) algorithm, which is an iterative nonlinear optimization. Optimization took less than a minute in general on a 64-bit Windows 10 operating system (Intel i7-3667U CPU; 2.00 GHz; 8.00 GB RAM). The search space was investigated and the cost function was plotted across the bounding volume as shown in **Figure 3-14**. The cost function is convex in the bounding volume, so most optimization methods should work fine. Since the optimization was fast, no other optimization algorithms was explored.

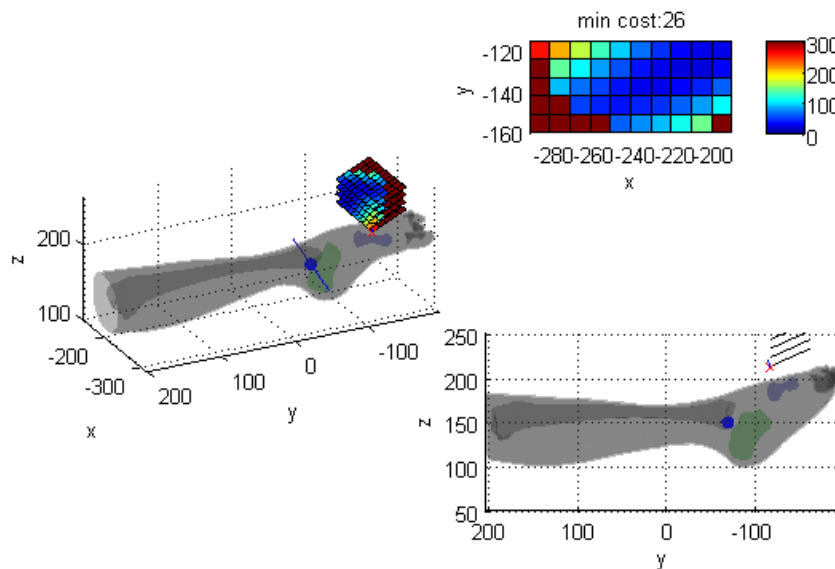


Figure 3-14 Plot of cost function across bounding volume for one particular ankle joint axis and position. Other ankle joint axes and positions yield similar plots.

This optimization was applied on the patient data described in Section 3.7 in four experiments described in Chapter 6. The results of the optimized external fixator configuration are shown in **Figure 3-15**. The deformity parameters are tabulated in **Table 3-3**. For the same patient data, fairly consistent deformity parameters was achieved even with some variation in the orientation and position of the ankle joint. The ankle joint varies because the each experiment was done on a new model. Therefore, the location of the ankle joint may not always be exactly the same.

3.10 Optimization of Distraction Schedule

The distraction schedule was optimized based on the optimal external fixator configuration. The distraction of soft tissues is affected by the rate at which the trajectory joints and the equinus joint are adjusted. The details of how soft tissue stretching is defined are given in Section 3.6.

The objective of this optimization is to set the target soft tissue stretching to 2 mm/day^{35, 47} to avoid damaging surrounding nerves and vasculature. The total amount of distraction going from deformed pose to target pose was first computed and this distraction was divided by 2 mm to get the minimum number of days necessary to complete the correction. The spline length was estimated by taking the Euclidean distance between the control points. Two of the control points move with the calcaneus while the other two move with the first metatarsus. The distraction schedule was also constrained to be monotonically increasing. The objective function was:

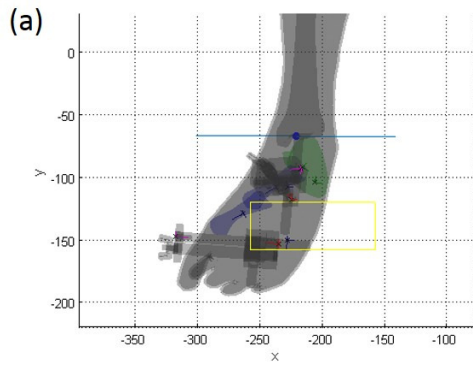
$$\min_{\bar{s}_e, \bar{s}_r, \bar{s}_t} \left(\sum_i ((\text{abs}(\text{footLength}_i - \text{footLength}_{i-1}) - d_{\max})^2) \right) \quad (6)$$

$$\text{footLength}_i = \text{splineLength}_i - \text{splineLength}_0 + s_{e,i} r_{cal} \quad (7)$$

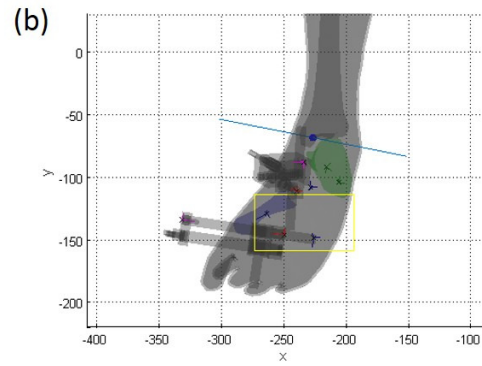
$$\text{splineLength}_i = \|CP_{1,i} - CP_{2,i}\| + \|CP_{2,i} - CP_{3,i}\| + \|CP_{3,i} - CP_{4,i}\| \quad (8)$$

where $\bar{s}_e, \bar{s}_r, \bar{s}_t$ is the distraction schedule for the equinus joint, the revolute trajectory joint and the prismatic trajectory joint, respectively; footLength_i is the cumulative increase in foot length on day i

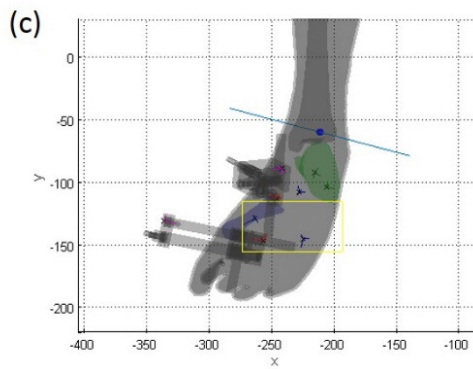
since day 0; $d_{\max} = 2mm$ is the maximum distraction length; $s_{e,i}$ is the equinus joint angle; r_{cal} is the estimated radius of the calcaneus; and $\|CP_{1,i} - CP_{2,i}\|$ is the Euclidean distance between two control points.



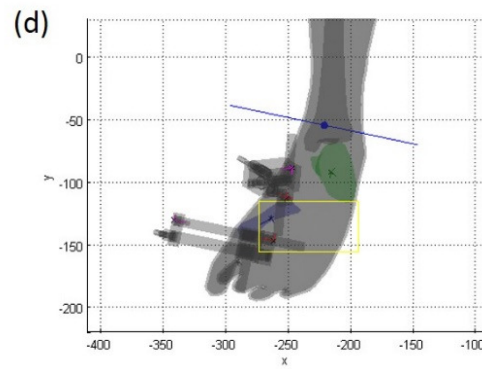
(a) Experiment 1.



(b) Experiment 2.



(a) Experiment 3.



(b) Experiment 4.

Figure 3-15 Computer generated 2DOF external fixator configuration after optimization. Blue line indicates the ankle joint axis. Yellow box indicates the bounding volume for the placement of the revolute trajectory joint.

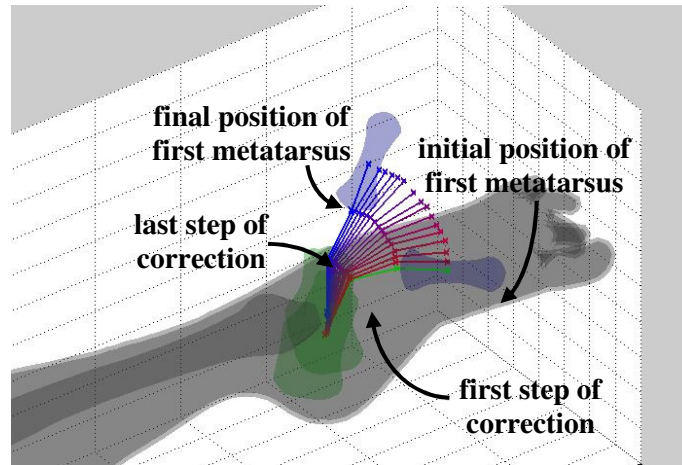


Figure 3-16 Control points for B-spline connecting calcaneus and first metatarsus are plotted for every day of the distraction schedule to visualize the amount of stretch in soft tissues. The first step and last step of the correction are plotted in green and blue respectively.

Table 3-3 Deformity parameters. Negative angle values indicate rotation in the clockwise direction and the rotation axes are positive in the positive z direction.

Expt.	Rotation axis	Rotation point	Rotation angle (deg)	Translation axis	Translation magnitude (mm)	Ankle joint axis	Ankle joint position	Equinus angle (deg)
1	$\begin{bmatrix} -0.364 \\ 0.429 \\ 0.827 \end{bmatrix}$	$\begin{bmatrix} -224.7 \\ -118.2 \\ 239.7 \end{bmatrix}$	52.6	$\begin{bmatrix} -0.996 \\ 0.072 \\ -0.048 \end{bmatrix}$	-36.6	$\begin{bmatrix} 1.000 \\ -0.004 \\ 0.012 \end{bmatrix}$	$\begin{bmatrix} -291.2 \\ -67.4 \\ 148.5 \end{bmatrix}$	-34.4
2	$\begin{bmatrix} -0.460 \\ 0.256 \\ 0.850 \end{bmatrix}$	$\begin{bmatrix} -239.8 \\ -111.9 \\ 241.6 \end{bmatrix}$	56.5	$\begin{bmatrix} -0.982 \\ 0.147 \\ -0.119 \end{bmatrix}$	-24.3	$\begin{bmatrix} 0.941 \\ -0.186 \\ 0.284 \end{bmatrix}$	$\begin{bmatrix} -292.6 \\ -55.9 \\ 129.4 \end{bmatrix}$	-33.9
3	$\begin{bmatrix} -0.545 \\ 0.272 \\ 0.793 \end{bmatrix}$	$\begin{bmatrix} -246.2 \\ -113.5 \\ 239.5 \end{bmatrix}$	59.6	$\begin{bmatrix} -0.960 \\ 0.191 \\ -0.206 \end{bmatrix}$	-28.2	$\begin{bmatrix} 0.899 \\ -0.236 \\ 0.370 \end{bmatrix}$	$\begin{bmatrix} -274.6 \\ -44.0 \\ 118.2 \end{bmatrix}$	-28.1
4	$\begin{bmatrix} -0.527 \\ 0.305 \\ 0.793 \end{bmatrix}$	$\begin{bmatrix} -251.3 \\ -113.3 \\ 249.6 \end{bmatrix}$	58.3	$\begin{bmatrix} -0.957 \\ 0.197 \\ -0.211 \end{bmatrix}$	-33.2	$\begin{bmatrix} 0.935 \\ -0.196 \\ 0.297 \end{bmatrix}$	$\begin{bmatrix} -286.4 \\ -41.3 \\ 120.9 \end{bmatrix}$	-28.0

Figure 3-16 shows the control points of the B-spline for each day of the correction. The B-splines appear to change gradually and smoothly. The results of the optimization for experiments 1-4 are given in **Figure 3-17**, **Figure 3-18**, **Figure 3-19** and **Figure 3-20**, respectively. The optimizer was able to find a smooth and gradual distraction path for the correction, as visualized in the plot of control points in part (a) of the figures. Part (b) shows that fairly constant distraction rates below the target of 2 mm/day were achieved for all experiments. The actual joint values are plotted in part (c) and they increase very gradually. Part (d) shows that the increments in joint values are indeed maintained within a narrow range. The gradual joint adjustments explain the gradual distraction path.

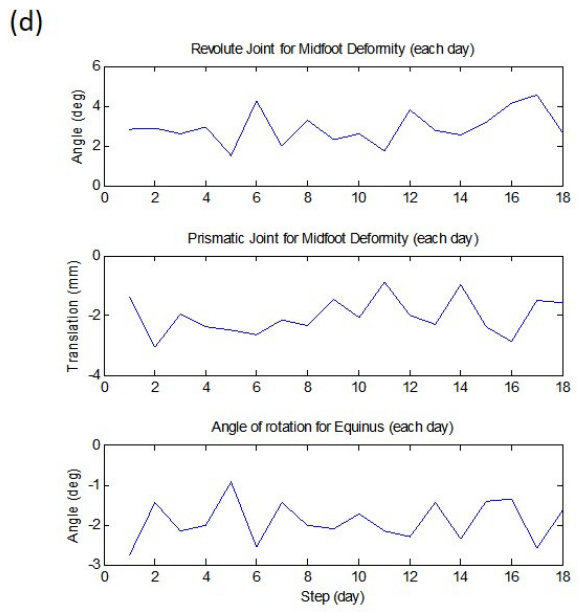
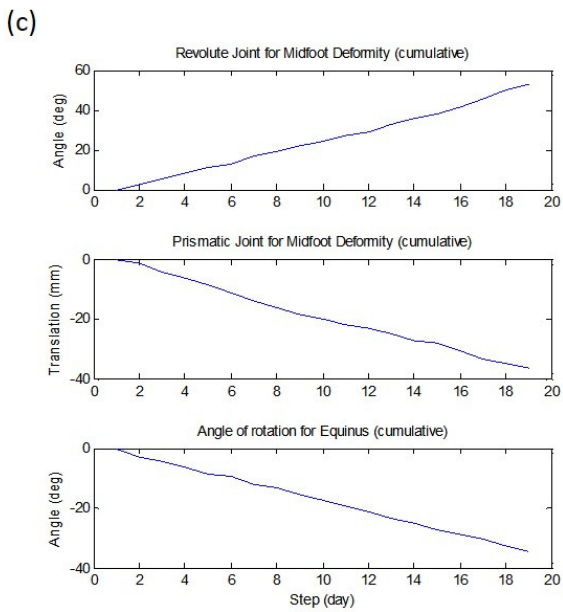
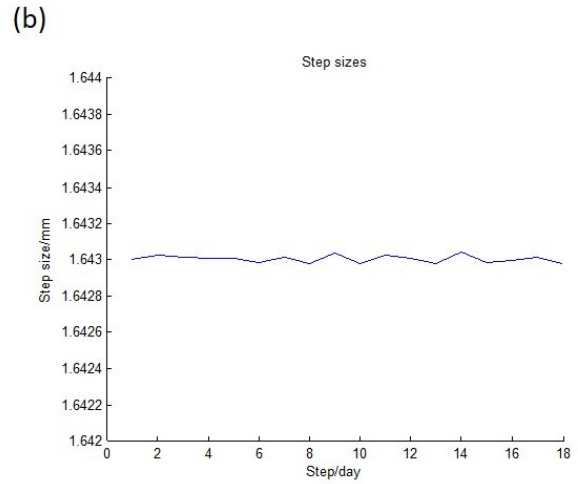
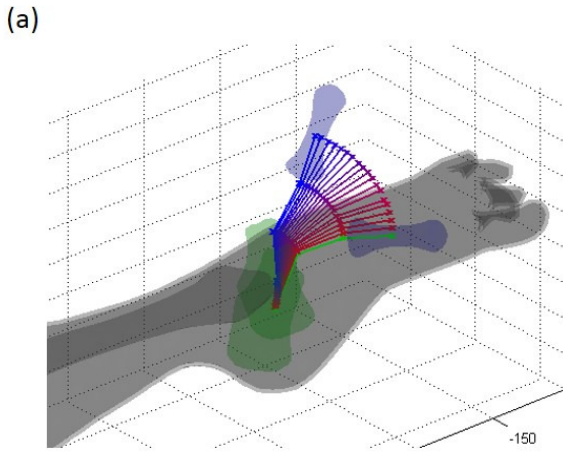
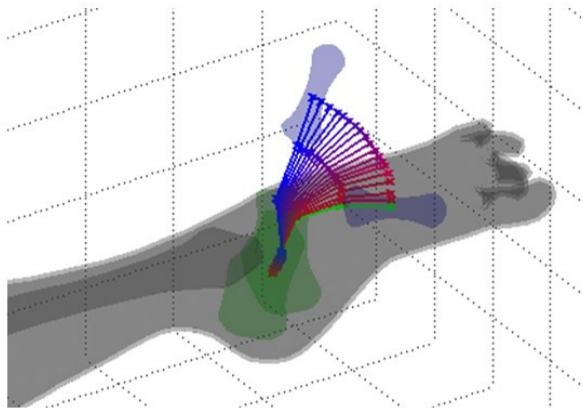


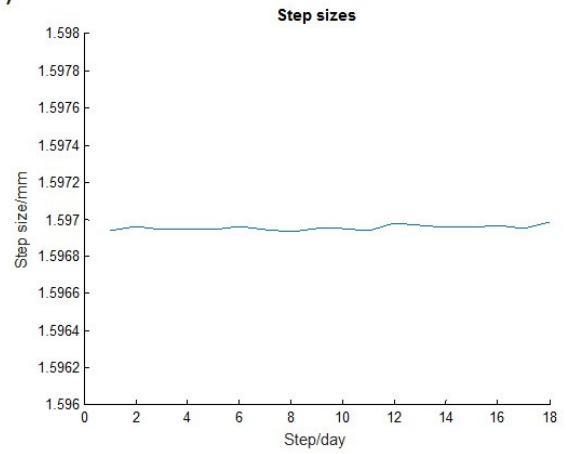
Figure 3-17 Results of distraction schedule optimization in experiment 1.

(a)



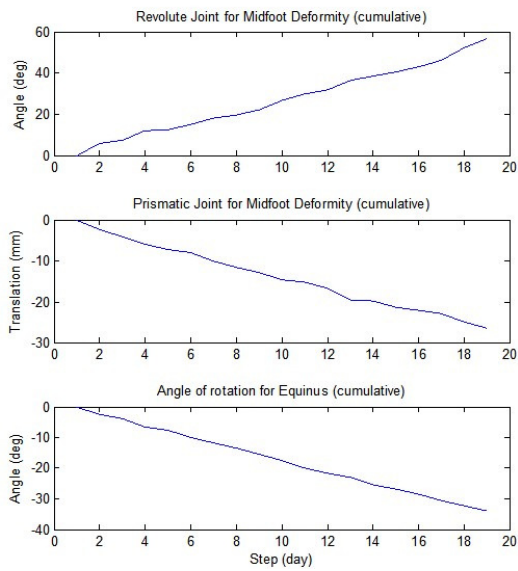
(a) Control points of B-spline.

(b)



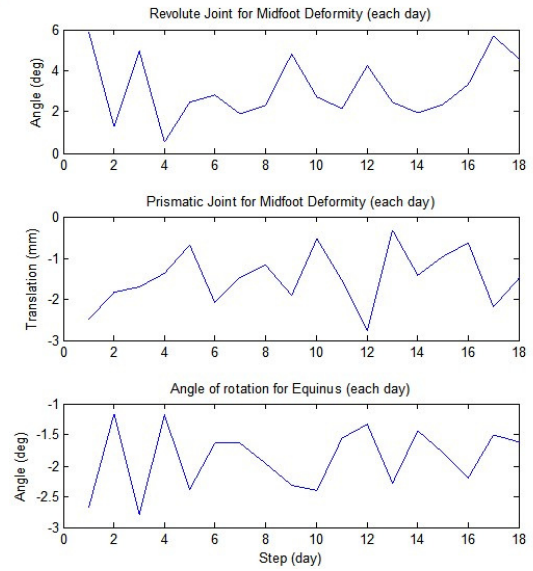
(b) Distraction length per day of correction.

(c)



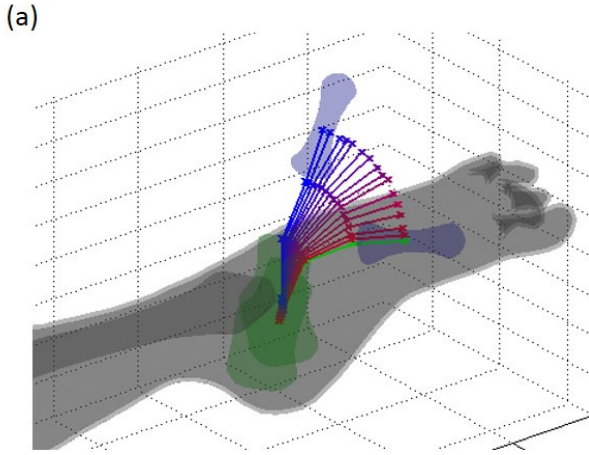
(c) Schedule of joint values.

(d)

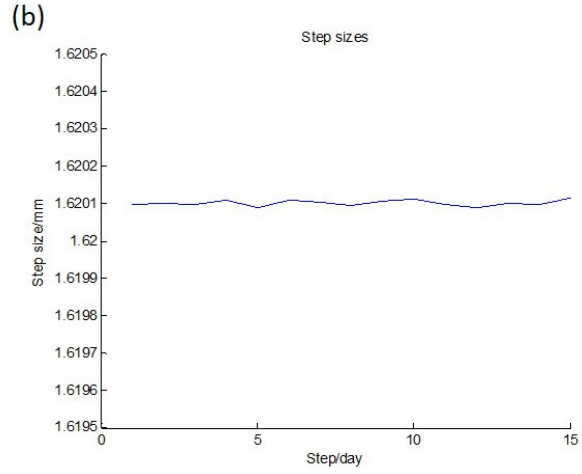


(d) Schedule of joint increment every day.

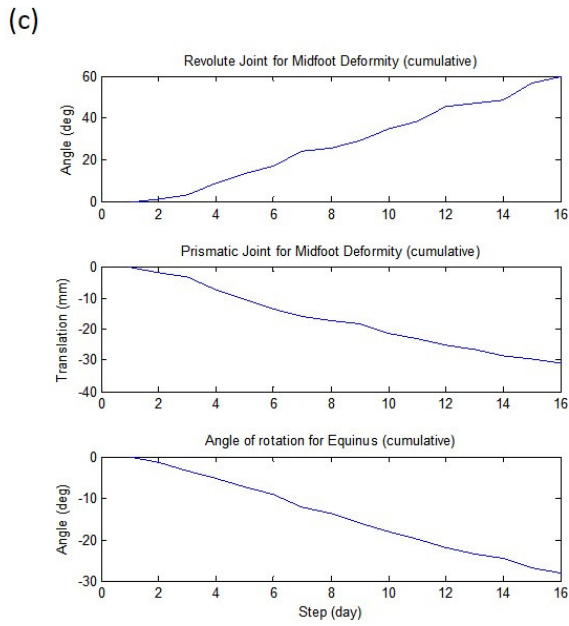
Figure 3-18 Results of distraction schedule optimization in experiment 2.



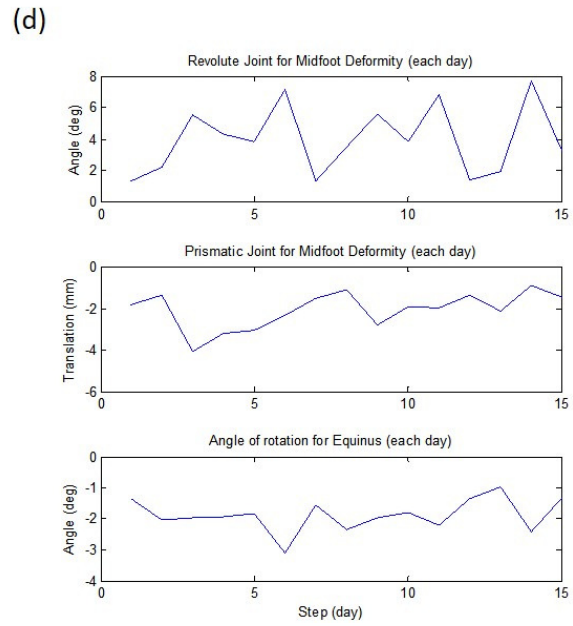
(a) Control points of B-spline.



(b) Distraction length per day of correction.

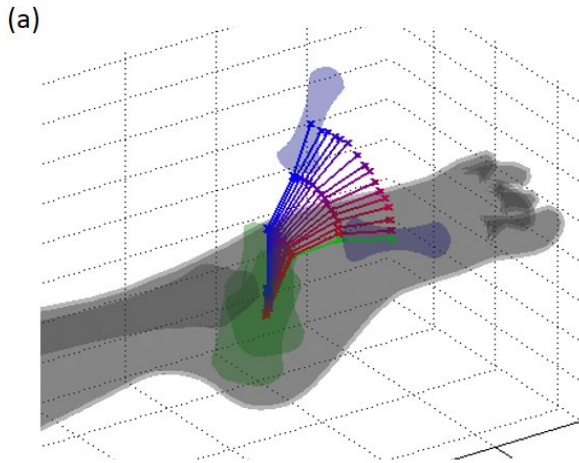


(c) Schedule of joint values.

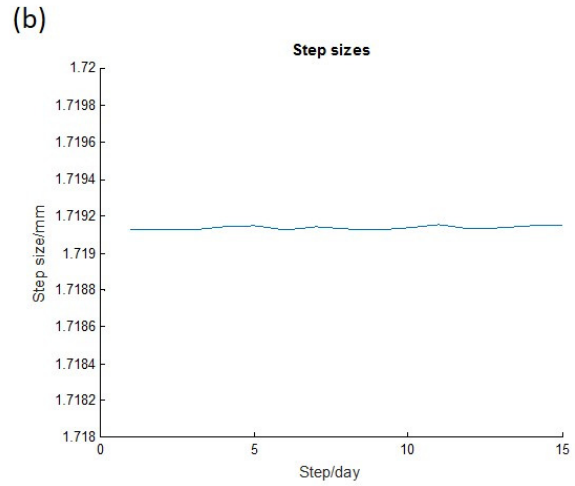


(d) Schedule of joint increment every day.

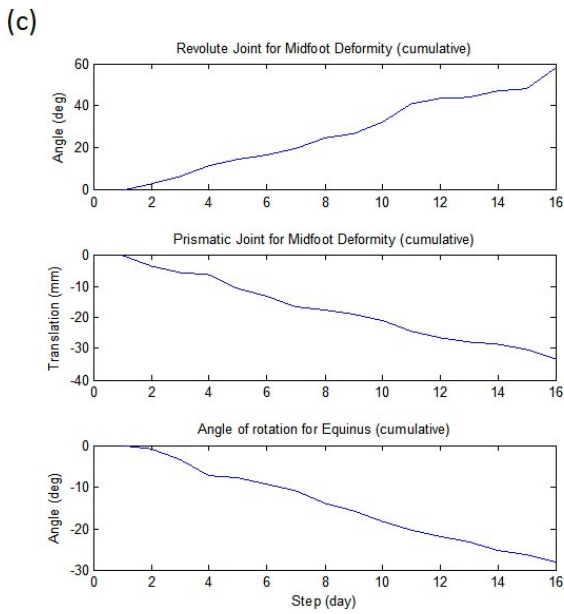
Figure 3-19 Results of distraction schedule optimization in experiment 3.



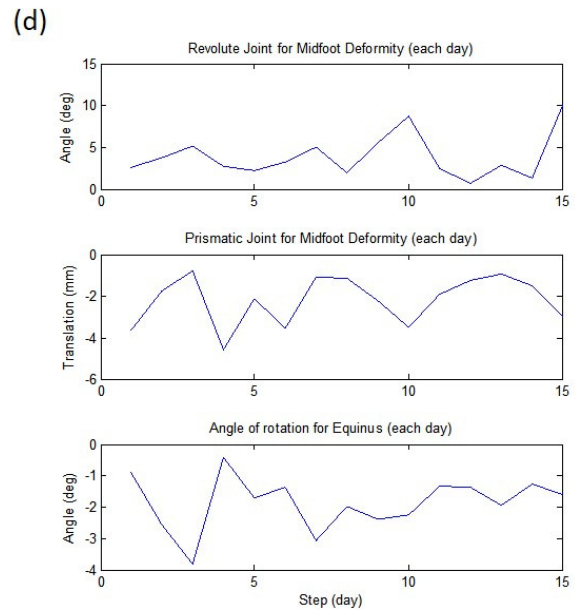
(a) Control points of B-spline.



(b) Distraction length per day of correction.



(c) Schedule of joint values.



(d) Schedule of joint increment every day.

Figure 3-20 Results of distraction schedule optimization in experiment 4.

3.11 Conclusion

This chapter introduced the clubfoot deformity correction as a 6DOF rigid body transformation. External fixation is indicated only for the correction of relapsed or neglected clubfoot in children older who have sufficient calcification of the skeleton to support the external fixator.

This chapter detailed the application of the proposed 2DOF approach on clubfoot correction. Firstly, clubfoot correction was simplified as a combination of equinus at the heel and midfoot deformity. 6DOF midfoot deformity correction was then reduced to 2DOF using axis-angle representation. A 2DOF external fixator specifically designed for clubfoot correction was described.

A method was developed and described to optimize the external fixator configuration to achieve the most compact fixator configuration while constraining the main bulk of the fixator to an area above and in front of the foot. For the optimal fixator configuration, the distraction schedule was optimized to achieve soft tissue stretching of 2 mm/day, which reduces the risk of soft tissue damage. Both optimizations were applied to an anonymized patient data and the result was a compact 2DOF external fixator and an average stretch of 1.6 mm/day.

Chapter 4. Passive Positioning Linkage

The passive positioning linkage is a non-actuated arm developed to assist surgeons in achieving precision in deformity correction using external fixation. It functions as both a positioning device to improve the accuracy of device configuration and a digitizer to capture deformity data, as well as to perform registration. Given there are no active actuators, the risk to patients is minimal and the relevant regulations will be less stringent.

In this chapter, the passive positioning linkage is described as: (1) a surgical assistive device to assist the surgeon in achieving accuracy in the fixator configuration; and (2) a digitizer to perform registration between the system and the patient during surgery. Several iterations of the linkage were made and a control system was designed with several different control strategies to improve its accuracy.

4.1 Positioning Device

The main function of this passive positioning linkage is to assist the surgeon in building the external fixator during surgery.⁷⁶ The trajectory joints attach to the end effector of this passive positioning linkage. Given a target end effector pose, the surgical planner calculates the inverse kinematics and the joint angle of each joint to bring the end effector into its target pose.

In the default state, all of its joints are loose so that the surgeon can easily manipulate it. At their target joint angles, the joints stiffen to hold their position. With a few easy maneuvers, all joints reach their target joint values so that the end effector is held rigidly at the calculated pose. This enables the surgeon to then attach the trajectory joints to the rest of the external fixator. To perform this function, each joint of the linkage has two main components: (1) a brake to hold the joint position; and (2) an angular encoder to measure joint value.

The brake in all prototypes is an electromagnetic brake. It is a flange mounted power-on brake (S90BF9-11A04, Designatronics Inc., NY, U.S.A.) that can be powered on in 5 ms. It has a static torque of 5 lbin with 5 W of power at 24 V DC, which is later found to be too low. Thus, it will be replaced in future.

Each joint measures its angular position using an optical encoder. The optical encoder is chosen over smaller magnetic encoder because the optical encoder is very stable and will not be affected by the magnetic field generated by the electromagnet. A miniaturized rotary optical encoder (E4P, US Digital, Washington, U.S.A.) was used in all prototypes. It makes 300 quadrature counts in a full revolution, giving a resolution of 1.2 deg/count.

4.2 Digitizer

During surgery, the surgical system has to locate the patient to ensure its accuracy as a positioning device. Since the linkage has embedded angular encoders, each joint can easily send its current joint value to the surgical planner, which in turn applies forward kinematics to calculate its end effector position. By attaching a pointed end effector to the linkage and probing bony features, a 3D point cloud is created and it is then matched to the 3D model of the patient. This effectively locates the patient in the coordinate system of the passive positioning linkage.

4.3 Specifications

The requirements for the passive positioning linkage as a positioning device and a registration tool is tabulate in **Table 4-1** and **Table 4-2**.

Table 4-1 Must-have specifications, in order of importance.

No.	Specifications	Description/ explanation
1	≥ 7 DOF	Linkage has to have at least 6DOF to reach all positions and orientations in 3D space within a workspace. Having at least one redundant DOF gives it more flexibility to reach an end effector pose.

2	±0.2 deg accuracy for each joint	Accuracy of joint angle is estimated to give an error of below 5 mm.
3	Diameter of <2in	Linkage should be compact so that it does not obstruct the surgeon's view.
4	Minimal joint resistance when brake is not activated	Minimal joint resistance enables minimal effort by the surgeon to maneuver the joint to the target joint value. Surgeon should only need to make a few smooth maneuvers.
5	Able to hold its own weight	Linkage should hold its own weight with all joints extended to horizontal.
6	Able to resist loading of 2 lbs at end effector	Surgeons may bump into or exert forces on the end effector when they are trying to connect the component to the rest of the external fixator. 2 lbs is an estimate of this impact force.
7	Modular design	Modularity enables us to extend or shorten the linkage as necessary.
8	Easy release and engage mechanism on end effector	The mechanism holding the trajectory joint to the end effector should release and engage easily to ensure a good user experience and to avoid any iatrogenic injuries.

Table 4-2 Good-to-have specifications, in order of importance.

No.	Specifications	Description/ explanation
1	Indicator of target joint value	Visual/tactile/sonar indication of which direction the joint should be rotated to reach target joint value.
2	Sleek and minimal design	Reduce confusion for surgeons.

4.4 Prototypes

To achieve the specifications for this linkage, a brake and an encoder at each joint is needed as shown in **Figure 4-1**. Four prototypes were made in total and all of them were designed to have the same repeating unit making up the linkage.

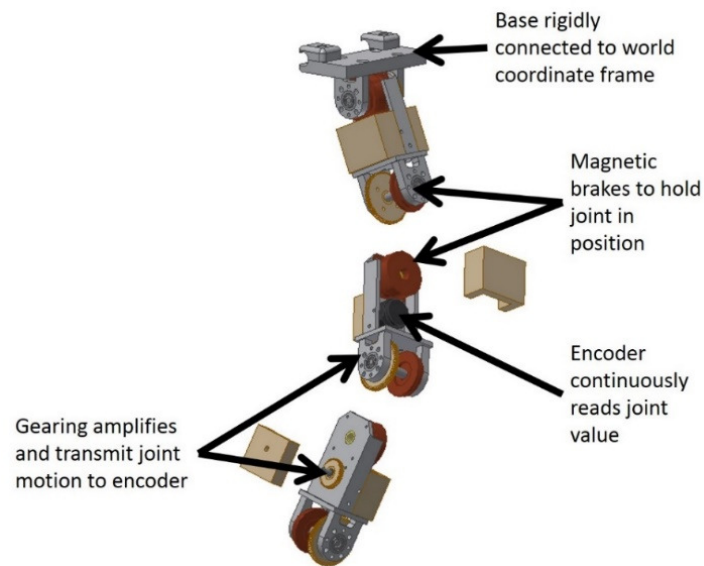


Figure 4-1 Basic elements of passive positioning linkage.

Design iterations are described in detail in Appendix B. In all design iterations, a gear train of 2:1 ratio was used to achieve an encoder resolution of 0.56 deg/count, and the same electromagnetic brake was used to generate the braking force. Through the iterations, the manufacturability of the prototypes were improved and the materials were selected to give greater rigidity to the structure. Anti-backlash gears were used to improve the accuracy of the linkage.

After four iterations, it was concluded that an electromagnetic brake is not powerful enough for this application. It was observed that the magnet does not have sufficient torque to hold its own weight at full horizontal extension. If a larger brake was used, the linkage becomes too bulky. When a gear train was used to amplify the stopping torque, the backdrive torque became so high that the joint was very stiff. The

alignment precision was also crucial if high gearing ratio was used. Hence, none of the prototypes were fully functional and new methods of braking are being investigated as further work.

4.5 End Effector

Besides the seven joints providing the 7DOF, the linkage also requires an end effector to hold on to the trajectory joints. A design that incorporates spring plungers is shown in **Figure 4-2**. The two spring plungers align to matching holes in the component while the bolt tightens to secure the connection. A wingnut makes it very easy to attach or release the trajectory joint.

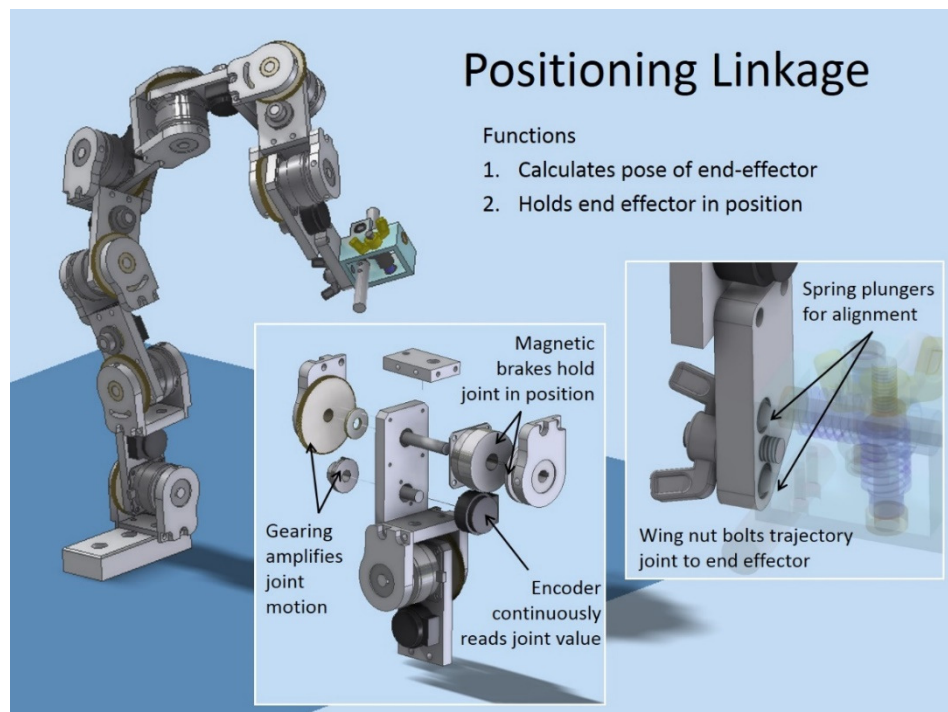


Figure 4-2 CAD model of full passive positioning linkage with revolute trajectory joint attached to its end effector.

4.6 Controller

To ensure that the joint stops within 0.2 deg of the target joint value, a controller was developed on Arduino Micro to control the activation of the electromagnetic brakes. Three units of the second prototype were tested and the units were linked in series, with each unit connected to a controller. The 3-unit linkage and the controllers are shown in **Figure 4-3**. Target angles were manually given to or coded in the controllers. The controller then calculates the voltage to supply to the electromagnet. The goal was to develop a controller and interface that intuitively guide the user towards the target joint value and achieve accuracy in the maneuvering.

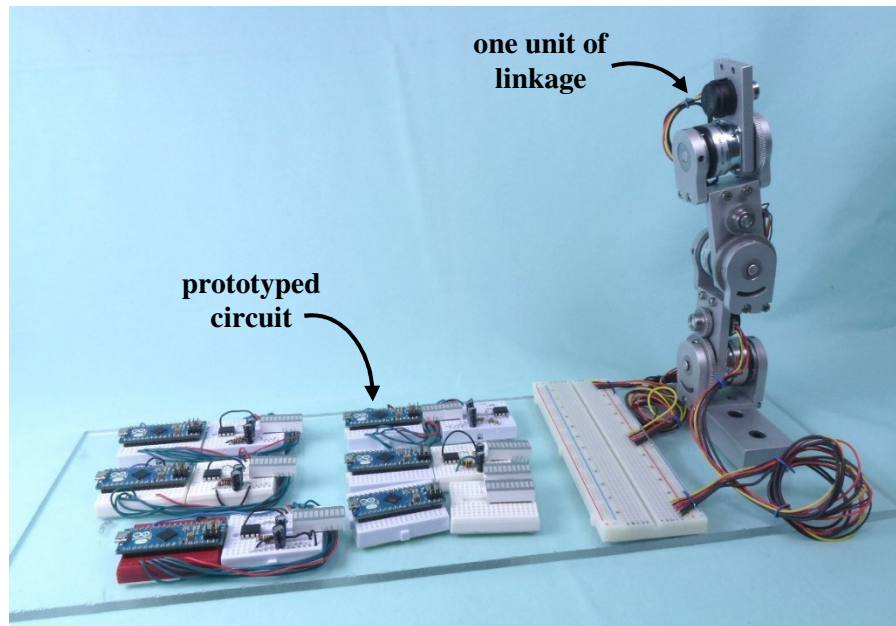


Figure 4-3 Photo of 3-unit linkage and control circuits on Arduino Micro.

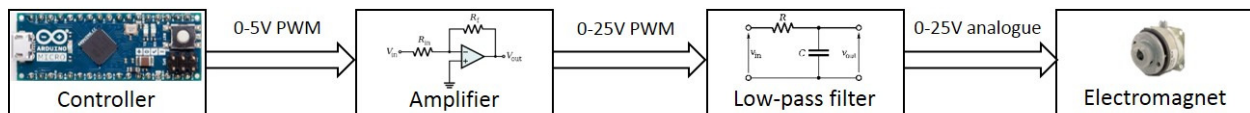


Figure 4-4 Block diagram of main steps in getting output signal from controller to electromagnet.

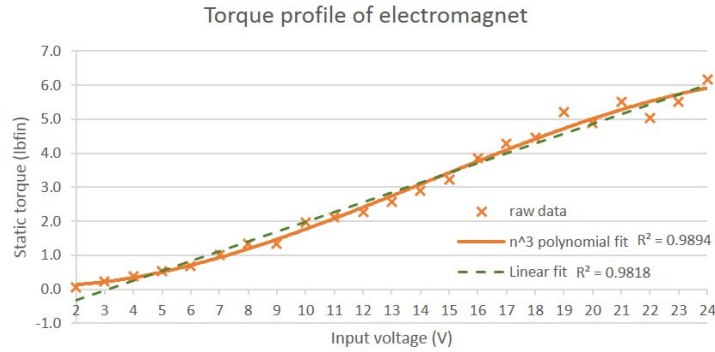


Figure 4-5 Profile of torque output vs input voltage of the electromagnet.

In general, the higher the voltage supplied to the electromagnet, the greater the holding power and the resistance to joint motion. A simplified block diagram of the control circuit is shown in **Figure 4-4**. As the Arduino Micro can only output a maximum of 5 V via its pins, the signal was amplified from 5 V to 25 V to power the 25 V electromagnet. In addition, the Arduino Micro cannot generate true analogue signals. A low-pass filter was used to convert the pulse-width modulation (PWM) generated by the Arduino Micro into a smooth pseudo-analogue signal.

The torque profile of the electromagnetic brake was measured to get a better control model of the linkage. The input voltage to the magnet was varied and the amount of static torque that it can resist before slipping was measured. The results are plotted in **Figure 4-5**. The R-squared value of a linear model is 0.9818 while that of an n^3 polynomial model is 0.9894. The difference between the two models is very small and therefore, the output torque was assumed to be linearly proportional to the input voltage.

4.6.1 Static Braking Profile

The initial controller featured static braking profile types to control the braking force. **Figure 4-6** shows the plots of profiles that were tested. The normal profile is a generic Gaussian curve that gives a gradually increasing resistance to joint motion as the joint approaches its target angle, while the step profile

gives a stepped increase in resistance. The ramp profile has a sudden drop in resistance to mimic the tactile feedback given by a physical snap-fit mechanism.

During joint movement, an indicator light turns on to indicate where the current joint position is relative to the target value. A close-up photo of the indicator LED lights is shown in **Figure 4-7**.

A user study was performed to investigate if the time taken to get to the target angle changes with the profile type. In this study, a LabJack (LabJack T7 Pro, LabJack Corporation, Lakewood, CO, U.S.A.) was used instead of an Arduino Micro, but the controller program is exactly the same. A single unit of the linkage was modified to include a handle as shown in **Figure 4-8** so that the results will not be biased by variations in users' grip. The study was performed with 18 users, one of whom is pictured in **Figure 4-9** during a trial. Although a study with 18 users is not enough to provide statistical significance, it enables us to do a pilot or preliminary study to decide if any of the static braking profile is better than the others. These users were undergraduate and graduate students from the Mechanical Engineering Department. Each user went through three experiments, and each experiment consisted of a randomized order of trials with different parameter sets of one profile type. Thus, every parameter set in each profile was repeated three times. There were 14 different profile parameter sets for the normal and ramp profiles, and 15 different parameter sets for the step profile. Parameter sets include parameters affecting the shape of the profile type and also four different target joint values of 25 deg, 45 deg, 90 deg and 135 deg.

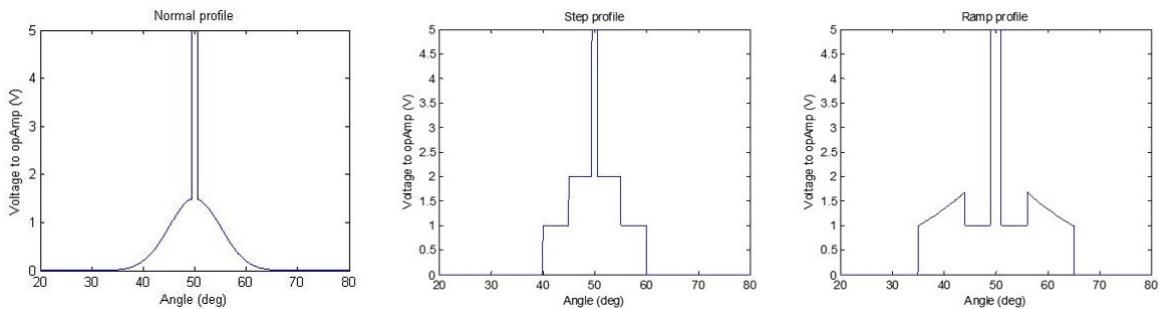


Figure 4-6 Braking profile types to control activation of brake of each joint. Target angle is set at 50 deg.

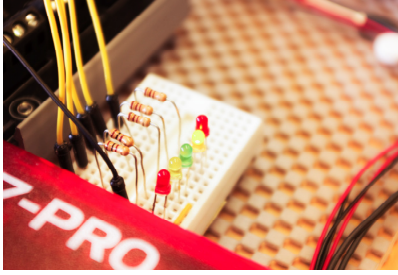


Figure 4-7 LED lights to indicate where the current joint value is relative to the target value. Red: joint value is very far out. Yellow: joint value is closing in on target value. Green: joint value is within accuracy limits of target.

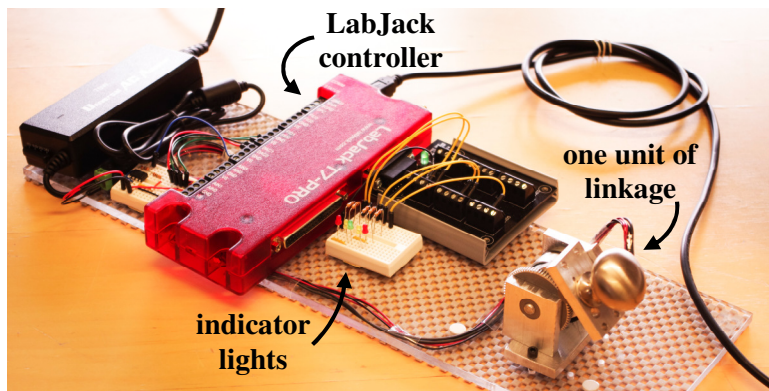


Figure 4-8 Setup of single unit of linkage and indicator lights during user study.

The linkage unit started at the home position and the user had to rotate it to the target joint value with the help of the indicator lights (visual cue) and joint resistance (tactile feedback). After each trial, users had to return the linkage unit to the home position before beginning the next trial. Time taken for each trial was started when the linkage unit was at the home position and stopped when it was at target joint value. After each experiment, the user was offered the option to take a break before continuing.

The user was instructed on how to interpret the indicator lights and allowed to complete as many example runs as needed to familiarize themselves with the setup. Users were informed of how time was taken and encouraged to complete the trials as fast as they could. They were also given a chocolate at the end of their session as a token of appreciation.

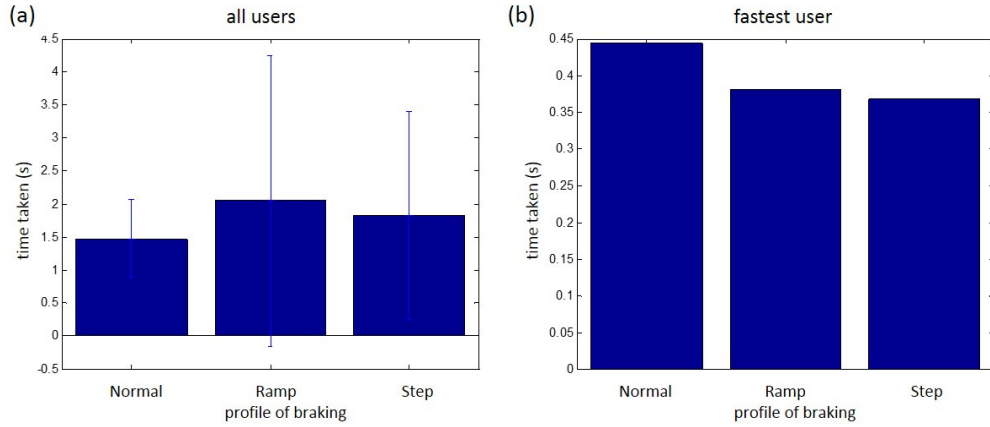


Figure 4-9 Photo of a user during the user study.

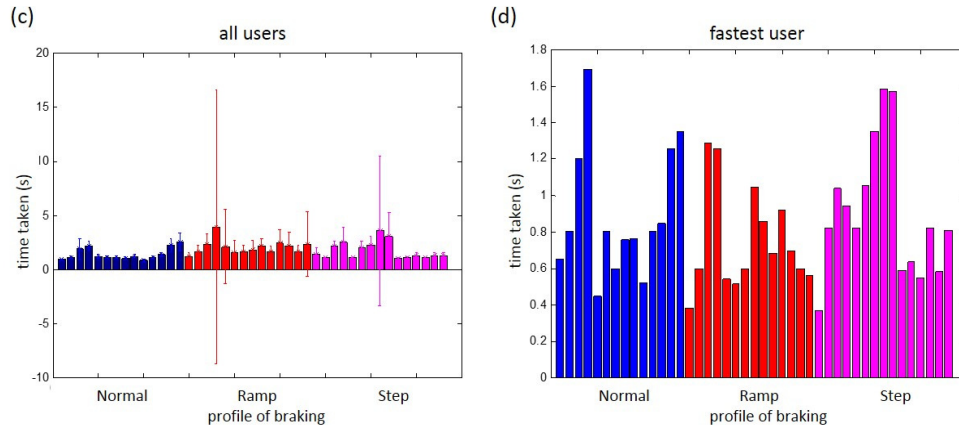
The results show little advantage of one profile over the other. In addition, parameter changes within each profile had little effect, but the target angle significantly affects the performance within a profile type. The average time taken across all parameter sets of each profile type is plotted in **Figure 4-10(a)** and the fastest time recorded within each profile type is plotted in **Figure 4-10(b)**. Separating the results of each parameter set of the profile types, the average time and fastest time for each is plotted in **Figure 4-10(c,d)**.

Large variations of 2 s (one standard deviation) in the time taken for each trial indicated to us that static profiles may have to be tuned for the individual user. While it is purported that static profiles were unable to react fast enough to high rotation speeds that was observed in many trials, it is not possible to determine if this is the main factor as the rotation speed was not recorded during each trial.

Given the large time variations and that none of the profiles conferred an obvious advantage over the others, it was concluded that static braking profiles may be inadequate to capture the joint rotation trajectories of the majority of the users. Therefore, dynamic braking profiles were explored as a more adaptive alternative to static braking profiles.



(a) Average time across all parameter sets of each profile type. (b) Fastest time across all parameter sets of each profile type.



(a) Average time for each parameter sets of each profile type. (b) Fastest time for each parameter sets of each profile type.

Figure 4-10 Results of user study on static braking profiles. None of the profiles gave a significantly improved results.

4.6.2 Dynamic Braking Profile

As static profiles proved inadequate, the system was modified to use dynamic profiles that predict the joint trajectory from a recent history of joint speed. The first choice of a predictive algorithm is the Kalman filter as it is very easy to implement and is computationally efficient. This dynamic profile was implemented on the Arduino Micro.

The Kalman filter was applied to the joint trajectory to predict the joint angle, joint angular velocity and joint angular acceleration. The state model is defined as

$$\bar{x} = \begin{bmatrix} \theta \\ \dot{\theta} \\ \ddot{\theta} \end{bmatrix} \quad (9)$$

where θ is the joint angle.

The variable θ was the only measured variable during the trials. The observation noise was estimated as $\sigma_{observation} = 1$ with covariance of $R = \sigma_{observation}^2 = 1$, and the process noise in the model was estimated as $\sigma_{process} = 0.01$ with a covariance of $Q = GG^T\sigma_{process}^2$ where $G = \left[\frac{dt^3}{6} \quad \frac{dt^2}{2} \quad dt \right]^T$.

The transition model is defined as

$$F = \begin{bmatrix} 1 & dt & \frac{dt^2}{2} \\ 0 & 1 & dt \\ 0 & 0 & 1 \end{bmatrix} \quad (10)$$

where $dt = 3 \text{ ms}$ is the time step for each prediction.

Besides predicting and updating the current angle at the sampling rate of 3 ms, it is also necessary to predict the stopping angle 12 ms ahead. Any braking mechanism will have an inherent activation delay time between receiving the activation signal to achieving full braking power. Part of that delay is due to the powering up of the electromagnet. The controller also takes time perform its calculation before it decides if it should activate the brake. The total activation delay was measured empirically to be 12 ms.

To predict 12 ms ahead, a new prediction step was added to the original Kalman filter to predict the stopping angle. **Figure 4-11** shows the schematic of the Kalman filter with an additional prediction step. The stopping angle is simply predicted using a similar state transition model with $dt = 12 \text{ ms}$.

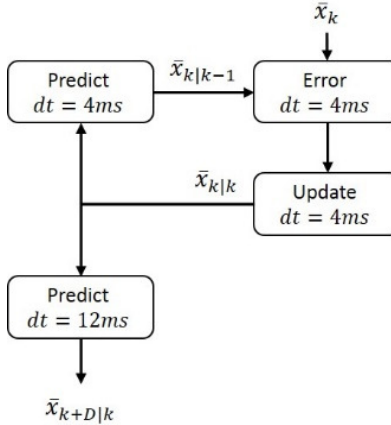


Figure 4-11 Schematic of Kalman filter with additional predict step to estimate the stopping angle. k indicates the current time step and D indicates the activation delay of 12 ms.

Another modified version of the Kalman filter was also developed. This version has an addition loop for predicting and updating the stopping angle. **Figure 4-12** shows the schematic of the modified Kalman filter. It is very similar to the original Kalman except the error term is the error in prediction 12 ms ago. It uses the history of errors to update its current prediction of the stopping angle 12 ms into the future.

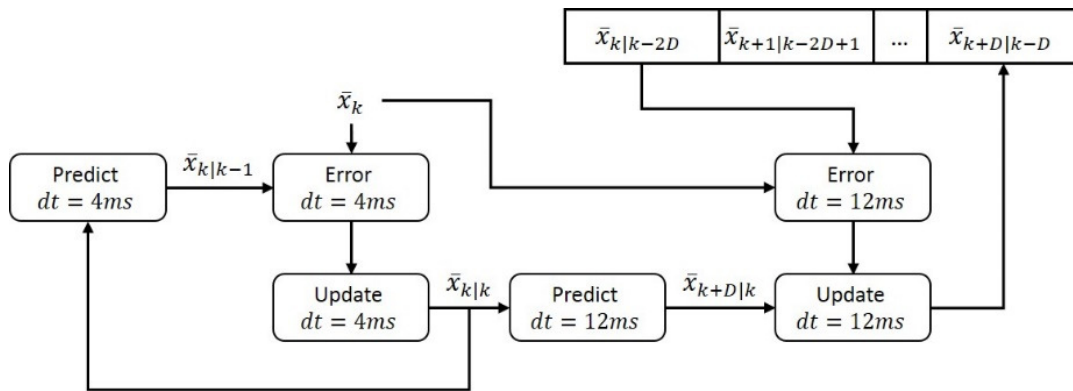


Figure 4-12 Schematic of modified Kalman filter, which predict and update of current angle and stopping angle. k indicates the current time step and D indicates the activation delay of 12 ms. A history of prediction of stopping angle is maintained to calculate the error term for $dt = 12$ ms.

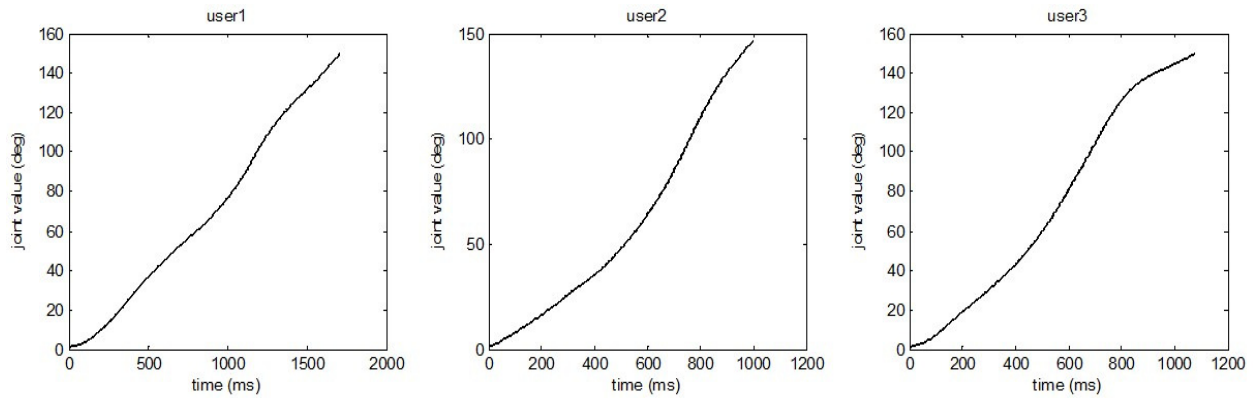


Figure 4-13 Joint trajectory for each user.

The angle trajectory of three users was recorded and applied with the different versions of Kalman filter. None of them gave enough accuracy. The joint trajectory for each user is plotted in **Figure 4-13**. The three experiments are (1) control experiment with no prediction and brake is activated at target joint value; (2) Kalman filter with just a predict step for estimating stopping joint value; and (3) modified Kalman filter with predict and update steps for estimating stopping joint value. The results are plotted in **Figure 4-14**.

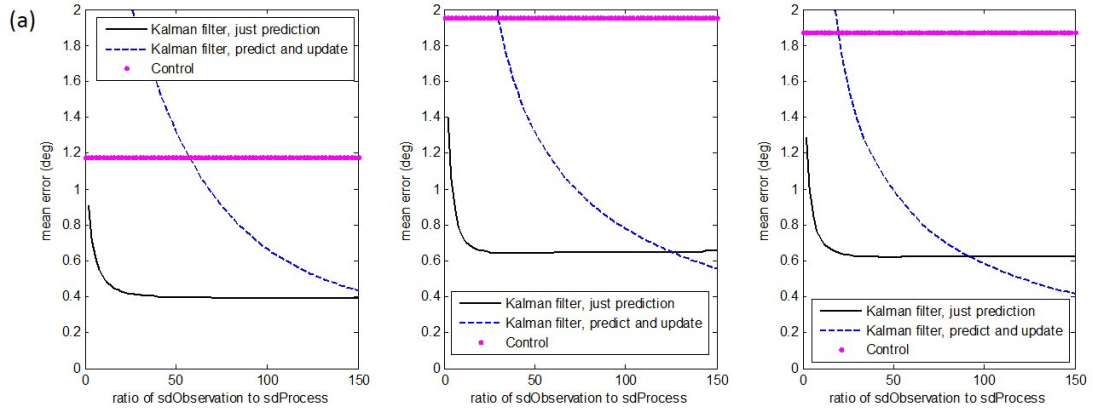
Considering mean and max error over the trajectory, the Kalman filters performed better than the control for a $\sigma_{observation}$ value that is much higher than $\sigma_{process}$. In addition, the Kalman filter performed better than the modified version at low ratios. Considering modal error, the Kalman filters perform much better than the control. The target accuracy of 0.2 deg was met only when the modal error is considered. Taken together, these results may indicate that the joint trajectory changes very quickly so the measured data has a lot of variance and does not follow the model. Further fine tuning may be necessary.

4.7 Current Status and Further Work

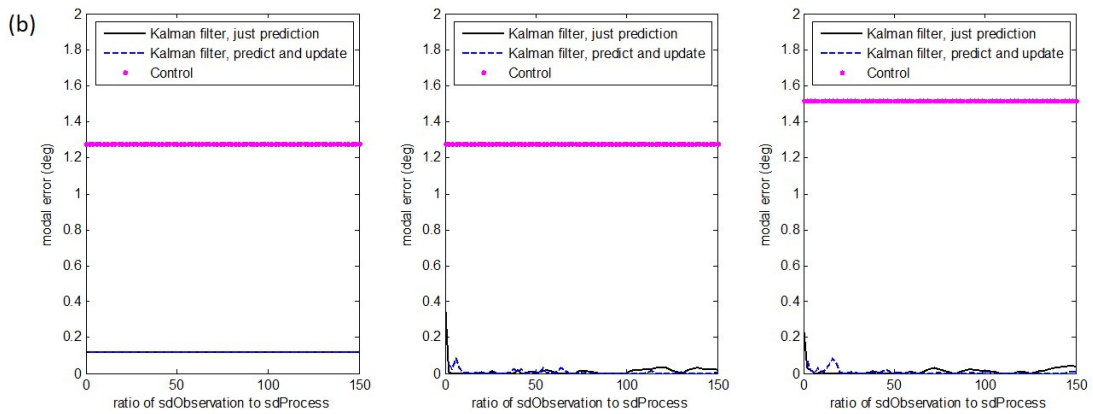
The use of more complex gears with higher gear ratios, such as harmonic gears, was briefly explored. However, for the gear ratio needed, the backdrive torque is so high that the user has to manipulate each joint individually. Thus, increasing the gear ratio does not seem to be the right direction. The current

approach is to apply different types of braking mechanisms such as pneumatic brakes to achieve higher braking force while maintaining a small form factor.

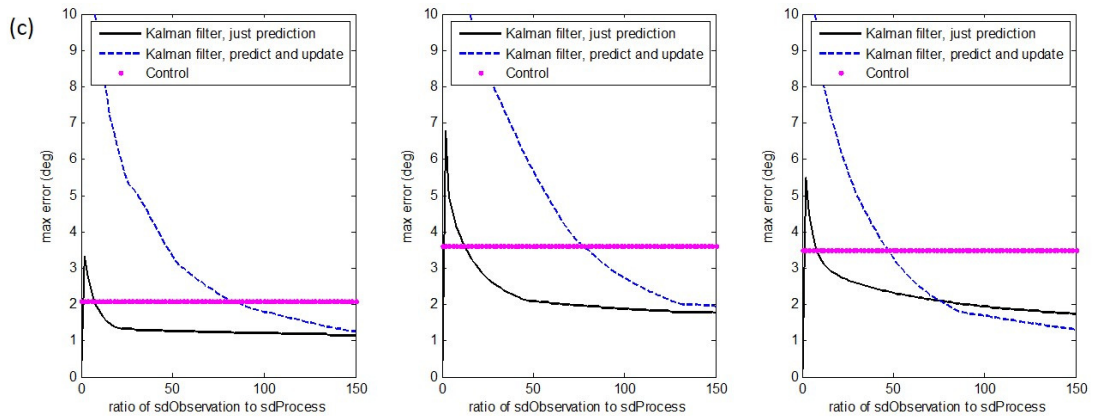
At the same time, dynamic braking profiles are explored. Dynamic braking profiles predict the joint trajectory to improve accuracy or user interaction. There are still many other filters or predictive methods that may work better than the Kalman filter. More work is needed to explore and develop alternative dynamic braking profiles.



(a) Mean error over entire trajectory.



(b) Modal error over entire trajectory.



(a) Max error over entire trajectory.

Figure 4-14 Results of Kalman filters applied to three user data. Each plot in a row shows the results a user data.

Chapter 5. Flexible Clubfoot Model

For this thesis, a realistic articulated model was needed to demonstrate the external fixation process of clubfoot correction and to measure the correction accuracy. This model must have a rigid skeletal structure to support the insertion of bone pins and/or k-wires, and a soft tissue layer to demonstrate the change in foot shape. Cadavers are not ideal as they are expensive and require specialized handling and storage facilities. In contrast, a synthetic model is cheaper and more convenient to work with. It is also culturally more acceptable to have the proposed 2DOF external fixator on a synthetic model, as opposed to a cadaver, for demonstrations.

This chapter describes some of the current models available and the new phantom model developed as part of this thesis work. The phantom model is a patient-specific clubfoot model that is intended to demonstrate the correction of clubfoot using the proposed 2DOF external fixator. It has the unique composition of rigid skeletal structure embedded in a synthetic soft tissue layer that mimics human muscles. Further application of this model to other areas such as medical education is discussed later.

5.1 Current Models

Current clubfoot models in the market are either made up of just rubber or rigid bone models. MD Orthopedics (MD Orthopedics, Inc., Wayland, IA, U.S.A.) develops infant clubfoot models that are specifically for teaching the Ponseti method⁶⁰, a multistep manipulation and casting method for treating clubfoot in infants. One of the models is a series of rubber models of infant clubfoot at various stages of correction, which enables clinicians to practice their casting technique. Another is an articulated and scaled-up skeletal model for clinicians to learn the relationship between foot bones in a clubfoot and to better understand the principles and nuances of the Ponseti method. Lastly, a tenotomy model of the ankle is available with a section or the skin flap removed to show the underlying Achilles tendon, nerves and vasculature for the teaching of heel cord tenotomy. None of these models simulates realistic tactile feedback for the procedure as they only mimic one part of the anatomy (skin or skeleton) and not the full composition.

5.2 Phantom Model

Must-have specifications are qualities of the model that are essential to the function of the clubfoot model for demonstrating our proposed 2DOF external fixator, and these are listed in **Table 5-1**. The good-to-have specifications that improve the function of the model are listed in **Table 5-2**.

Table 5-1 Must-have specifications, in order of importance.

No.	Specifications	Description/ explanation
1	Strong and rigid skeletal structure	Skeletal structure must support bony operations such as bone pin insertion and osteotomy.
2	Articulated joints	Joints have to be articulated to demonstrate clubfoot correction.
3	Elastic outer layer	Outer layer has to be elastic to accommodate the stretching during correction without tearing or permanently deforming.
4	Actual scale	Foot model has to be true to scale so that commercially available components can be used without modifications.
5	Low cost manufacturing	A foot model should cost below \$500.
6	Patient specificity	Foot model should be made based on patient's CT data.

Table 5-2 Good-to-have specifications, in order of importance.

No.	Specifications	Description/ explanation
1	Transparent outer layer	Transparent outer layer shows how internal bone structure shifts during correction.
2	Automated or semi-automated manufacturing process	Process should require minimal number of skilled manpower hours to make a model, especially when duplicating a model.
3	Fast manufacturing process	Process should take less than a week for a model.

4	Generic manufacturing that applies to conditions beyond clubfoot	Would be good if method of modeling can be generalized to other conditions or body parts to cater to other teaching or simulation needs in medical field.
5	Manufacturing process does not require special equipment	Preferable that manufacturing does not involve any hazardous materials that require special handling or storage.

A new patient-specific model for clubfoot was developed. This new model has both the rigid skeletal structure and a flexible layer covering the skeleton. A photo of this model is shown in **Figure 5-1**. The procedure of making the model is described in greater detail in this paper⁷⁸ and will not be repeated in this thesis. Briefly, the skeletal structure was segmented from patient CT data and 3D printed. The skeletal structure was printed using the 3D printing service (Selective Laser Sintering technique) provided by Shapeways (Shapeways, Inc., New York, NY, U.S.A.) in a polyamide material labelled as White, Strong and Flexible plastic. A plaster mold was created to cast ballistic gel over the skeleton. The ballistic gel (Clear Ballistics, Fort Smith, AR, U.S.A.) is a 10% synthetic non-fouling gel. It is designed to mimic the density and viscosity of human muscle tissue¹⁰ and is thus an excellent choice for modelling the soft tissue.

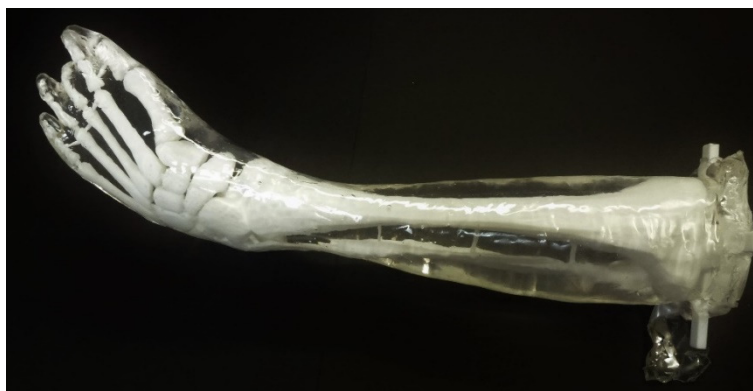


Figure 5-1 Photo of foot phantom model⁷⁸ with rigid 3D printed skeletal structure surrounded by elastic ballistic gel.

The 3D printed skeletal structure and the elastic outer layer combine to create an articulated and elastic model that can support an external fixator and demonstrate the correction process. The entire skeletal structure was initially printed as a single piece with links holding each bone in position relative to each other. After casting the gel layer, these links were broken so that each bone piece was independently embedded in the gel matrix. The composition of having independent bone pieces embedded in a gel matrix creates a fully articulated model for demonstrating the correction.



Figure 5-2 Photo of clubfoot model⁷⁸ manipulated to normal foot shape. Model did not show signs of tear.

During the experimentation, the foot model was able to sustain the deformation from a clubfoot configuration to a normal plantigrade foot configuration without breaking. In **Figure 5-2**, the clubfoot model was manually twisted back to normal configuration as a preliminary test of the model's elasticity. For a quantitative study, stress-strain tests was performed on the model and the model was shown to be capable of being stretched four times its original length without breaking.⁷⁸

In terms of functionality, this model meets all the specifications in **Table 5-1** and **Table 5-2**, and clubfoot correction using the proposed 2DOF external fixator was demonstrated on this model. Bone pins and wires can be drilled and lodged securely into the skeletal structure of the model without breaking it.

The model as a whole is elastic and articulate, and able to sustain significant deformation during the correction process. It is a full-scale model and is thus compatible with commercially available external fixator components. The soft tissue layer is completely transparent, enabling users to see how the bone pieces moves during correction by the proposed 2DOF external fixator.

The manufacturing of the model was labor-intensive, involving multiple steps of casting and molding. However, areas of automation were identified that may reduce the amount of in-house man-hours needed, with a possible increase in manufacturing costs. The mold for casting costs \$370 (one-off) and took 5 hours to make⁷⁸, while the model itself costs \$196 and took a day⁷⁸. The plaster mold can be replaced with a 3D printed mold, which is more expensive but would take less than a day to design and send for printing. The cost of manufacturing will also be drastically reduced if an in-house 3D printer is available.

5.3 Further Work and Other Applications

In this thesis, the foot model was used as a demonstration model for the proposed 2DOF external fixator. Nevertheless, this model would be useful in many other medical applications.

A straightforward extension for this model is as a pre-operative planning tool. For external fixation of clubfoot, relatively few details such as skeletal structure, nerves and vasculature are needed for pre-operative planning. For other surgeries such as brain surgeries, other soft tissue anatomy may be necessary. Using multi-material 3D printing, more detailed structures can be easily included.

With these details included, the model is also a potential tool for training residents. For this application, the transparency is especially valuable as it provides visual feedback for residents when they practice and enables them to visualize the internal structures *in vivo*. While computer models are prevalent, physical models remains the more effective tool as they take advantage of stereoscopic vision to interpret the 3D structures,⁴² whereas computer models may instead tax the brain's resources to reconstruct the mental 3D model^{42,61}. In some studies,^{42,61} virtual models are found to be less effective than physical models. In one study, training with virtual models imbued greater confidence in the trainee even though they did not perform better.⁶¹ In addition, these models could serve as standardized tools to evaluate residents.

Physical models are also less expensive and more readily available than cadavers, so residents can train for any medical procedure whenever they want to. Currently, this model is limited to bony operations, but the range of medical conditions that the model can simulate will expand if more anatomical details were included in the model.

Patient education is another area where physical models come in handy. Clinicians often have to explain to patients their current conditions and the treatment options. A good transparent model with great visuals reduce the effort of explaining the complex human anatomy, while articulated models help patients to immediately grasp what the treatment process entails and the expected result.

Chapter 6. Accuracy of Surgical System: Experimental Surgery for Clubfoot Correction

To evaluate the accuracy and feasibility of the proposed system, an experiment was designed to perform the installation of the proposed 2DOF external fixator on the foot model described in Chapter 5.

The accuracy and feasibility of the surgical system was evaluated on a controlled experimental foot model. It is assumed that in the case of operating on a patient's foot, there is a way to accurately register and fixate its pose. The development of safe and effective methods to register and fixate a patient's foot is beyond the scope of this thesis.

In addition, the proposed surgery workflow involving a passive positioning linkage described earlier in Section 1.5 was modified as the positioning linkage was not available during the experiments. Two substitute systems were implemented: (1) a camera system; and (2) a universal positioning arm.

This chapter begins with a description of the camera system. The camera system registers the surgical system to the foot model and it collects other point data by triangulating the position of fiducial markers in two camera views. The accuracy of the camera system is then evaluated and the sources of errors are discussed. The universal positioning arm is then described as an intermediate construct to transfer the optimal trajectory joint pose from the Denso robot arm to the trajectory joint at the surgical table.

Four experiments were performed in total on four identical foot models, with slight variations in the ankle joint axis. The surgical procedure that was followed in the experiments is described and illustrated with photos taken during the experiment. A fiducial marker construct was designed and tracked using the camera system to evaluate the amount of midfoot deformity correction that was achieved by the 2DOF external fixator built during these experiments. The amount of correction measured was then compared to the target correction to evaluate the accuracy of the surgical system.

When the external fixator is connected to the foot model, the average error in the transformation is 41 mm and 11.7 deg. When the external fixator is not connected to the foot model on one end, the error is drastically reduced to 11 mm and 3.5 deg. Thus, the conclusion is that, while the external fixator has to be

more rigid to overcome resistance from the foot model, the surgical system is fairly accurate. This chapter ends with a discussion on the possible sources of error and a qualitative evaluation of the 2DOF external fixator.

6.1 Camera System for Registration and Data Collection

The function of the passive positioning linkage as an encoder chain for registration during surgery was substituted with a camera system during the experiments. Instead of probing the foot model to obtain either surface data or position of landmarks features for registration, fiducial markers were embedded and an array of cameras was used to locate them. Given two camera images and their respective camera matrices, the location of a marker in the two camera views can be triangulated to give the 3D position of the marker. By identifying multiple markers on an object, the pose of the object can be determined. The fiducial markers used in these experiments are ball bearings painted bright green or orange for easy identification and selection. An interactive program enables users to pick the centers of ball bearings on each camera view and the program would triangulate the ball bearing locations in 3D space. Besides registration, the same method was used to obtain data such as the ankle joint axis and transformation accuracy, during the surgery.

Four cameras were empirically found to be the least number necessary to localize all points of interest for this experiment. Theoretical determination of the number of cameras needed is a coverage problem and depends on several factors such as the coverage area and the extent of occlusion. All four cameras were calibrated using the calibration module in OpenCV⁴, an open source computer vision library. Instructions for camera calibration are available online and will not be elaborated in detail here. Briefly, the cameras were mounted at a high vantage point, without obstructing the surgeon's access to the foot model and with all objects of interest visible to at least two cameras. Once the cameras were secured in place, a checkerboard with a known grid size was placed in the camera's view in 24 different poses for calibration. During camera calibration, the calibration was repeated until re-projection error was less than 1 mm. Camera calibration generates (1) a single internal camera matrix that models distortion in the camera view,

and (2) an external camera matrix that encodes the camera's pose to the checkerboard. The full camera matrix is the multiple of the internal and external camera matrices.

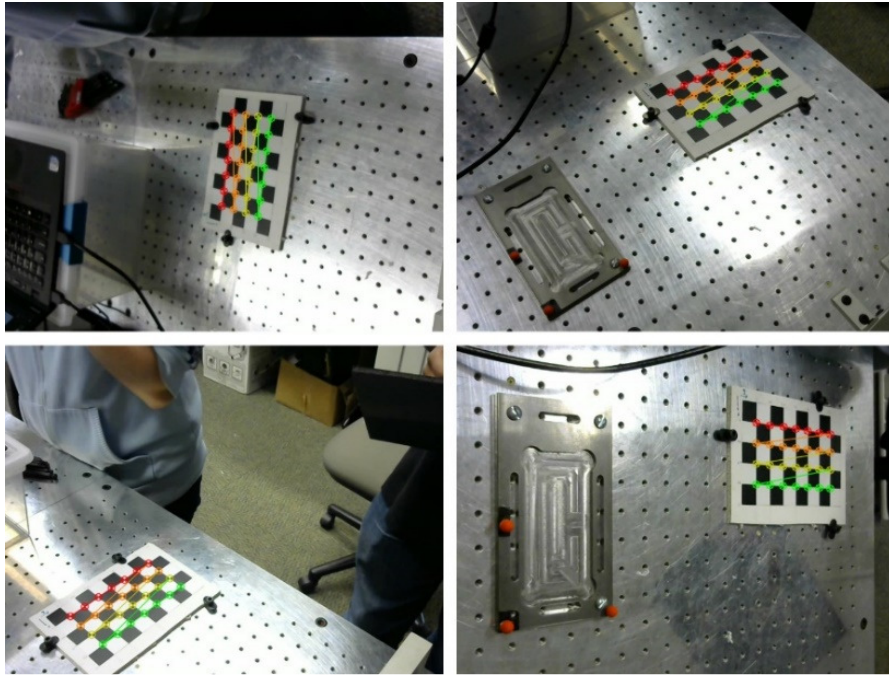


Figure 6-1 Camera views of common checkerboard pose that establishes a common workspace coordinate. Colored lines on checkerboard indicates the grid intersections identified by the calibration program.

A common workspace coordinate was established by having one checkerboard pose that was visible to all cameras. The camera view of the common checkerboard pose from each of the four cameras during calibration is shown in **Figure 6-1**. The external camera matrix was taken when the common checkerboard pose was shown to obtain the full camera matrix. The inherent error of using a camera system to locate ball bearings is evaluated in Section 6.2.

6.2 Accuracy of Camera Triangulation

In this experiment, various components of the 2DOF device and the foot model itself were registered using green ball bearings as fiducial markers. Thus, before determining the accuracy of the correction, the accuracy of the localization process must first be determined.

Accuracy of the camera system was evaluated by measuring the distance between ball bearings as opposed to the absolute position of each ball bearing. Green ball bearings were secured to a checkerboard at known distances apart. The 3D location of the ball bearings were then determined using the interactive program and the distances between ball bearings were calculated and compared to the actual value.

To investigate if ball bearing diameter affects accuracy of selection on the interactive program, the experiment was repeated using ball bearings that are either $3/8$ in or $3/16$ in in diameter. The ball bearings were also placed in a pattern that includes a range of gap sizes between two ball bearings, to investigate if the error is absolute or proportional to distance.

6.2.1 Results

Green ball bearings were selected on the camera views as shown in **Figure 6-2**. The triangulated 3D positions of the ball bearings calculated by the interactive program were plotted in **Figure 6-3**. The plots show that the measured positions were in agreement with the actual setup.

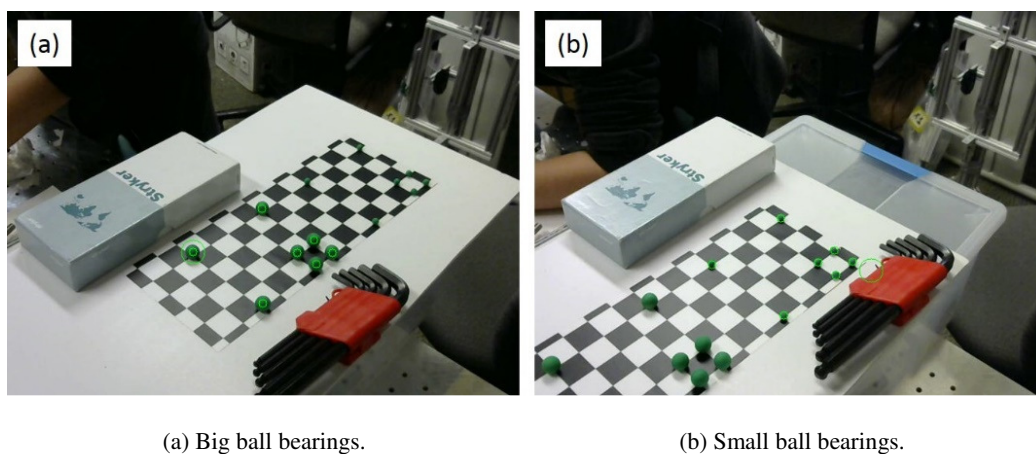


Figure 6-2 Ball bearing setup as viewed by one camera. The ball bearings (green circles) were placed approximately in the middle of the camera view for triangulation.

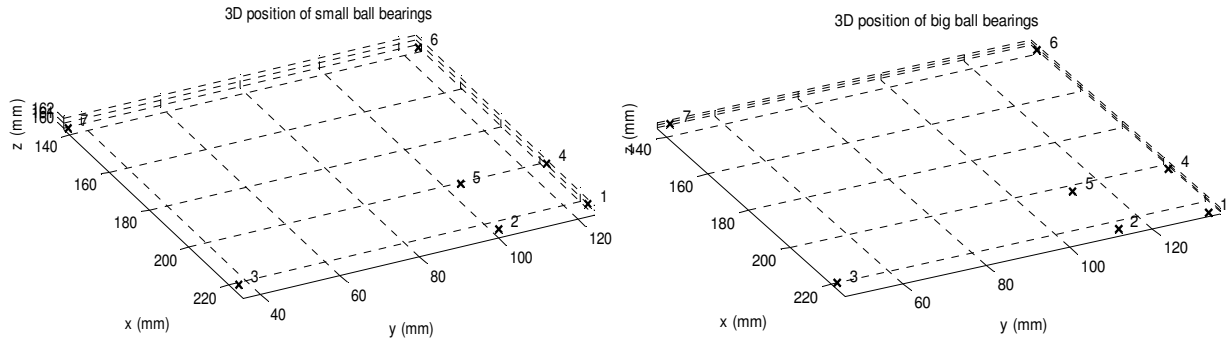


Figure 6-3 Triangulated 3D positions of ball bearings (marked 'x') based on selected points on each camera view in Figure 6-2.

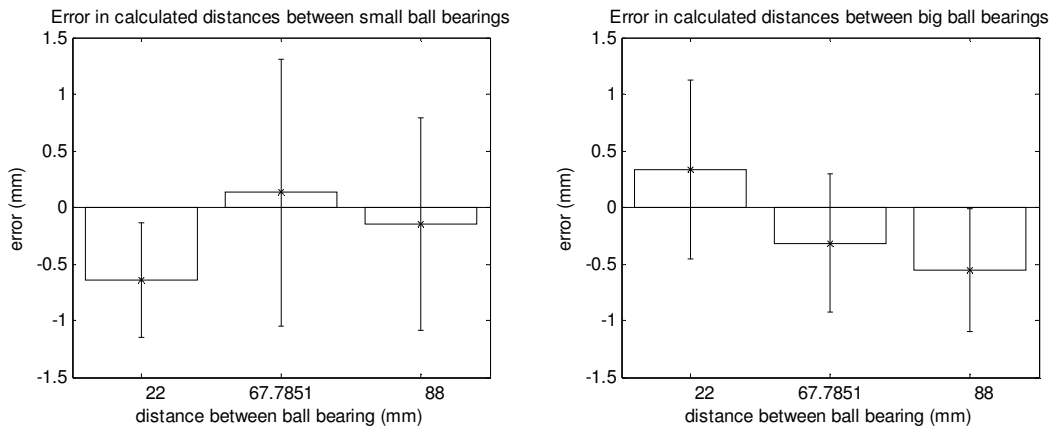


Figure 6-4 Error plots of measured distance between ball bearings. Error bars: one standard deviation.

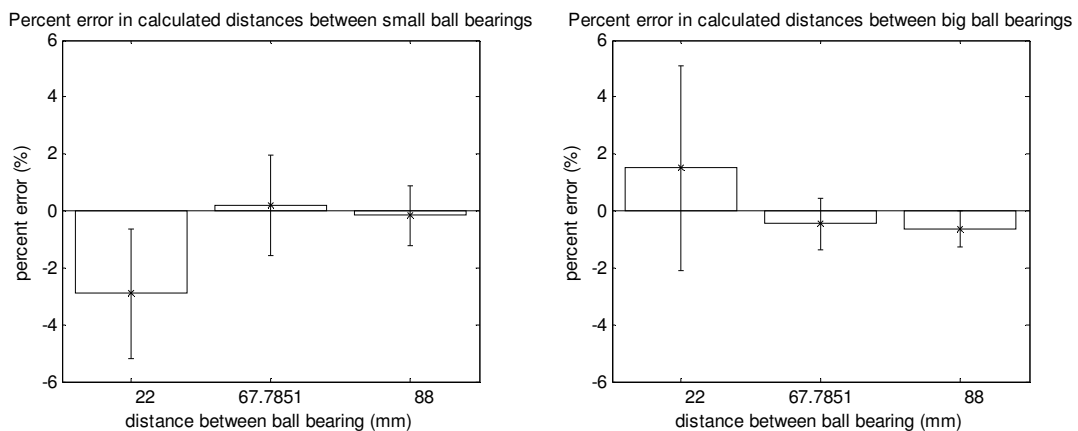


Figure 6-5 Error plots of distance between ball bearings triangulated by the camera array as a percentage of the actual distance. Error bars: one standard deviation.

To quantify the error, distances between ball bearings were investigated. The absolute error in the measurements as plotted in **Figure 6-4** were below 1.5 mm for all distances, with no significant difference between size of ball bearings or distances. **Figure 6-5** shows the same error values as percentages of the actual distances. As the absolute errors are similar across distances and ball bearing diameters, the percentage errors are much lower at larger distances.

6.2.2 Sources of Error

First and foremost, there is a limitation to how accurately a generic camera lens can be modelled during the calibration process. To minimize error propagation, the calibration was repeated until the re-projection error was below 1 mm.

Another potential source of error is in the selection of ball bearing locations on each camera view. As a camera image is discretized, there is a finite resolution to this selection process. Given the camera image is 480 px tall by 640 px wide, it has a diagonal of 800 px. Furthermore, given that its field of view is 60 deg and the distance between camera and the plane of interest is approximately 500 mm, the physical diagonal distance is $2 \times 500 \times \tan(30^\circ) = 577.35 \text{ mm}$. Thus, a single pixel in the image represents a physical distance of $577.35 \text{ mm}/800 \text{ px} = 0.72 \text{ mm/px}$. Assuming an average error of 3 px when selecting the center of ball bearings, the estimated selection error is 2 mm in one dimension.

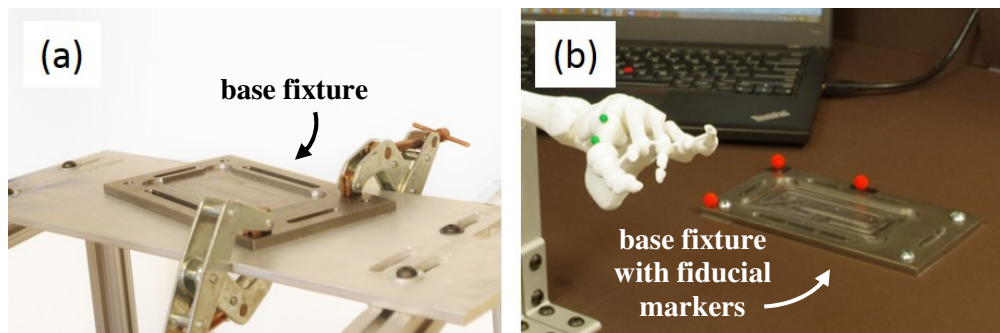
Taking these errors into consideration, the measurement error of below 1.5 mm is comparable to the sum of the re-projection error and a selection error of 1 pixel. While the average user is expected to have a larger selection error, this experiment showed that it is possible to achieve a very small error in the measurement of fiducial markers using a camera array.

6.3 Robot and Universal Positioning Arm for Trajectory Joint Placement

The proposed method of reducing 6DOF correction to 2DOF is possible by constraining the pose of the trajectory joints. Thus, to achieve accurate correction, these joints have to be placed accurately

relative to the foot. The passive positioning linkage described in Section 1.5.4 is envisioned to perform this function. However, as this passive positioning linkage was not fully developed yet, a universal positioning arm (Jumbo Flexbar, Flexbar Machine Corporation, Islandia, NY, U.S.A) and a 6DOF Denso robot (VS6577-E, DENSO Robotics, Southfield, MI, U.S.A) were used instead.

Two workspaces are defined in this experiment: (1) the surgery workspace, which is also referred to as simply the workspace; and (2) the robot workspace, which is a separate area containing the robot. Both workspaces were connected mathematically by the presence of two identical base fixtures for the universal positioning arm as shown in **Figure 6-6**. In the robot workspace, the base fixture was placed in a known pose by the robot to establish a robot workspace coordinate at one corner of the base fixture. In the surgery workspace, the base fixture had three ball bearings attached to define the same coordinate at the same corner. The steel base fixture was designed as a snug fit to the base of the universal positioning arm and held it firmly in place when the magnetic base of the arm is turned on.



(a) Base fixture in robot workspace.

(b) Base fixture in surgery workspace.

Figure 6-6 Photos of base fixture for universal positioning arm in surgery and robot workspaces.

The purpose of the universal positioning arm is to transfer the pose of the trajectory joint from the robot to the trajectory joint itself. A custom end effector was designed to replicate a fixture pattern on the trajectory joint so that an adapter for the universal positioning arm could connect to either the trajectory joint or this custom end effector. The robot placed the custom end effector in the calculated pose and the

adapter and universal positioning arm were connected to the custom end effector as shown in **Figure 6-7**. After tightening the universal positioning arm, the adapter was detached from the end effector and the adapter-arm construct was transferred to the surgery workspace. The trajectory joint was then attached to the adapter as shown in **Figure 6-8**. Since the base fixtures are identical in the two workspaces, when the adapter-arm construct was transferred to the surgery workspace, the pose would be effectively transferred from the robot to the trajectory joint.

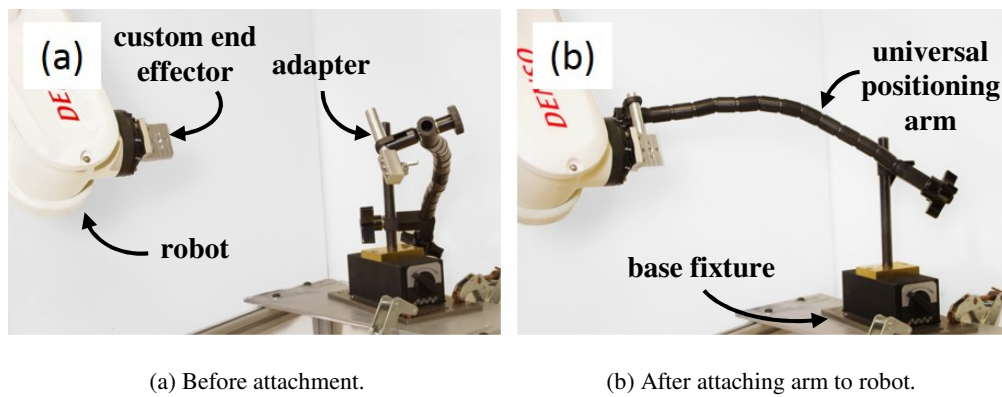


Figure 6-7 Photo of universal positioning arm with the adapter and the robot with the custom end effector. Adapter attached to the robot end effector to configure the universal positioning arm to the calculated pose.

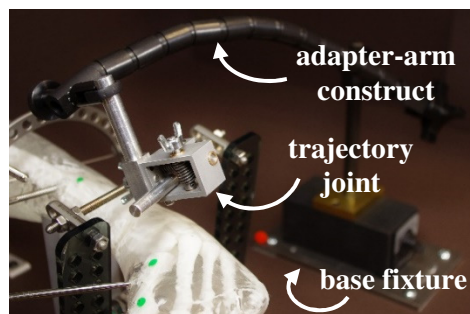


Figure 6-8 Photo showing revolute trajectory joint attached to the adapter-arm construct, which was configured by the robot. The adapter-arm construct places the trajectory joint in the calculated pose relative to the foot.

6.4 Surgery Procedure on Foot Model

In preparation for the experiment, the camera array was calibrated to a common coordinate. Throughout the experiment, the foot model was attached to the table via a custom fixture. The setup of the foot model, cameras and workspace coordinate are as annotated in **Figure 6-9**.

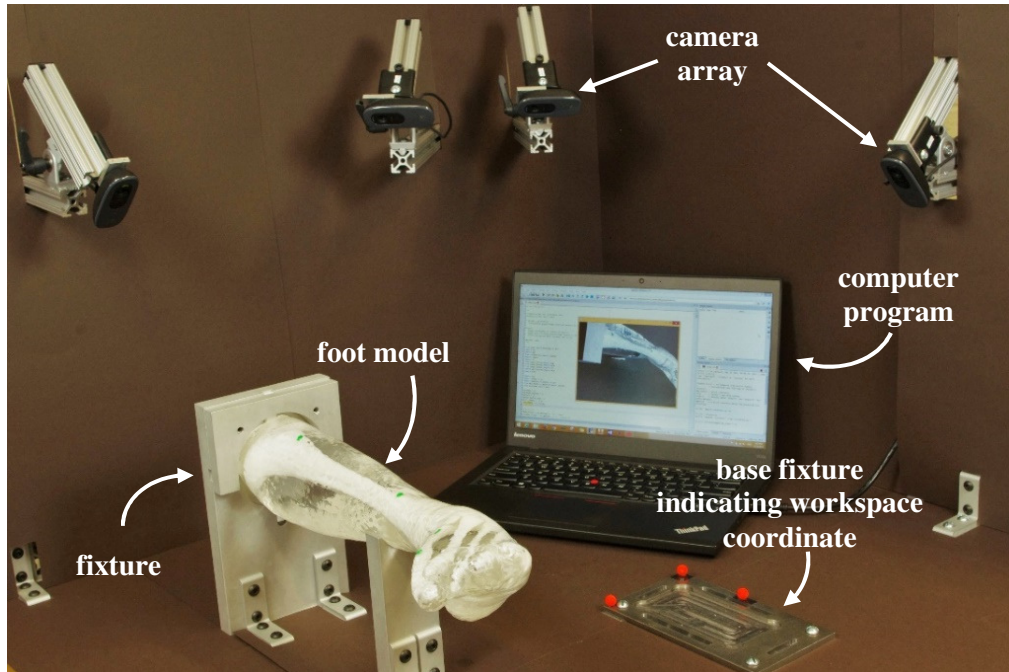


Figure 6-9 Setup of experimental surgery for clubfoot correction.

1. Register foot model to workspace coordinate using fiducial markers.

An array of cameras registered the foot model to the workspace to convert CAD data to real world coordinates. Fiducial markers were predefined on the CAD model as shown in **Figure 6-10**, and placed in the same positions on the 3D printed foot skeleton prior to casting. **Figure 6-11** shows the foot model with the ball bearings, which are located using the camera system. A transformation from CAD coordinate to workspace coordinate was calculated using least squares.

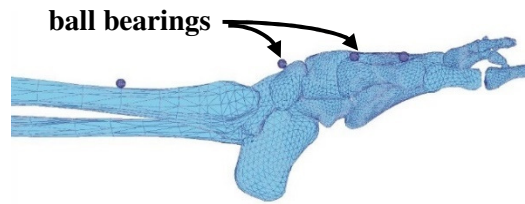
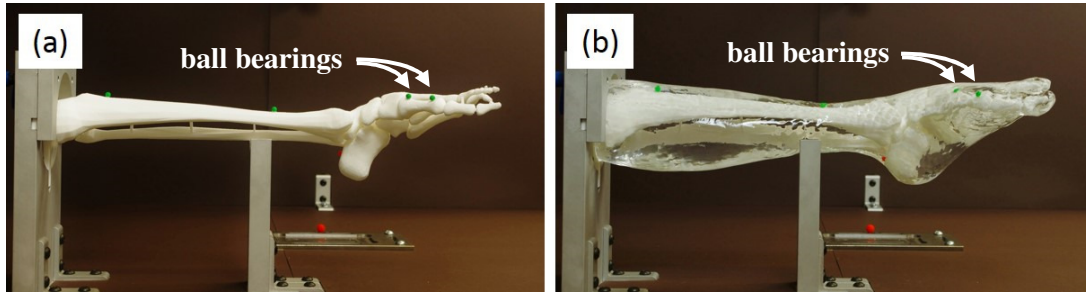


Figure 6-10 CAD model of clubfoot skeleton with ball bearings at predefined positions.



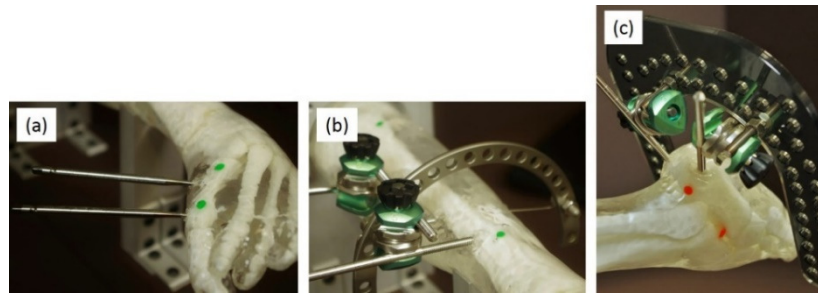
(a) Foot skeleton with ball bearings attached.

(b) Foot model with ball bearings embedded.

Figure 6-11 Actual foot models with ball bearings for registration to CAD model.

2. Insert bone pins and set up base frames at tibia, calcaneus and first metatarsus.

Bones pins were inserted into the tibia, calcaneus and first metatarsus as shown in **Figure 6-12**, to attach the fixator to the skeleton. At least two bone pins were inserted into each bone to resist torque and force loadings. The base frames at the tibia and calcaneus were attached rigidly via bone pins or k-wires to the bone. **Figure 6-13** shows the foot model with the base frames.



(a) Bone pins at first metatarsus. (b) Tibial frame. (c) Calcaneal frame.

Figure 6-12 Tibial and calcaneal frames were attached to the skeleton via bone pins and sometimes k-wires. The first metatarsus had just the bone pins but no plate as a frame.

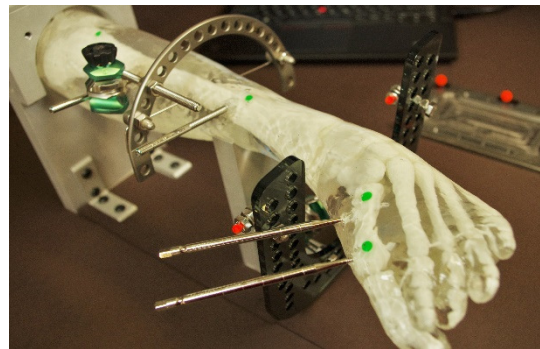


Figure 6-13 Full view of foot model with base frames.

3. Install hinges between tibial frame and calcaneal frames to establish ankle joint for correcting equinus.

By locating the hinges, the extent of equinus correction and thus the amount of midfoot deformity that remains to be corrected can be calculated. The rest of the device was then optimized to correct this remaining deformity. **Figure 6-14** shows the ball bearings attached to the hinges along the rotation axis as viewed from one camera. This would typically be done with the help of a C-arm, but as the model is transparent, the ankle joint can be directly located.

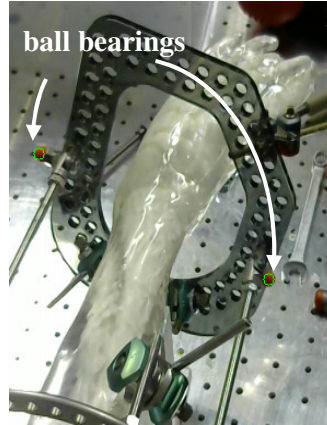


Figure 6-14 The ankle axis was located (green circles) using two ball bearings attached to the hinge joints.

- 4. Optimize fixator configuration and review the final configuration to make sure the joint values are feasible, and that there are no impingement or collision between joints. Adjust the joints to the calculated initial values.**

The optimization was discussed in detail in Section 3.9. **Figure 6-15** shows the computer rendering of the trajectory joints relative to the foot. By changing parameters in the program such as shifting the bounding box for the rotation point, the optimization constraints was modified to generate alternative configurations.

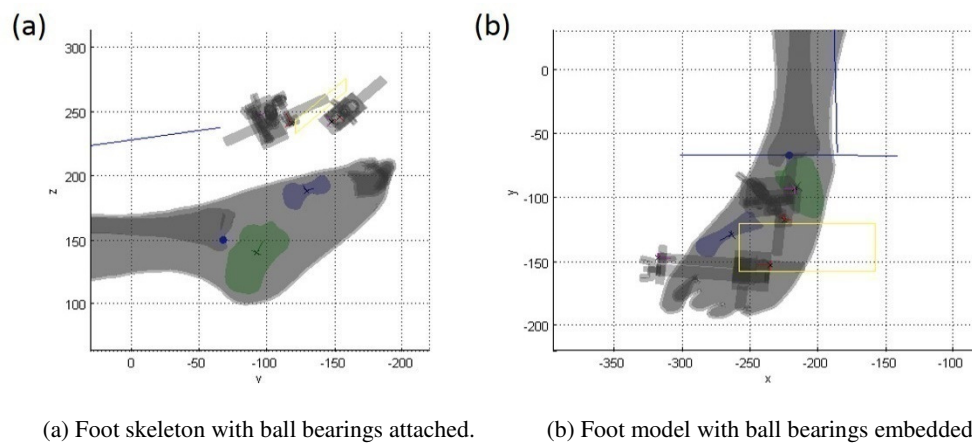


Figure 6-15 Final configuration from the optimization of fixator configuration. The calcaneus is depicted in green and the first metatarsus in blue. The yellow rectangle indicates the bounding box for the rotation point.

5. Set up base fixture in robot workspace.

A special end effector with a right angle corner positioned the base fixture before the base fixture was clamped securely in the robot workspace.

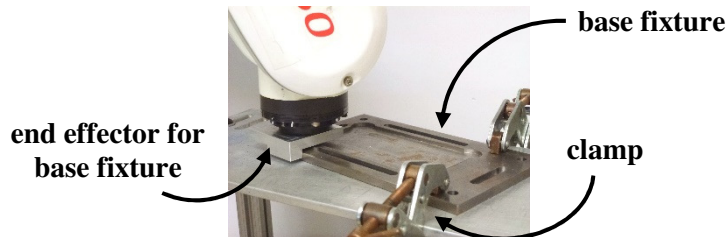


Figure 6-16 Robot positioned the base fixture using a special end effector and the base fixture was secured with clamps.

6. Place revolute trajectory joint relative to foot and secure to the base frames.

The robot positioned its end effector in the calculated pose for the revolute trajectory joint. The adapter was connected to the end effector and secured this pose on the universal positioning arm as shown in **Figure 6-17**.



Figure 6-17 Robot positioned the end effector in the calculated pose and the universal positioning arm was attached to the end effector via the adapter.

The revolute trajectory joint was attached to the universal positioning arm via the adapter and the whole construct was then secured onto the base fixture in the workspace as shown in **Figure 6-18**. This effectively transferred the calculated pose from the robot to the trajectory joint. The surgeon then secured the joint to the calcaneal frame via rods and clamps as shown in **Figure 6-19**.

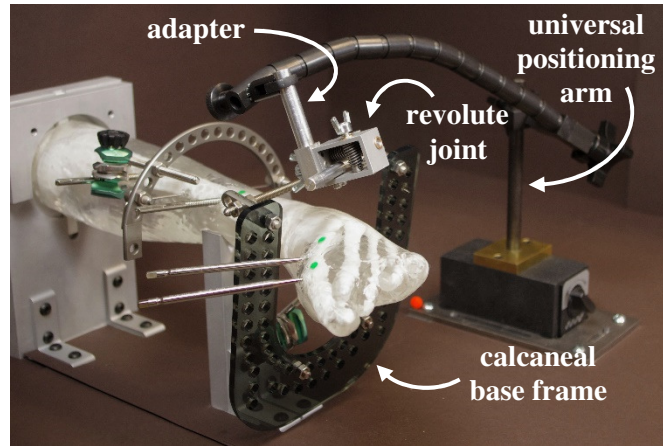
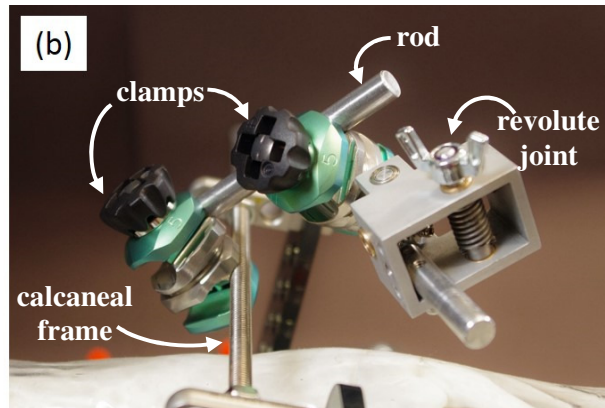


Figure 6-18 Universal positioning arm effectively transferred the calculated pose from the robot in the robot workspace to the revolute trajectory joint in the surgery workspace.



(a) Top view with arm attached.



(b) Revolute joint rigidly attached to calcaneal frame.

Figure 6-19 Photos showing one possible way of using rods and clamps to secure the revolute trajectory joint to the calcaneal base frame.

7. Place prismatic trajectory joint relative to foot and secure it to revolute trajectory joint.

This step was essentially the same as the previous step, except the prismatic trajectory joint was attached to the revolute trajectory joint instead of the base frame, as shown in **Figure 6-20**.



Figure 6-20 Prismatic trajectory joint was positioned by the universal positioning arm and secured to the revolute trajectory joint.

8. Secure prismatic trajectory joint to bone pins at first metatarsus.

The prismatic trajectory joint was secured to the bone pins at the first metatarsus. **Figure 6-21** shows the completed connection between the first metatarsus and the calcaneal frame.

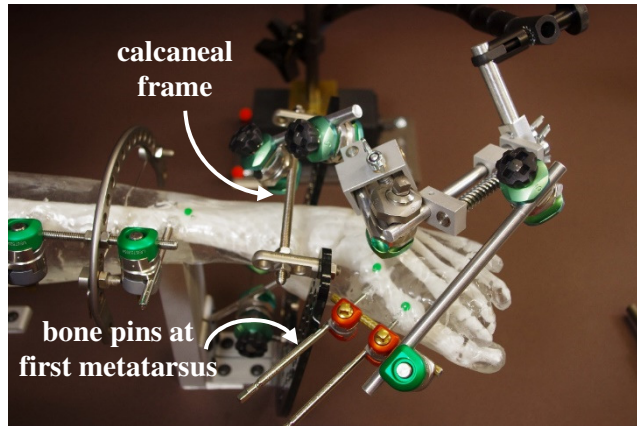


Figure 6-21 Photo of connection from calcaneal base frame to first metatarsus via the two trajectory joints.

9. Secure a prismatic joint between the calcaneal and tibial frames for equinus correction.

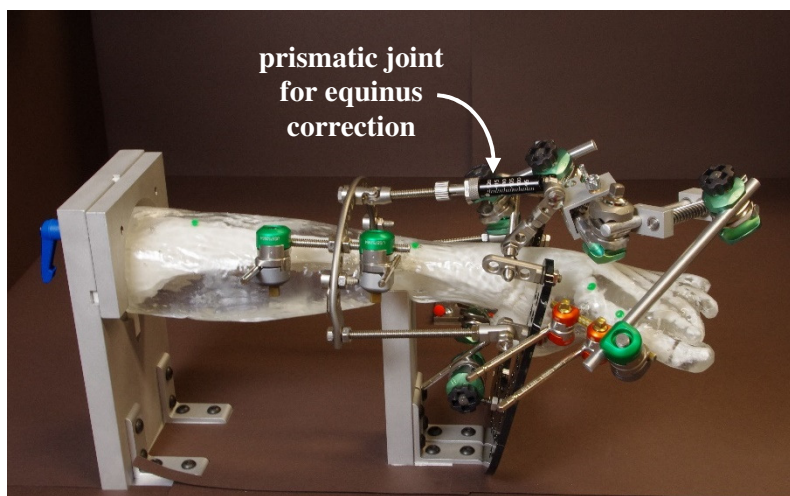


Figure 6-22 Completed 2DOF fixator.

10. Optimize joint schedules for correction.

The details of this optimization is described in Section 3.10. Briefly, the schedule for each joint was calculated so that the overall soft tissue stretching was under 2 mm/day.

6.5 Accuracy of Correction using 2DOF External Fixator

After setting up the 2DOF external fixator, midfoot correction was performed on the foot model. The accuracy of the external fixator was measured by tracking a fiducial marker attached to the external fixator near the first metatarsus. The movement of the marker was thus equivalent to the movement of the forefoot. Equinus correction was not included because, in all experiments, it was not possible to correct equinus with a single prismatic joint. Swapping the prismatic joint for a longer one is common in external fixation on patients. However, this could introduce errors as the foot model imposes a large resistive force that can cause slippage or bending during the swap. On a patient's foot, this resistive force does not increase indefinitely with the correction as the soft tissues grow under gradual distraction.

The fiducial marker is a planar construct with three ball bearings attached onto its surface in an L pattern as shown in **Figure 6-23**. The three ball bearings were located before and after midfoot correction to measure the rigid body transformation of the marker. This transformation was then compared to the target correction to evaluate the accuracy of midfoot correction.

In each experiment, the accuracy measurement was obtained for both with and without loading. In the case of without loading, midfoot correction was performed when the device was not connected to the first metatarsus. Between measurements on the same fixator configuration, trajectory joints were repositioned to eliminate errors due to the previous measurement. Four different experiments, each with a different fixator configuration, were performed.

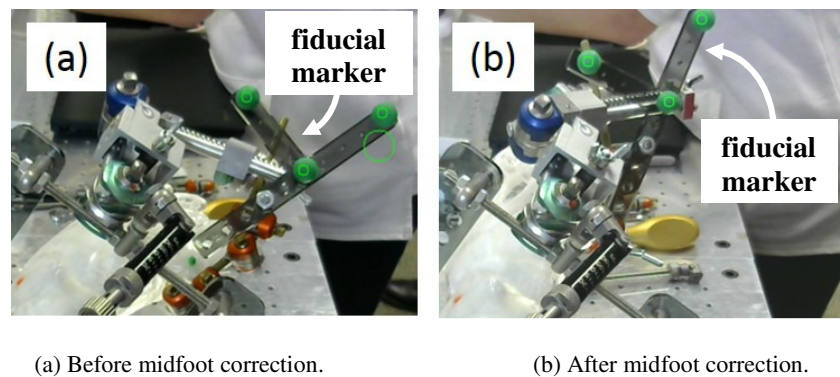


Figure 6-23 Fiducial marker for checking the accuracy of midfoot correction. The fiducial marker is a planar construct with three ball bearings attached to track the pose of the forefoot.

6.5.1 Results

The errors in midfoot correction, with and without loading, are tabulated in **Table 6-1** and the transformations are plotted as coordinate matrices in **Figure 6-24**. Since the setup in each experiment was different, the target matrices were different. To make it easier to visualize and compare the error across experiments, the transformation matrices are plotted with the target transformation as the basis coordinate.

The errors in translation and orientation were both higher with loading than without loading. Without loading, the errors were minimal, averaging 11 mm and 3.5 deg respectively. With loading, these numbers increased to 41 mm and 11.7 deg respectively.

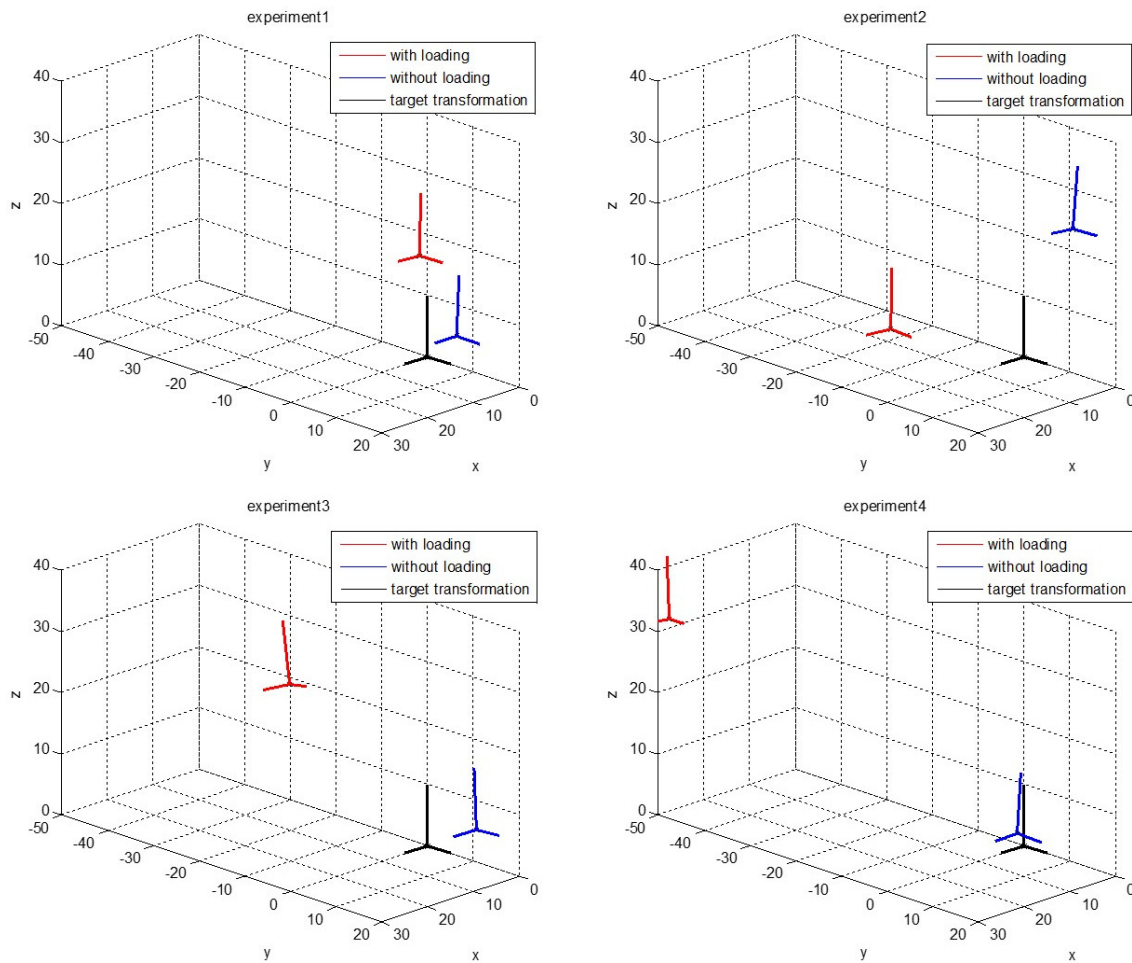


Figure 6-24 Plots of target transformation (black) and measured transformation with loading (red) and without loading (blue), for experiments 1-4. Transformations shown here are relative to the target transformation.

Table 6-1 Table of error in position and orientation of midfoot correction.

Experiment	With loading						Without loading					
	1	2	3	4	Ave	SD	1	2	3	4	Ave	SD
Error in translation (mm)	25	34	38	65	41	17.3	8	23	8	5	11	8.3
Error in rotation (deg)	4.0	7.4	16.7	18.8	11.7	7.2	2.8	4.7	3.0	3.6	3.5	0.9

6.5.1 Sources of Error

The measurement error of the camera system as discussed in Section 6.2 comes into play during registration of the foot model and the tracking of the fiducial marker before and after midfoot correction.

Besides measurement error, there were also errors in the placement of the trajectory joints. Firstly, the adapter of the universal positioning arm was tightened manually to the robot end effector and this could introduce misalignments. Also, as the universal positioning arm was tightened with a tension cable, there was internal tension that caused the adapter to spring away once it was detached from the custom end effector. These errors were minimized by carefully aligning the adapter to the custom end effector and visually observing the adapter to ensure minimal movement when it was released.

There may also be internal tension in the clamps and other fasteners used as part of the external fixator. The universal clamps used were spring loaded and will shorten when tightened. This shortening can generate internal tension in the external fixator and cause its configuration to change.

Last but not least, the rigidity of the external fixator and foot model were not high enough to resist torsion and bending forces. The foot model does not grow with the correction as a patient's foot would and so it imposed increasing resistance during the demonstration of midfoot correction. On the other hand, the 2DOF fixator was essentially a unilateral construct, which converted the resistive force into a huge cantilever moment. Under loading, the aluminum trajectory joints showed signs of wear and the acrylic

base plate could bend and twist. In addition, the foot model itself was also less rigid than the real foot and its compliance to the torsional and bending forces adds to the error in the midfoot correction.

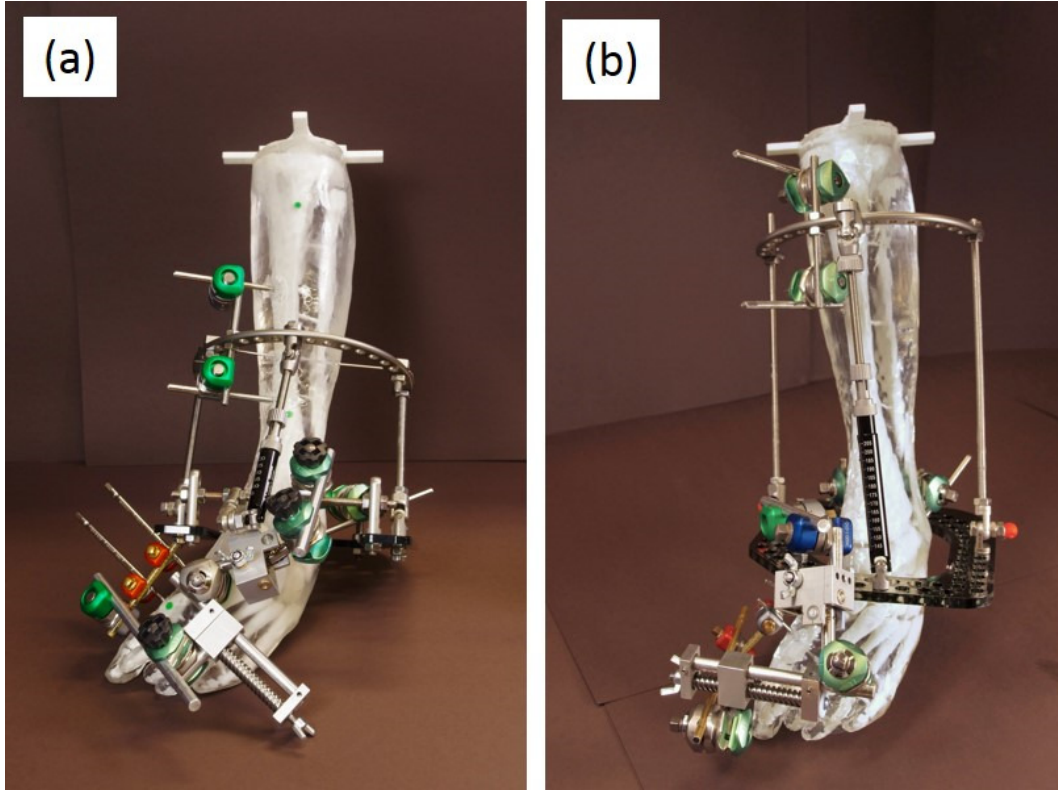
These errors were mostly related to hardware and loading. Thus, when there was no load and the compliance of the foot model and external fixator was irrelevant, the error was much smaller.

6.6 Qualitative Evaluation of 2DOF External Fixator

The experiments produced external fixator configurations that were simple and compact. Examples of the 2DOF external fixator configurations in two different experiments are shown in **Figure 6-25** and **Figure 6-26**. There were only two joints at the front of the foot and another joint in front of the shin, as opposed to multiple joints in current fixator setup. The trajectory joints can be made smaller and more rigid with better manufacturing resources.

Each experiments took less than 2 hours from registration to completion of the device setup. This is a huge and reliable savings in surgery time as opposed to the current method where surgeons may spend hours in the surgery to get a good fixator configuration. In addition, this speed was achieved despite having multiple extra steps to manipulate the Denso robot and universal positioning linkage. With the passive positioning linkage, the surgery time is expected to decrease further.

The proposed surgical system also required minimal input from the surgeon. Inputs included the correction target and a couple other parameters for ensuring that there were no impingements during correction and that there was sufficient skin gap for the tissues to swell.



(a) Example setup 1.

(b) Example setup 2.

Figure 6-25 Photos of the external fixator for two different experiments. Both configurations were compact and simple. They only occupy the volume in front of the shin and above the foot.

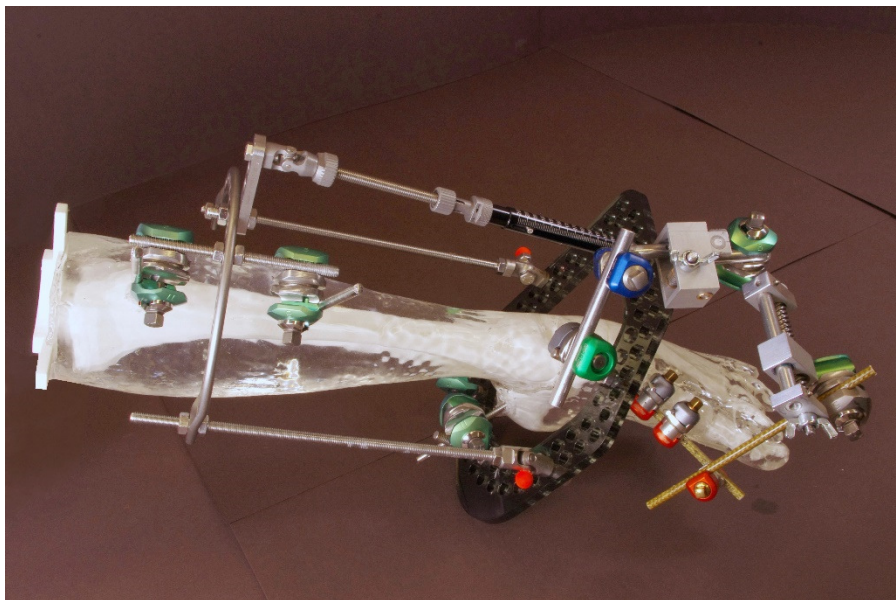


Figure 6-26 A different view of external fixator showing simplicity of the setup.

Chapter 7. Conclusion and Further Work

This thesis describes (1) a new method of defining orthopedic deformity correction procedures, (2) a new 2DOF external fixator for long bone deformity correction and clubfoot correction, (3) the reduction of 6DOF correction to 2DOF, (4) a new surgical planner that generates the most compact external fixator configuration and a distraction schedule to minimize the risk of soft tissue damage, (5) a passive positioning linkage to assist in the building of external fixator in surgery, and (6) a novel model with soft tissues over rigid 3D printed skeleton to demonstrate the external fixation. Measured over four experiments on the foot model, an accuracy in midfoot deformity correction of 11 mm and 3.5 deg without loading and 41 mm and 11.7 deg with loading was measured. Thus with more rigid external fixator design, better accuracy can be achieved.

The proposed 2DOF external fixator is essentially an axial fixator but with more benefits. The 2DOF external fixator has a revolute joint and a prismatic joint attached in series. This makes the design inherently less rigid than a generic ring fixator, which have support structures in parallel around the limb. This is the same design tradeoff when the surgeon chooses an axial fixator over a ring fixator. However, in this case, there are more benefits using the proposed 2DOF external fixator than the generic axial fixator. Even while being more compact with only two joints, the 2DOF external fixator is able to correct a 6DOF external fixator. In addition, the 2DOF approach enables control of the distraction path by optimization of the distraction schedule according to the needs of the specific correction. In the case of long bone deformity correction, the distraction schedule is optimized to follow a target distraction path that regenerates the original or contralateral bone shape. In the case of clubfoot deformity correction, the distraction schedule is optimized to reduce the risk of soft tissue damage by limiting the soft tissue stretching.

There are limitations to the 2DOF approach for orthopedic corrections. The two trajectory joints of the 2DOF external fixator have to be placed fairly accurately. This necessitates the use of a surgical system that includes a surgical assistive device to achieve accuracy in the placement of the joints. This thesis proposed a passive positioning linkage for this purpose, and demonstrated how an alternative system using

a Denso robot arm and a universal positioning arm can be implemented to achieve accuracy. Although this implies higher overhead costs in having the surgical system, the long term savings come from shortened surgeries and greater accuracy in the corrections. With a surgical system to assist them in pre-surgical planning and in building the external fixator during surgery, surgeons are expected to spend less time for each patient, and inexperienced surgeons will receive more guidance. The experiments described in this thesis took less than two hours each, as opposed to 2.5 or 4.5 hours on average.³⁹

The experiments described in this thesis are competent for a lab experiment, but will still need further refinement and validation before it can be commercialized. The correction accuracies of 11 mm and 3.5 deg are sufficient as preliminary results to support this concept, but are not yet good enough as a commercial surgical system. The prototypes made as part of this thesis are also not commercially viable. As discussed earlier, the components are not rigid enough to overcome the resistance of the foot phantom model. The design and selection of materials to create a more rigid external fixator are product development processes. The development of commercially viable external fixator and surgical system are not part of the scope of this academic thesis.

The phantom foot model is an effective phantom for the demonstration of external fixation on a clubfoot. It not only has the rigid skeletal structure that supports the external fixator, it also has a soft tissue layer to replicate the shape of the clubfoot and mimic the texture of soft tissues. This model is able to show the change in foot shape as the clubfoot is corrected. In its current form, the foot phantom model has only the skeletal structure and a soft tissue layer with no internal structures. It is possible to include more details in the model from CT scan data using multi-materials printers that can print more than one materials simultaneously to achieve complex and anatomically accurate models. For example, vasculatures, nerves and ligaments can be included in the model to make it more realistic. With more details and a transparent gel layer, this model has potential as a teaching or educational tool. Further work is necessary to explore its application in medical education, medical training and patient education.

In this thesis, a surgical system was developed to implement the 2DOF approach to orthopedics deformity corrections, specifically on long bone deformity correction and clubfoot correction. Key

components of the surgical system such as the 2DOF external fixator, the surgical planner, the registration system, and the surgical assistance via a Denso robot and a universal positioning arm, were developed and four experiments were performed. While the surgical system may not be ready for commercialization in its current form, it demonstrated the feasibility of implementing this 2DOF approach and the benefits of this approach.

7.1 Summary of Contributions

The original contributions by this thesis are:

1. A mathematical expression of bone deformity correction as a rigid body transformation that enables quantification of correction target and accuracy.
2. A method of optimizing the 2DOF external fixator configuration for long bone deformity correction and clubfoot correction to minimize the overall size of the device.
3. A method of optimizing the device distraction schedule to limit distraction rate in long bone deformity correction and clubfoot correction, and to regenerate the original or contralateral bone shape in distraction osteogenesis.
4. A novel foot phantom model consisting of a rigid skeletal structure embedded in flexible transparent ballistic gel that mimics the consistency of human muscle. This model has generated much interest as a teaching tool for residency programs.

7.2 Extensions

Some of the concepts or components developed as part of this thesis can be further explored or extended for other applications.

1. The development of the passive positioning linkage was not completed due to time and resource constraints. The passive positioning linkage could further reduce surgery time and accuracy of correction as it is a less convoluted method than the use of the Denso robot.
2. The same passive positioning linkage could be applied to other procedures such as 3D ultrasound imaging.
3. The application of the novel phantom foot model in residency programs for the training of new residents, particularly in the orthopedics department.

References

1. A.D.A.M., I. Clubfoot. <http://www.nlm.nih.gov/medlineplus/ency/article/001228.htm> 2013, 2011.
2. Abe, I., N. Ochiai, H. Ichimura, A. Tsujino, J. Sun, and Y. Hara. Internodes can nearly double in length with gradual elongation of the adult rat sciatic nerve. *J. Orthop. Res.* 22:571-577, 2004.
3. Anand, A. and D. A. Sala. Clubfoot: etiology and treatment. *Indian. J. Orthop.* 42:22-28, 2008.
4. Bradski, G. and A. Kaehler. *Learning Opencv*, 1st Edition. : O'Reilly Media, Inc., 2008.
5. Burns, J. K. and R. Sullivan. Correction of severe residual clubfoot deformity in adolescents with the Ilizarov technique. *Foot Ankle Clin.* 9:571-82, ix, 2004.
6. Caja, V., W. Kim, S. Larsson, and Y. C. E. Comparison of the mechanical performance of three types of external fixators: linear, circular and hybrid. *Clin. Biomech. (Bristol, Avon)* 10:401-406, 1995.
7. Carter, D. R., G. S. Beaupre, N. J. Giori, and J. A. Helms. *Mechanobiology of skeletal regeneration.* *Clin. Orthop. Relat. Res.* :S41-55, 1998.
8. Chao, E. Y. and T. J. Hein. Mechanical performance of the standard Orthofix external fixator. *Orthopedics* 11:1057-1069, 1988.
9. Choi, I. H., M. S. Yang, C. Y. Chung, T. J. Cho, and Y. J. Sohn. The treatment of recurrent arthrogryptic club foot in children by the Ilizarov method: A PRELIMINARY REPORT. *Journal of Bone & Joint Surgery, British Volume* 83-B:731-737, 2001.
10. Clear Ballistics llc. *About Ballistic Gelatin.* 2015.
11. Codivilla, A. The classic: On the means of lengthening, in the lower limbs, the muscles and tissues which are shortened through deformity. 1905. *Clin. Orthop. Relat. Res.* 466:2903-2909, 2008.
12. Cooke, S. J., B. Balain, C. C. Kerin, and N. T. Kiely. Clubfoot. *Current Orthopaedics* 22:139-149.
13. Dammerer, D., K. Kirschbichler, L. Donnan, G. Kaufmann, M. Krismer, and R. Biedermann. Clinical value of the Taylor Spatial Frame: a comparison with the Ilizarov and Orthofix fixators. *J. Child. Orthop.* 5:343-349, 2011.
14. Dell'Osso, G., F. Celli, V. Bottai, G. Bugelli, C. Citarelli, G. Agostini, G. Guido, and S. Giannotti. Single-Use Instrumentation Technologies in Knee Arthroplasty: State of the Art. *Surg. Technol. Int.* XXVIII:sti28/727, 2016.
15. Demarais, D. M., R. A. Bachschmidt, and G. F. Harris. The instantaneous axis of rotation (IAOR) of the foot and ankle: a self-determining system with implications for rehabilitation medicine application. *IEEE Trans. Neural Syst. Rehabil. Eng.* 10:232-238, 2002.
16. Dobbe, J. G., K. J. Pre, P. Kloen, L. Blankevoort, and G. J. Streekstra. Computer-assisted and patient-specific 3-D planning and evaluation of a single-cut rotational osteotomy for complex long-bone deformities. *Med. Biol. Eng. Comput.* 49:1363-1370, 2011.

17. Dobbs, M. B., J. R. Rudzki, D. B. Purcell, T. Walton, K. R. Porter, and C. A. Gurnett. Factors predictive of outcome after use of the Ponseti method for the treatment of idiopathic clubfeet. *J. Bone Joint Surg. Am.* 86-A:22-27, 2004.
18. El Barbary, H., H. Abdel Ghani, and M. Hegazy. Correction of relapsed or neglected clubfoot using a simple Ilizarov frame. *Int. Orthop.* 28:183-186, 2004.
19. El-Sayed, M. Ilizarov external fixation for management of severe relapsed clubfeet in older children. *Foot Ankle Surg.* 19:177-181, 2013.
20. Feldman, D. S., S. S. Shin, S. Madan, and K. J. Koval. Correction of tibial malunion and nonunion with six-axis analysis deformity correction using the Taylor Spatial Frame. *J. Orthop. Trauma* 17:549-554, 2003.
21. Ferreira, R. C. and M. T. Costa. Recurrent clubfoot--approach and treatment with external fixation. *Foot Ankle Clin.* 14:435-445, 2009.
22. Fitzpatrick, D. C., W. S. Foels, D. R. Pedersen, J. L. Marsh, C. L. Saltzman, and T. D. Brown. An articulated ankle external fixation system that can be aligned with the ankle axis. *Iowa Orthop. J.* 15:197-203, 1995.
23. Foster, P. A., S. B. Barton, S. C. Jones, R. J. Morrison, and S. Britten. The treatment of complex tibial shaft fractures by the Ilizarov method. *J. Bone Joint Surg. Br.* 94:1678-1683, 2012.
24. Franke, J., F. Grill, G. Hein, and M. Simon. Correction of clubfoot relapse using Ilizarov's apparatus in children 8-15 years old. *Arch. Orthop. Trauma Surg.* 110:33-37, 1990.
25. Fuller, D. J. and C. J. McCullough. Malunited fractures of the forearm in children. *J. Bone Joint Surg. Br.* 64:364-367, 1982.
26. Galante, V. N., L. Molfetta, and C. Simone. The treatment of club foot with external fixation — A review of results. *Current Orthopaedics* 9:185-188, 1995.
27. Ganger, R., C. Radler, A. Handlbauer, and F. Grill. External fixation in clubfoot treatment - a review of the literature. *J. Pediatr. Orthop. B* 21:52-58, 2012.
28. Gentili, A., S. Masih, L. Yao, and L. L. Seeger. Pictorial review: foot axes and angles. *Br. J. Radiol.* 69:968-974, 1996.
29. Goldstein, R. Y., C. J. Jordan, T. M. McLaurin, and A. Grant. The Evolution of the Ilizarov Technique Part 2: The Principles of Distraction Osteogenesis. *Bulletin of the Hospital for Joint Diseases* 71:96-103, 2013.
30. Grant, A. D., D. Atar, and W. B. Lehman. The Ilizarov technique in correction of complex foot deformities. *Clin. Orthop. Relat. Res.* (280):94-103, 1992.
31. Grill, F. Correction of complicated extremity deformities by external fixation. *Clin. Orthop. Relat. Res.* (241):166-176, 1989.
32. Gunay, M., M. B. Shim, and K. Shimada. Cost- and time-effective three-dimensional bone-shape reconstruction from X-ray images. *Int. J. Med. Robot.* 3:323-335, 2007.

33. Gurnett, C. A., S. Boehm, A. Connolly, T. Reimschisel, and M. B. Dobbs. Impact of congenital talipes equinovarus etiology on treatment outcomes. *Developmental Medicine & Child Neurology* 50:498-502, 2008.
34. Hasler, C. C. and A. H. Krieg. Current Concepts Review - Current Concepts of Leg Lengthening. *Journal of Children's Orthopaedics* :1863-2521, 2012.
35. Hassan, A. and M. Letts. The management of the neglected congenital foot deformity in the older child with the Taylor spatial frame. *J. Pediatr. Orthop.* 32:85-92, 2012.
36. He, L. S., H. T. Shang, and Y. Xue. A novel method for transferring press during curvilinear distraction. *Br. J. Oral Maxillofac. Surg.* 48:658-659, 2010.
37. Hibi, H. and M. Ueda. New internal transport distraction device for reconstructing segmental defects of the mandible. *Br. J. Oral Maxillofac. Surg.* 44:382-385, 2006.
38. Horn, B. D. and R. S. Davidson. Current treatment of clubfoot in infancy and childhood. *Foot Ankle Clin.* 15:235-243, 2010.
39. Hosny, G. A. Correction of foot deformities by the Ilizarov method without corrective osteotomies or soft tissue release. *J. Pediatr. Orthop. B* 11:121-128, 2002.
40. Ilizarov, G. A. The tension-stress effect on the genesis and growth of tissues: Part II. The influence of the rate and frequency of distraction. *Clin. Orthop. Relat. Res.* :263-285, 1989.
41. Jeong, H. S., K. J. Park, K. M. Kil, S. Chong, H. J. Eun, T. S. Lee, and J. P. Lee. Minimally invasive plate osteosynthesis using 3D printing for shaft fractures of clavicles: technical note. *Arch. Orthop. Trauma Surg.* 134:1551-1555, 2014.
42. Khot, Z., K. Quinlan, G. R. Norman, and B. Wainman. The relative effectiveness of computer-based and traditional resources for education in anatomy. *Anat. Sci. Educ.* 6:211-215, 2013.
43. Koo, T. K., E. Y. Chao, and A. F. Mak. Development and validation of a new approach for computer-aided long bone fracture reduction using unilateral external fixator. *J. Biomech.* 39:2104-2112, 2006.
44. Lewis, G. S., H. J. Sommer 3rd, and S. J. Piazza. In vitro assessment of a motion-based optimization method for locating the talocrural and subtalar joint axes. *J. Biomech. Eng.* 128:596-603, 2006.
45. Lie, C. W. and W. Chow. Limb lengthening in short-stature patients using monolateral and circular external fixators. *Hong Kong Med. J.* 15:280-284, 2009.
46. Lockett, M. R., P. Hosseinzadeh, P. A. Ashley, R. D. Muchow, V. R. Talwalkar, H. J. Iwinski, J. L. Walker, and T. A. Milbrandt. Factors predictive of second recurrence in clubfeet treated by ponseti casting. *J. Pediatr. Orthop.* 35:303-306, 2015.
47. Makhdoom, A., P. A. Qureshi, M. F. Jokhio, and K. A. Siddiqui. Resistant clubfoot deformities managed by Ilizarov distraction histogenesis. *Indian. J. Orthop.* 46:326-332, 2012.
48. Mayer, G., H. Seidlein, and T. Hunfeld. Clubfoot correction by external ring fixator. *Foot and Ankle Surgery* 2:223-227, 1996.

49. Melincoff, R. H. and R. H. Davis. The development of lower extremity deformity. *J. Am. Podiatry Assoc.* 68:631-635, 1978.
50. Morcuende, J. A., L. A. Dolan, F. R. Dietz, and I. V. Ponseti. Radical reduction in the rate of extensive corrective surgery for clubfoot using the Ponseti method. *Pediatrics* 113:376-380, 2004.
51. Moseley, C. F. Leg lengthening. A review of 30 years. *Clin. Orthop. Relat. Res.* :38-43, 1989.
52. Ng, C. Y. and M. M. McQueen. What are the radiological predictors of functional outcome following fractures of the distal radius? *J. Bone Joint Surg. Br.* 93:145-150, 2011.
53. Niu, X. G., Y. M. Zhao, and X. X. Han. Multiplanar and combined distraction osteogenesis for three-dimensional and functional reconstruction of unilateral large maxillary defects. *Br. J. Oral Maxillofac. Surg.* 47:106-110, 2009.
54. Orthofix Holdings Inc. M2 MultiPlanar MiniRail. , 2009.
55. Paley, D. *Principles of Deformity Correction.* Germany: Springer-Verlag, 2002.
56. Paley, D. Current techniques of limb lengthening. *J. Pediatr. Orthop.* 8:73-92, 1988.
57. Paley, D. and K. Tetsworth. Mechanical axis deviation of the lower limbs. Preoperative planning of multiapical frontal plane angular and bowing deformities of the femur and tibia. *Clin. Orthop. Relat. Res.* (280):65-71, 1992.
58. Patil, S., A. Bunn, W. D. Bugbee, C. W. Colwell Jr, and D. D. D'Lima. Patient-specific implants with custom cutting blocks better approximate natural knee kinematics than standard TKA without custom cutting blocks. *Knee* 22:624-629, 2015.
59. Piazza, S. J. Mechanics of the subtalar joint and its function during walking. *Foot Ankle Clin.* 10:425-42, v, 2005.
60. Ponseti, I. V. Treatment of congenital club foot. *J. Bone Joint Surg. Am.* 74:448-454, 1992.
61. Preece, D., S. B. Williams, R. Lam, and R. Weller. "Let's get physical": advantages of a physical model over 3D computer models and textbooks in learning imaging anatomy. *Anat. Sci. Educ.* 6:216-224, 2013.
62. Radler, C., G. T. Mindler, K. Riedl, C. Lipkowski, and A. Kranzl. Midterm results of the Ponseti method in the treatment of congenital clubfoot. *Int. Orthop.* 37:1827-1831, 2013.
63. Richards, B. S., S. Faulks, K. E. Rathjen, L. A. Karol, C. E. Johnston, and S. A. Jones. A comparison of two nonoperative methods of idiopathic clubfoot correction: the Ponseti method and the French functional (physiotherapy) method. *J. Bone Joint Surg. Am.* 90:2313-2321, 2008.
64. Rosemeyer, B. and W. Pforringer. Basic principles of treatment in pseudarthroses and malunion of fractures of the leg. *Arch. Orthop. Trauma Surg.* 95:57-64, 1979.
65. Sailhan, F. Bone lengthening (distraction osteogenesis): a literature review. *Osteoporos. Int.* 22:2011-2015, 2011.

66. Sala, F., T. Talamonti, and M. A. Agus. Tetrafocal leg reconstruction using combined Ilizarov/TSF technique. *Musculoskelet. Surg.* 95:151-155, 2011.
67. Sangeorzan, B. P., R. P. Judd, and B. J. Sangeorzan. Mathematical analysis of single-cut osteotomy for complex long bone deformity. *J. Biomech.* 22:1271-1278, 1989.
68. Shang, H., X. Lin, J. Du, L. He, and Y. Liu. Use of a new curvilinear distractor to repair mandibular defects in dogs. *Br. J. Oral Maxillofac. Surg.* 50:166-170, 2012.
69. Simpson, A. L., B. Ma, B. Slagel, D. P. Borschneck, and R. E. Ellis. Computer-assisted distraction osteogenesis by Ilizarov's method. *Int. J. Med. Robot.* 4:310-320, 2008.
70. Spiegelberg, B., T. Parratt, S. K. Dheerendra, W. S. Khan, R. Jennings, and D. R. Marsh. Ilizarov principles of deformity correction. *Ann. R. Coll. Surg. Engl.* 92:101-105, 2010.
71. Suresh, S., A. Ahmed, and V. K. Sharma. Role of Joshi's external stabilisation system fixator in the management of idiopathic clubfoot. *J. Orthop. Surg. (Hong Kong)* 11:194-201, 2003.
72. Tripathy, S. K., R. Saini, P. Sudes, M. S. Dhillon, S. S. Gill, R. K. Sen, A. Agarwal, S. Dhatt, and A. K. Mootha. Application of the Ponseti principle for deformity correction in neglected and relapsed clubfoot using the Ilizarov fixator. *J. Pediatr. Orthop. B* 20:26-32, 2011.
73. United States Bone and Joint Initiative. In: *The Burden of Musculoskeletal Diseases in the United States* Anonymous Rosemont, IL: American Academy of Orthopedic Surgeons, 2011, pp. 129-179.
74. Vanderwilde, R., L. T. Staheli, D. E. Chew, and V. Malagon. Measurements on radiographs of the foot in normal infants and children. *J. Bone Joint Surg. Am.* 70:407-415, 1988.
75. Wiedemann, M. Callus distraction: a new method? A historical review of limb lengthening. *Clin. Orthop. Relat. Res.* (327):291-304, 1996.
76. Wu, Y. Y., A. Plakseychuk, and K. Shimada. 2DOF External Fixator and Surgical System for Clubfoot Correction (Poster). *American Society of Biomechanics*, 2015.
77. Wu, Y. Y., A. Plakseychuk, and K. Shimada. 2DOF Fixator System for Correcting 3D Clubfoot Deformity (Poster). *7th World Congress of Biomechanics 2014*, 2014.
78. Wu, Y. Y., M. Rajaraman, B. Lee, A. Plakseychuk, and K. Shimada. A Patient-Specific Flexible 3D Printed Orthopedic Model for Training and Teaching of Clubfoot Correction Surgery. *3D Printing and Additive Manufacturing* 3:98-105, 2016.
79. Wu, Y. Y. and K. Shimada. Computer-Aided Surgical Planner for a New Bone Deformity Correction Device Using Axis-Angle Representation (Poster). *Innovation in Healthcare Technology Conference 2014*, 2014.
80. Wu, Y. Y., A. Plakseychuk, and K. Shimada. Computer-aided surgical planner for a new bone deformity correction device using axis-angle representation. *Med. Eng. Phys.* 36:1536-1542, 2014.
81. Wu, Y. Y., R. Lucking, R. Oberreuter, and K. Shimada. New Distraction Osteogenesis Device With Only Two Patient-Controlled Joints by Applying the Axis-Angle Representation on Three-Dimensional Bone Deformation. *Journal of Medical Devices* 7:041010-041010, 2013.

82. Zhao, D., H. Li, L. Zhao, J. Liu, Z. Wu, and F. Jin. Results of clubfoot management using the Ponseti method: do the details matter? A systematic review. *Clin. Orthop. Relat. Res.* 472:1329-1336, 2014.
83. Zhao, D., J. Liu, L. Zhao, and Z. Wu. Relapse of clubfoot after treatment with the Ponseti method and the function of the foot abduction orthosis. *Clin. Orthop. Surg.* 6:245-252, 2014.
84. Zheng, J., P. Lamoureux, V. Santiago, T. Dennerll, R. E. Buxbaum, and S. R. Heidemann. Tensile regulation of axonal elongation and initiation. *J. Neurosci.* 11:1117-1125, 1991.
85. Zionts, L. E. What's New in Idiopathic Clubfoot? *J. Pediatr. Orthop.* 35:547-550, 2015.

Appendix A. Iterations of 2DOF External Fixator for Clubfoot

Correction

A1. First Prototype

The first prototype was a rod and clamp system, borrowing components from other fixators in the market. Existing components were used to reduce the acceptance barrier of this system and to avoid reinventing the wheel. The design was first created in CAD environment as shown in **Figure A-1**, and clubfoot correction was simulated. **Figure A-2** shows the decomposition of clubfoot into heel and midfoot deformities. **Figure A-3** shows the various views of the foot and fixator before and after clubfoot correction.

The trajectory joints are custom designed as there are no components in current external fixators that perform the same function. The revolute trajectory joint has a worm gear mechanism with a 1:60 gearing ratio. The prismatic trajectory joint has 50 mm of extension and is constrained so that it does not rotate about its own axis. Current external fixators have prismatic joint components, but those joints are hinged and free to rotate about their own axes, so they cannot be used as a structural component on their own.

The entire frame and structure were assembled using mainly carbon fiber rods and universal clamps obtained from the clinical consultant. The trajectory joints were made in the University's machine shop using raw materials, such as aluminum and steel, and purchased components. The external fixator was then attached to an articulated Sawbones model using bone pins as shown in **Figure A-4**. **Figure A-5** and **Figure A-6** show the Sawbones and external fixator before and after correction using this external fixator setup. The prototype has a total of 33 components (excluding nuts) and the detailed breakdown is tabulated in **Table A-1**.

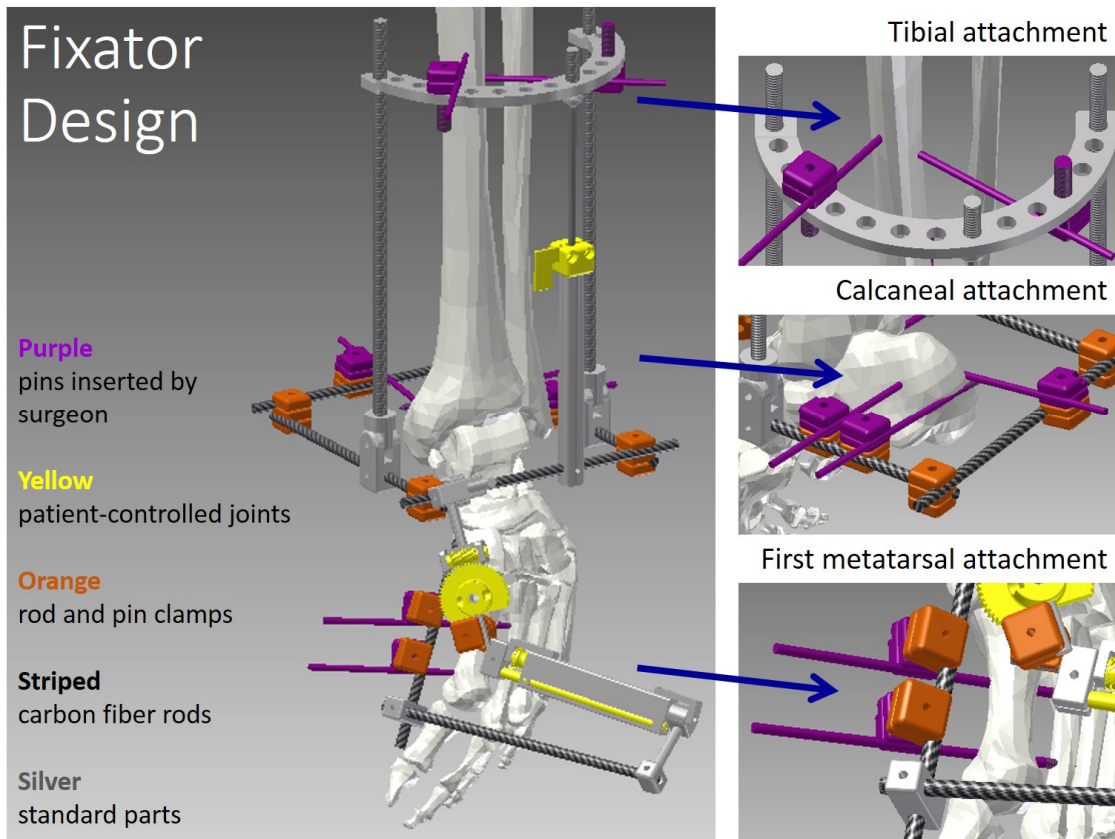
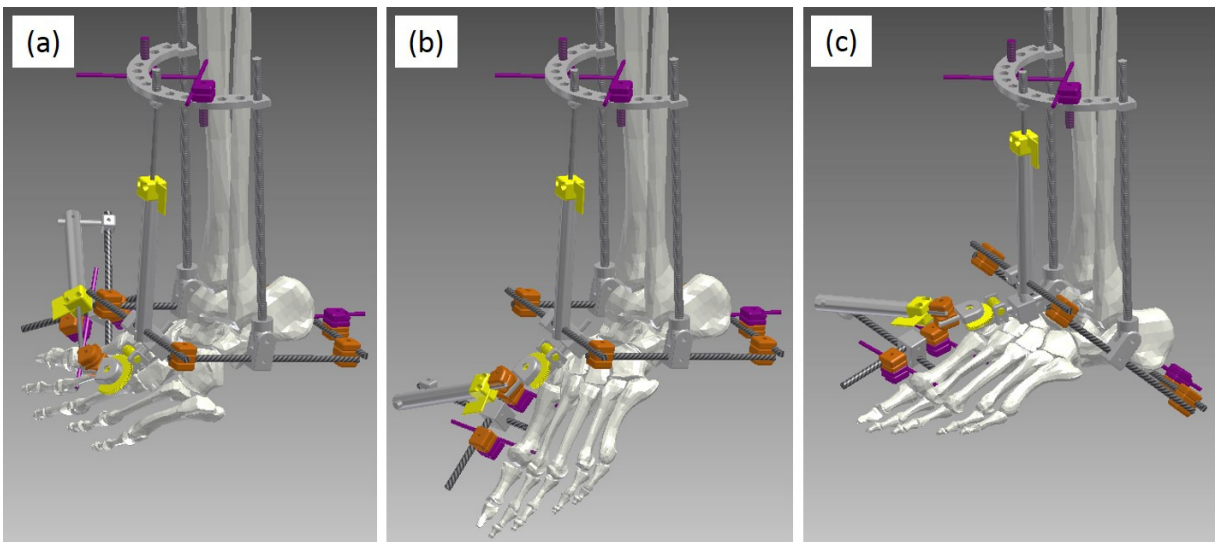


Figure A-1 First complete design of 2DOF external fixator. Trajectory joints and equinus joint are highlighted in yellow.



(a) Before correction. (b) After midfoot deformity is reduced. (c) After correction.

Figure A-2 CAD illustration of heel and midfoot deformities.

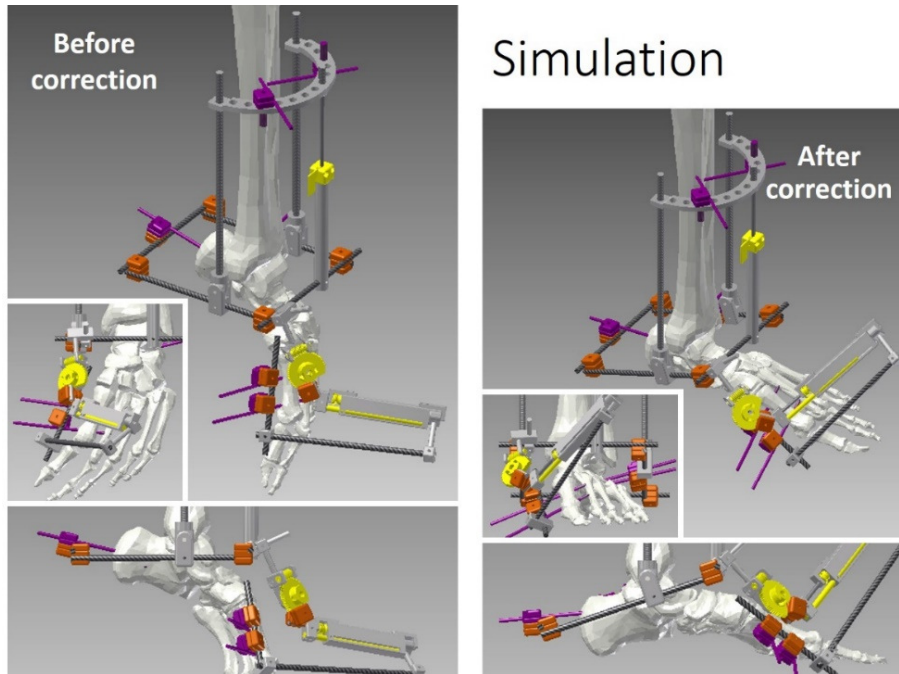
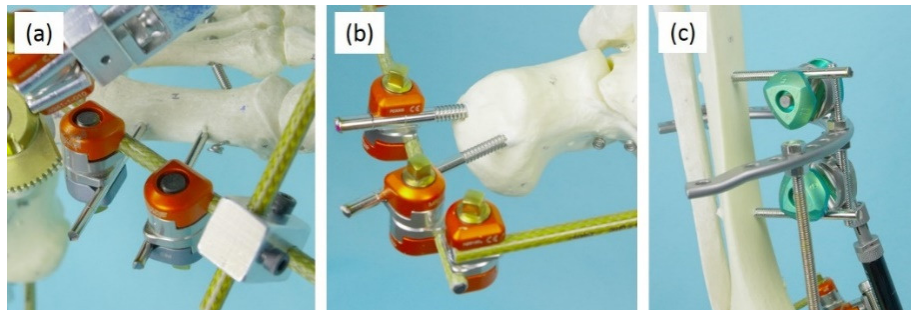
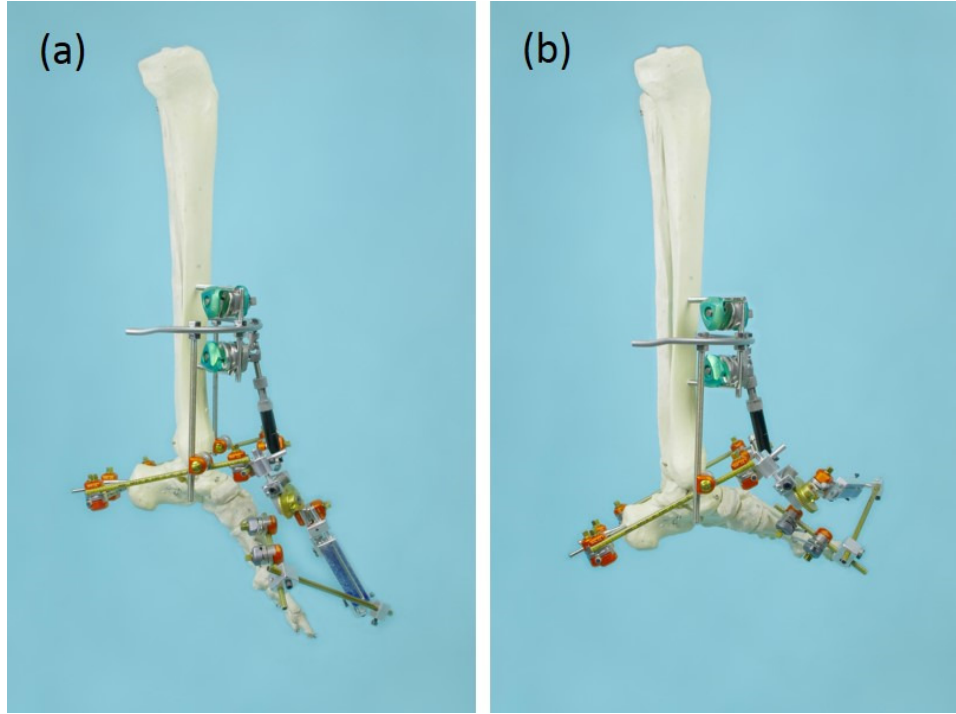


Figure A-3 CAD illustration of foot before and after simulated correction.⁷⁷



(a) Bone pins at first metatarsus. (b) Bone pins at calcaneus. (c) Bone pins at tibia.

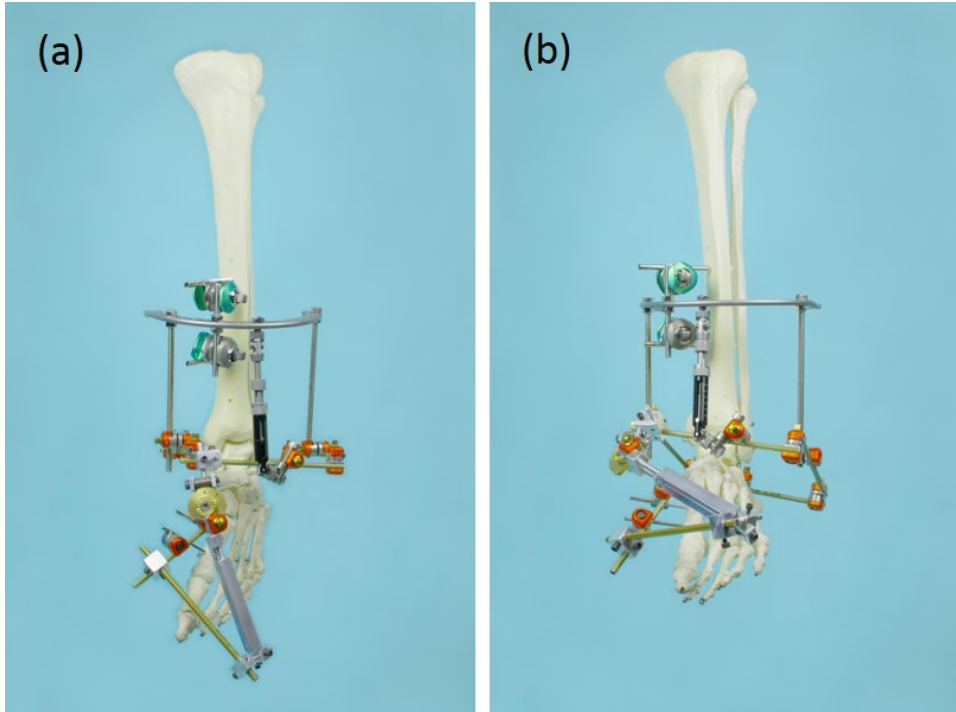
Figure A-4 Photos of bone pin attachment sites of first 2DOF external fixator prototype.



(a) Before correction.

(b) After correction.

Figure A-5 Side view of first 2DOF external fixator prototype, before and after correction.



(a) Before correction.

(b) After correction.

Figure A-6 Front view of first 2DOF external fixator prototype, before and after correction.^{76, 77}

Table A-1 Component count for first prototype.

Item	Count
Revolute trajectory joint	1
Prismatic trajectory joint	1
Prismatic equinus joint	1
Bone pin	6
Half ring	1
Hinge for ankle joint	2
Clamp	10
Extension plate	1
Rod	8
Custom universal joint	2
TOTAL	33

A2. Second Prototype

In the second prototype, improvements were made to the trajectory joint and the entire construct was made more rigid. Instead of purely a rod and clamp system, U-shaped plates were borrowed from existing systems and used bigger universal clamps and rods to increase the rigidity of the construct. This prototype was used in experiments 1-3 described in Chapter 6. The new components are annotated in **Figure A-7**. **Figure A-8** shows the second prototype on a patient-specific clubfoot model.

The trajectory joints were improved to increase rigidity and gearing ratio. **Figure 3-10** shows close-up photos of the revolute and prismatic trajectory joints. These joints were made with double-thread gears so the gearing ratio on the physical component was low. This was done deliberately for the convenience of demonstration. It is desirable for the joints to turn faster in these prototypes for demonstration so that the

audience can see the process immediately. Since there are always single-thread gears that can be swapped in, this design can be easily converted to high gearing ratios.

The mechanism of the revolute trajectory joint was a series of two worm gears. At the size of approximately 2 in by 1 in by 1 in, each worm gear pair can achieve a gearing ratio of 1:20. With two in a series, the gearing ratio can be designed to 1:400 gearing ratio so that one turn of the wing nut on the joint results in a rotation of 0.9 deg.

The prismatic trajectory joint was essentially a nut on a threaded rod. A precision ACME threaded rod could have a pitch as low as 1/16 in or 1.6 mm, so one full turn of the wing nut will result in a translation of only 1.6 mm.

While this prototype had the same component count of 33 as the first prototype, the breakdown was different. Custom made universal joints were replaced by generic clamps that were already commercially available. Using the U-shaped plate also saved us a few rods and clamps, which can be cumbersome to set up. Overall, the fixator was sturdier and more rigid. The breakdown of the component count is given in **Table A-2**.

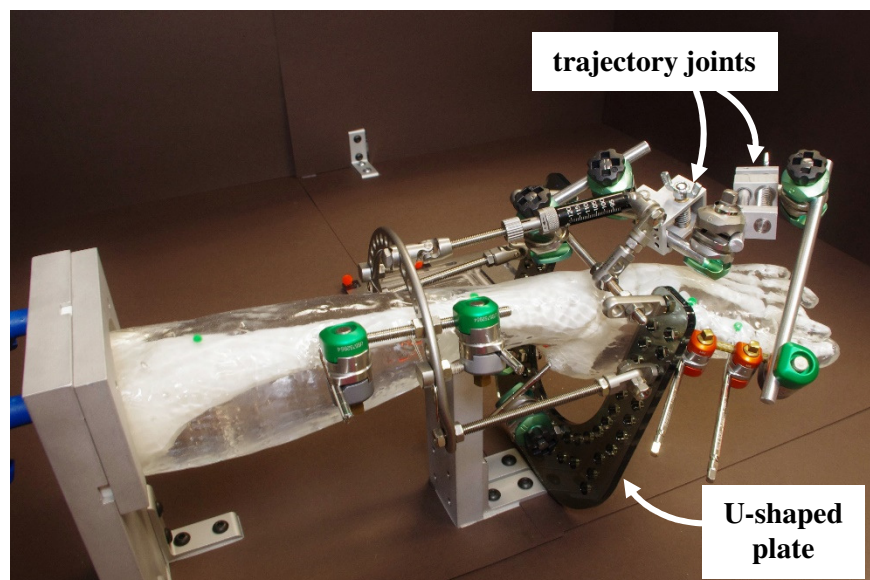
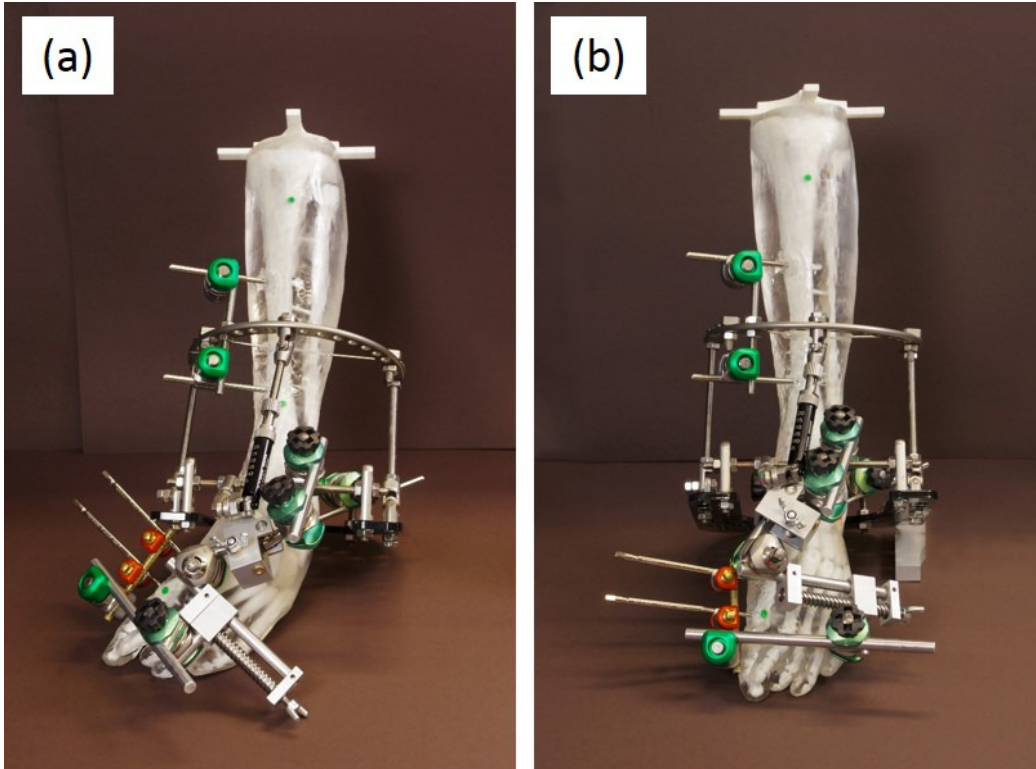


Figure A-7 Photo of second prototype showing plate and new trajectory joints.



(a) Before midfoot correction.

(b) After midfoot correction.

Figure A-8 Photos of foot model before and after midfoot correction.

Table A-2 Component count for second prototype.

Item	Count
Revolute trajectory joint	1
Prismatic trajectory joint	1
Prismatic equinus joint	1
Bone pin	6
Half ring	1
Hinge for ankle joint	2
Clamp	11
Extension plate	3
Rod	6
U-shaped plate	1
TOTAL	33

A3. Third Prototype

The third prototype was similar to the second prototype except the U-shaped plate was replaced with a D-shaped plate and a longer equinus joint was used. An annotated photo is shown in **Figure 3-11** and a front view of this prototype on the foot model is shown in **Figure 3-12**. The D-shaped plate reduced the number of components needed as a separate rod or bar going across the front of the ankle was no longer necessary. A single D-shaped plate also helped to simplify the fixator and make it more compact. The holes on the D-shape plate offered more flexibility in setting up the fixator as opposed to having just a rod. The total component count is down to 30, and the breakdown is given in **Table A-3**. The prototype looks simpler and less bulky than previous prototypes.

For this prototype, the procedure of installing the fixator was also modified. Instead of attaching the base frames directly on the foot, one component after the other, the frames were pre-built before attaching it to the foot. This enabled better control over the placement of the ankle hinges and minimized residual tension in the frame. This prototype was used in experiment 4 described in Chapter 6.

Table A-3 Component count for third prototype.

Item	Count
Revolute trajectory joint	1
Prismatic trajectory joint	1
Prismatic equinus joint	1
Bone pin	6
Half ring	1
Hinge for ankle joint	2
Clamp	11
Extension plate	1
Rod	5
D-shaped plate	1
TOTAL	30

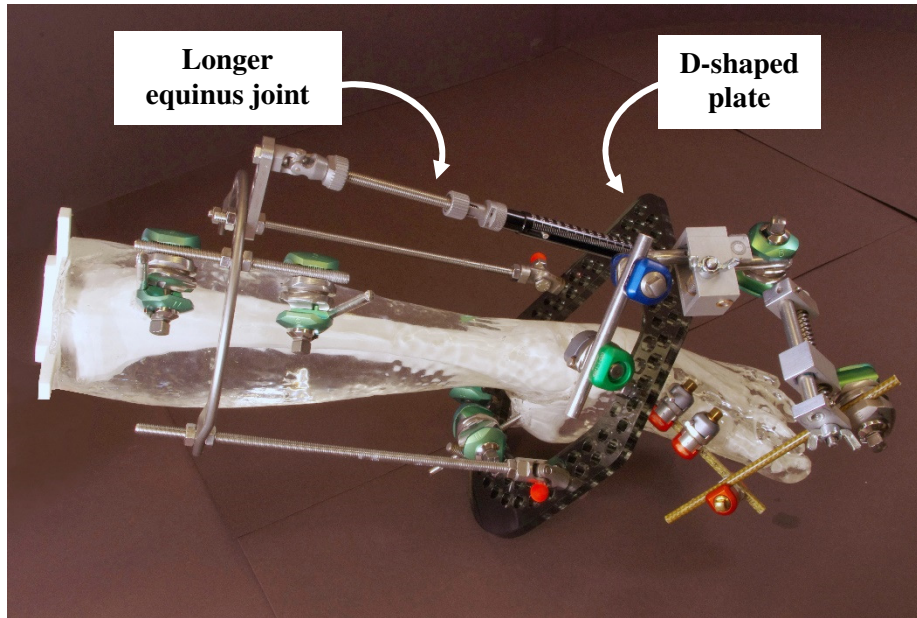


Figure A-9 Photo of third prototype showing new D-shaped plate and longer equinus joint.

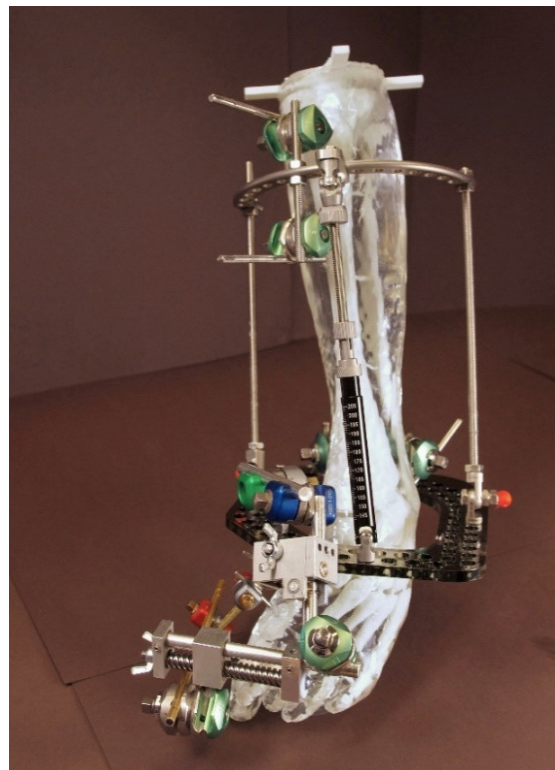


Figure A-10 Front view of third prototype of 2DOF external fixator for clubfoot correction.

Appendix B. Iterations of Passive Positioning Linkage

B1. First Prototype

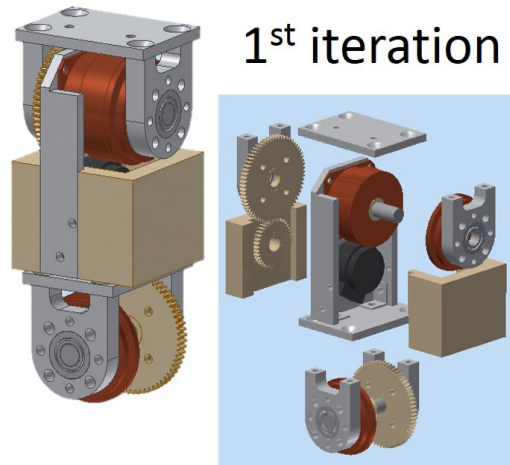
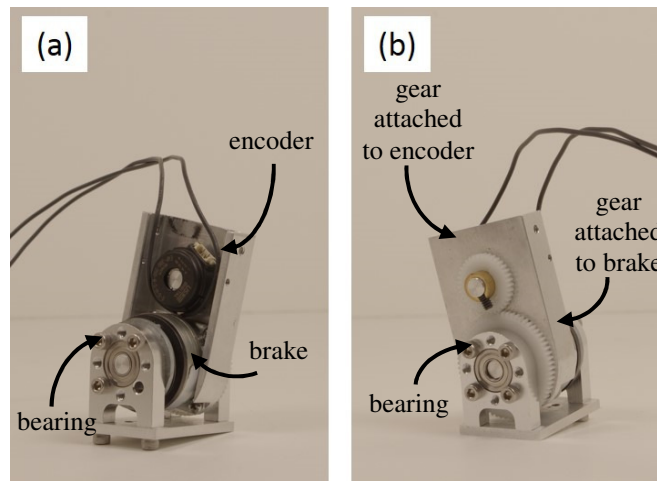


Figure B-1 First design of a linkage unit. Exploded view shows the electromagnet in copper color and the encoder in black.



(a) View of brake and encoder.

(b) View of gears.

Figure B-2 Photos of first prototype of linkage unit.

The first prototype of a linkage unit consisted of an electromagnetic brake, an encoder and a gear chain with two gears. The exploded view of this design is given in **Figure B-1** and photos of the physical

prototype is shown in **Figure B-2**. Plastic gears and aluminum brackets were used as proof of concept. The gear train had a ratio of 75:35, which gave an encoder resolution of 0.56 deg/count.

This prototype was very compact and rotated very smoothly but the design could be improved. Its components were not very rigid as the gears were plastic and the frame was made of aluminum pieces that had large tolerances in the manufacturing. The design also required many custom modifications to the components so the manufacturing process was slow and tedious.

B2. Second Prototype

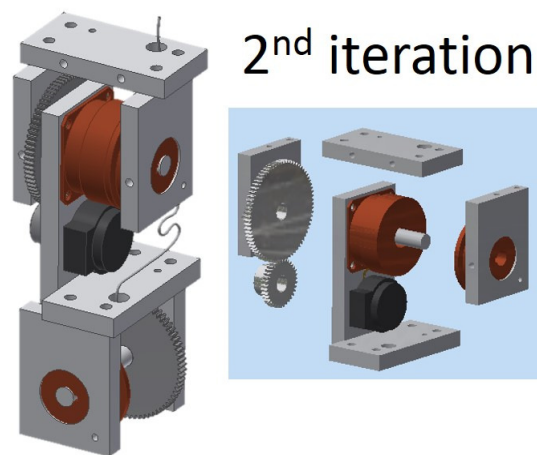
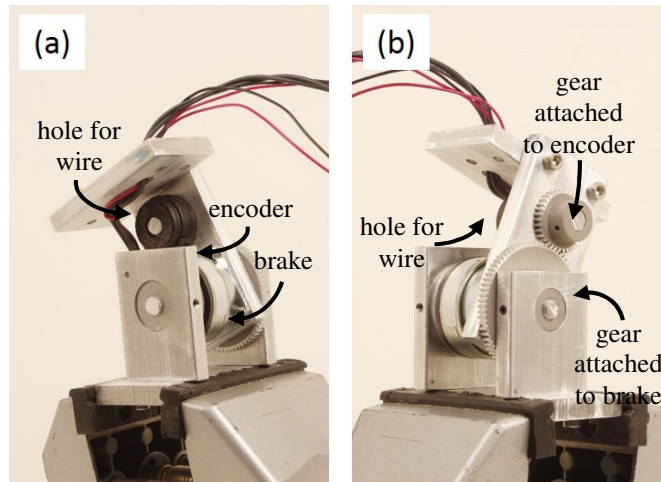


Figure B-3 Second iteration of linkage unit. Exploded view shows the electromagnet in copper color and the encoder in black.



(a) View of brake and encoder.

(b) View of gears.

Figure B-4 Photos of second prototype of linkage unit.

The second prototype had the same components as the first prototype, except the plastic gears were replaced with aluminum gears. The frame was made from aluminum plates that were thicker and stronger, and with the same gear ratio. The design is shown in **Figure B-3** and photos of the actual prototype are shown in **Figure B-4**. Holes in the frame were included specifically for wire management as the brake, encoder and controller required power supply and signal lines.

This prototype was designed for improved manufacturability. As a result of manufacturing and assembly being more precise, the joint moved more smoothly. However, relative to the required accuracy, this prototype had significant backlash in the gear train.

B3. Third Prototype

The third prototype had an anti-backlash gear coupled to an aluminum gear, with a ratio of 150:70, which still gave a resolution of 0.56 deg/count. As the anti-backlash gear was used to increase encoder resolution, it experienced very little loading and worked very well in reducing backlash.

The aluminum frame was designed with CNC machining in mind, so curves were included and features were designed to be mostly planar. The design looks more refined even though the components

specifications did not change. A gap was left in the frame for indicator lights that would tell the surgeon which direction to rotate the joint. The CAD design is shown in **Figure B-5** and photos of the actual prototype with annotated components are shown in **Figure B-6**.

However, the magnet did not have sufficient torque to hold its own weight at full horizontal extension. Thus, either a larger and stronger brake or a gear train at the magnet to increase its static torque loading was necessary. The current unit weighed about 10 oz, totaling 70 oz for the full 7DOF linkage, and each unit was about 3 in long. Considering its own weight and 2 lb of force at the end effector, the torque loading at the first joint is 90 lbin. The measured static torque loading of the brake was approximately 4 lbin. Using this value, the gear ratio needed was at least 23. Considering some safety margin, a gear ratio of above 30 was required.

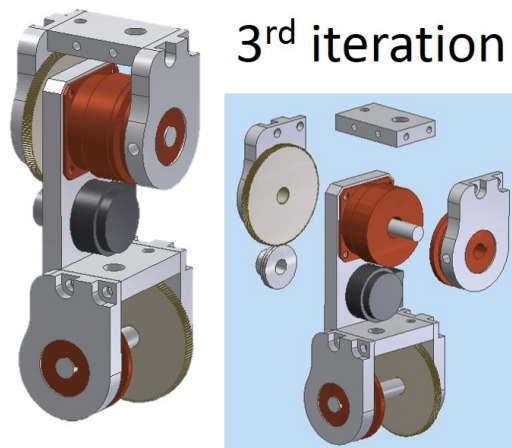
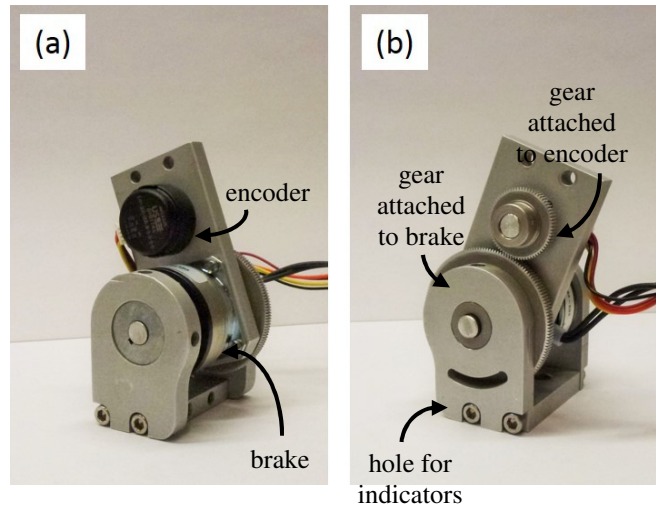


Figure B-5 Third design iteration of linkage unit. Exploded view shows the electromagnet in copper color and the encoder in black.



(a) View of brake and encoder. (b) View of anti-backlash gears.

Figure B-6 Photos of third prototype of linkage unit.

B4. Fourth Prototype

Multiple laser-cut plastic gears were made to explore the use of planetary gear systems that can achieve high gear ratio. High gear ratios between five and ten were possible, and the higher the gear ratio, the harder it was to operate since the backdrive torque was very high and the joint became very stiff. In addition, operating planetary gears in backdrive require tight tolerance in the alignment of rotation axes for each of the gears, especially for high gear ratios.

In this iteration, a planetary gear system with a gear ratio of six and a gear train of two gears with a ratio of six in series was included to create an overall gear ratio of 36. **Figure B-7** shows the exploded view of a linkage unit while **Figure B-8** shows a photo of the prototype. This prototype was much bigger because it had more components. The planetary gear system also made it necessary to have a bulkier frame to maintain alignment. The backdrive resistance was significant, especially since the alignment was not perfect and the gears frequently locked up.

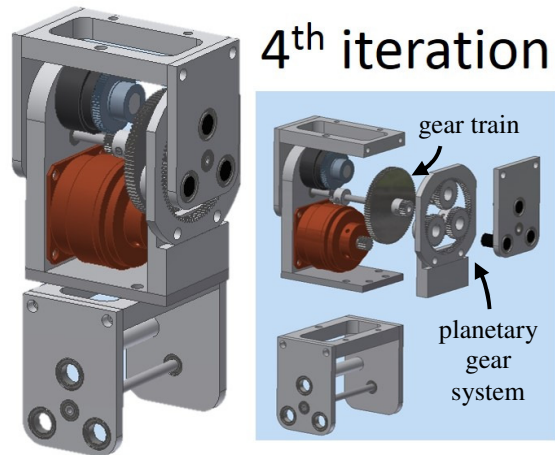


Figure B-7 Fourth design of a linkage unit. Exploded view shows the electromagnet in copper color and the encoder in black. The planetary gear system and the gear train are also shown in the exploded view.

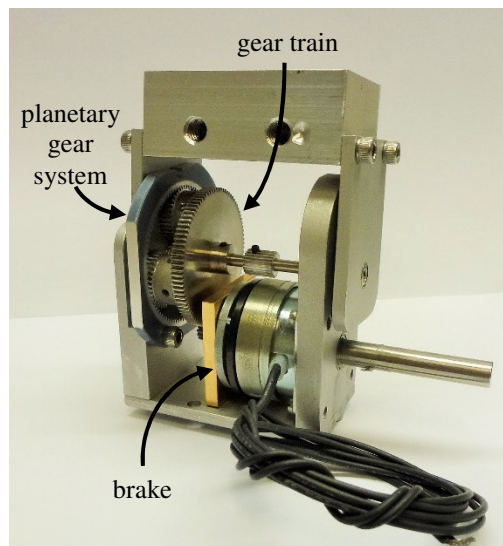


Figure B-8 Photo of fourth prototype of linkage unit. Encoder is not attached to prototype.